The Enhancement of Supermassive Black Hole Accretion Rates in Post-Merger Galaxies from Cosmological Simulations

by

Shoshannah Byrne-Mamahit
B.Sc., University of Waterloo, 2020

A Thesis Submitted in Partial Fulfillment of the
Requirements for the Degree of

MASTER OF SCIENCE

in the Department of Physics and Astronomy

The Enhancement of Supermassive Black Hole Accretion Rates in Post-Merger Galaxies from Cosmological Simulations

by

Shoshannah Byrne-Mamahit
B.Sc., University of Waterloo, 2020

Supervisory Committee

Dr. S. Ellison, Supervisor
(Department of Physics and Astronomy)

Dr. A. Babul, Departmental Member
(Department of Physics and Astronomy)

ABSTRACT

Numerical simulations of galaxy mergers predict that in a merger event, the angular momentum of gas is efficiently drained, leading to gaseous inflows resulting in high central gas densities and bursts of star formation. The merger-starburst connection is strongly corroborated by observational studies of interacting and post-merger galaxies. In addition to the enhancement of central star formation rate, simulations predict that gaseous inflows will increase the accretion onto central supermassive black holes (SMBHs) which may trigger or enhance nuclear activity. However, observational studies continue to debate the connection between galaxy mergers and active galactic nuclei (AGN), with contrasting conclusions on whether mergers are likely to trigger AGN and whether the majority of AGN are triggered by merger events. In this thesis, I present an analysis of the SMBH accretion rates in post-merger galaxies drawn from the IllustrisTNG, Illustris, and EAGLE cosmological simulations. The post-merger samples consist of galaxies that have experienced a merger in the last simulation snapshot in the redshift range $0< z <1$, with stellar mass ratios $> 1:10$ and post-merger stellar masses $> 10^{10}\mathrm{M}_{\odot}$. I compare the post-merger SMBH accretion rates to a control sample of galaxies that are matched to the post-mergers in stellar mass, redshift, environment (and AGN feedback mode in the case of IllustrisTNG) but that have not experienced a merger (of mass ratio $> 1:10$) within at least two Gyrs. I find that all three simulations demonstrate a population averaged enhancement in SMBH accretion rate in the post-merger sample, with accretion rates ~ 2 times higher than controls for IllustrisTNG and EAGLE and ~ 4 times higher in Illustris. In addition, I find that post-mergers are 2-4 times more likely to host a highly accreting SMBH compared with matched non-merger galaxies. In all three simulations, the population averaged SMBH accretion rate enhancement persists for $\sim 2-3$ Gyrs after coalescence, significantly exceeding the $\sim$500 Myr lifetime of star formation rate enhancements. In the IllustrisTNG simulation, I investigate the presence of simultaneous enhancements in both the star formation and SMBH accretion rates; I find that co-incidence occurs predominantly in the first few hundred Myrs post-coalescence and depends on both the mass ratio of the merger and on the gas mass of the post-merger galaxy. Furthermore, in TNG, I find that despite the overall SMBH accretion rate enhancement, only approximately 35% of post-mergers experience a luminous AGN ($L_{bol} > 10^{44}$erg/s) within 500 Myrs after coalescence, and fewer than 10% achieve a luminosity in excess of $L_{bol} > 10^{45}$erg/s. Moreover, only $\sim$10%

of the highest luminosity ($L_{bol} > 10^{45}$erg/s) AGN in the IllustrisTNG galaxy sample are recent mergers. My results are therefore consistent with a picture in which mergers *can* (but don't always) trigger AGN activity, but where the majority of galaxies hosting high luminosity AGN are not recent mergers.

Contents

List of Tables

List of Figures

ACKNOWLEDGEMENTS

I would like to thank:

Dr. Sara Ellison, for being an amazing supervisor and mentor. Your instruction, encouragement, and kindness have been invaluable towards my academic and professional development.

Drs. Maan Hani & Salvatore Quai, for your mentorship. I've been privileged to tackle interesting and exciting science questions alongside you.

M. Thorp, R. Bickley, S. Wilkinson, Dr. Patton, Dr. Woo, and D. Walters, for your regular support and insightful questions.

Dr. Arif Babul, for your positive encouragement and for teaching me to have a healthy dose of skepticism.

Matthew Pereira Wilson, for your encouragement, support, humour, and love.

Lucy, for being the best girl.

DEDICATION

I dedicate this body of work to my family, who have provided me with love, support, and the opportunity to pursue my passion.

Chapter 1

Introduction

In the Universe today there exists a diverse and complex population of galaxies. In some galaxies, stars are distributed within a disk that can have features such as spiral arms or bars, others instead look like smooth featureless ellipsoids, and some have disorganised and irregular morphologies (Hubble 1926; Sandage 1961). However, in the standard cosmological model, all galaxies ultimately formed from the same origins. Stars form from gas which collapsed into overdensities of dark matter, called dark matter halos, creating galaxies (White and Rees 1978; White and Frenk 1991; Springel 2005). Galaxies will evolve over cosmic time under the influence of both internal and external processes, and through hierarchical merging, creating the population observed today (Somerville and Davé 2015). In fact, the galaxy populations of the past, observed at higher redshifts, have different characteristics than the late universe, such as higher star formation rates (Madau and Dickinson 2014) and a higher abundance of disks and irregular morphologies (Conselice 2014). It therefore appears that galaxies are dynamic systems that can undergo significant changes in morphology and star formation activity over cosmic time. Understanding how galaxies evolve over cosmic time, what processes influence galactic evolution, and how the diversity of the galactic population came to be is a challenging problem which spans many orders of magnitude in spatial, temporal, and energy scales.

1.1 Galaxy bimodality

Despite a large amount of diversity in the galactic population, it is observed that most galaxies are well separated into two categories according to their colour and

morphology: the blue disky galaxies and red ellipsoidal galaxies (Strateva et al. 2001; Baldry et al. 2004; Schawinski et al. 2014). The distinction between the blue and red sequence also separates the populations by star formation activity, as blue light is associated with young stellar populations and ongoing star formation whereas red light is associated with older 'passive' or 'quenched' stellar populations. In addition, the two categories are also related to the stellar mass of the galaxy, with the more massive galaxies appearing in the red ellipsoidal category (Schawinski et al. 2014).

Within the star forming population of galaxies, there also exists variation in the rate of ongoing star formation. Star forming galaxies demonstrate a positive correlation between the star formation rate and the total stellar mass of the galaxy, known as the star forming main sequence (Brinchmann et al. 2004; Daddi et al. 2007; Noeske et al. 2007; Salim et al. 2007). Therefore, star forming galaxies are expected to evolve along the star-forming main sequence, but eventually cease star formation and transition into the passive population (Peng et al. 2010). In addition to the variation of star formation rate for galaxies of different stellar mass, there are also galaxies that can demonstrate exceptionally high star formation rates for their stellar mass, known as starburst galaxies.

1.2 Active Galactic Nuclei

In addition to the variation in star formation activity amongst galaxies, some galaxies also contain observational signatures of energetic processes that are believed to result from an accreting supermassive black hole (SMBH). Such systems are referred to as Active Galactic Nuclei or AGN hosts.

1.2.1 AGN structure and the unified AGN model

The classification of 'AGN' can depend on many types of emission from an accreting SMBH, resulting in a large diversity of AGN types which Padovani et al. (2017) refers to as the 'AGN zoo'. Antonucci (1993) and Urry and Padovani (1995) bridge together many of these separate categories into a unified AGN model, outlined in Figure 1.1. The unified AGN model separates the emission sources associated with AGN into several structures: the accretion disk, the corona, high density high velocity clouds known as the Broad Line Region (BLR), low density lower velocity clouds known as the Narrow Line Region (NLR), a dusty torus, and a radio jet (Netzer

2015). The various components emit over different ranges of the electromagnetic spectrum (or with different spectral characteristics in the case of the BLR and NLR), as demonstrated in Figure 1.2. Figure 1.2 shows the spectral energy distribution of an unobscured AGN, with the total (radio-quiet) AGN emission shown in the solid black line. The emission from the hot corona peaks in the x-ray. Next the plasma within the unobscured accretion disk will emit in the optical and UV range. The dusty torus emits reprocessed emission in the mid to near infrared. Finally, there may be additional emission in the radio range due to synchrotron emission within relativistic jets associated with SMBHs.

Antonucci (1993) and Urry and Padovani (1995) proposed that different AGN classifications can be explained as observations of different components of the unified model. For example, the distinction between Type I and Type II AGN can be explained via the obscuration of the broad line region by the torus, such that observers aligned with the plane of the torus will only detect AGN with narrow spectral lines. Additionally, alignment or misalignment with a radio jet can result in a radio loud or radio quiet AGN (as shown in Figure 1.2), though some AGN may not host a relativistic jet at all.

In addition to the larger scale AGN structure demonstrated in Figure 1.1, theoretical studies and simulations have also demonstrated variation in the gas structure surrounding the SMBH (Liu et al. 2002; Brinkmann 2009; Meyer-Hofmeister et al. 2012; Inayoshi et al. 2018). At high accretion rates, high density gas is able to sufficiently cool into a thin accretion disk structure in what is known as radiatively efficient AGN, as is demonstrated in Figure 1.1. However, when accretion rates are lower, the SMBH becomes surrounded by hot diffuse gas that is unable to efficiently cool via radiation (Brinkmann 2009), known as a radiatively inefficient AGN. In radiatively inefficient AGN, the gas structure in the innermost region surrounding the SMBH becomes geometrically thicker approaching a toroidal structure (Brinkmann 2009; Inayoshi et al. 2018). In fact, the inner disk may even completely disappear at very low accretion rates, and the gas is arranged in an ellipsoidal configuration (Liu 2013). In the radiatively inefficient configuration, magnetic fields play an increasingly dominant role allowing for the support of relativistic jets (Brinkmann 2009). The varying geometries of the near SMBH region are demonstrated in Figure 1.3, where the arrow denotes the increasing strength of the accretion flow.

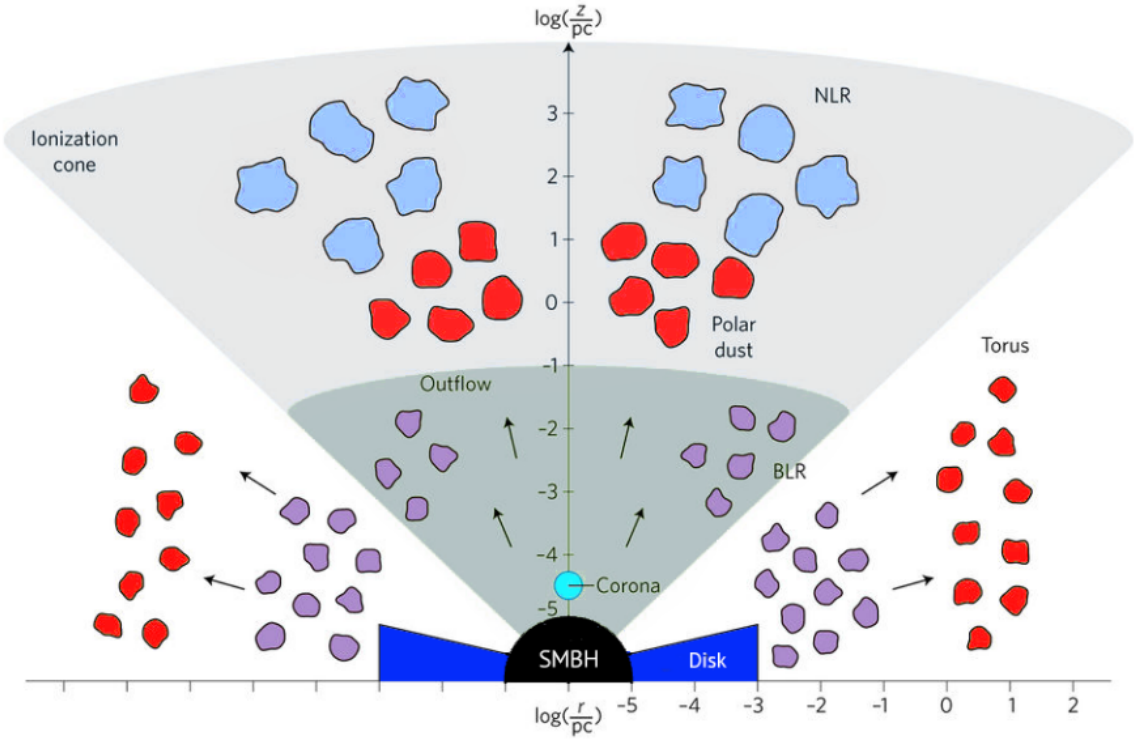

Figure 1.1: Schematic for the different components of the unified AGN model (for a radiatively efficient AGN), taken directly from Hickox and Alexander (2018) (adapted from Ramos Almeida and Ricci (2017))

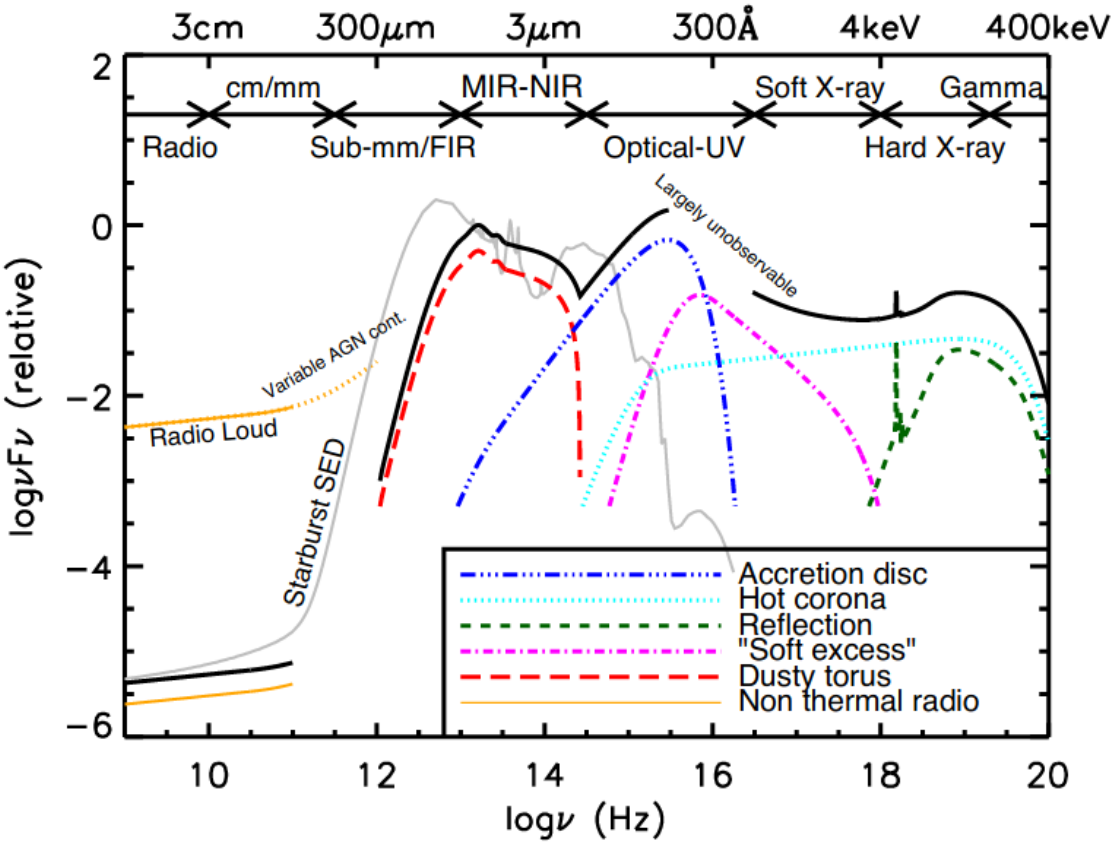

Figure 1.2: Schematic demonstrating the Spectral Energy Density (SED) for an unobscured AGN shown in black, and the contributions from the separate AGN model components, color coded to match the schematic in Figure 1.1. Taken directly from Hickox and Alexander (2018) (adapted from Harrison (2014)).

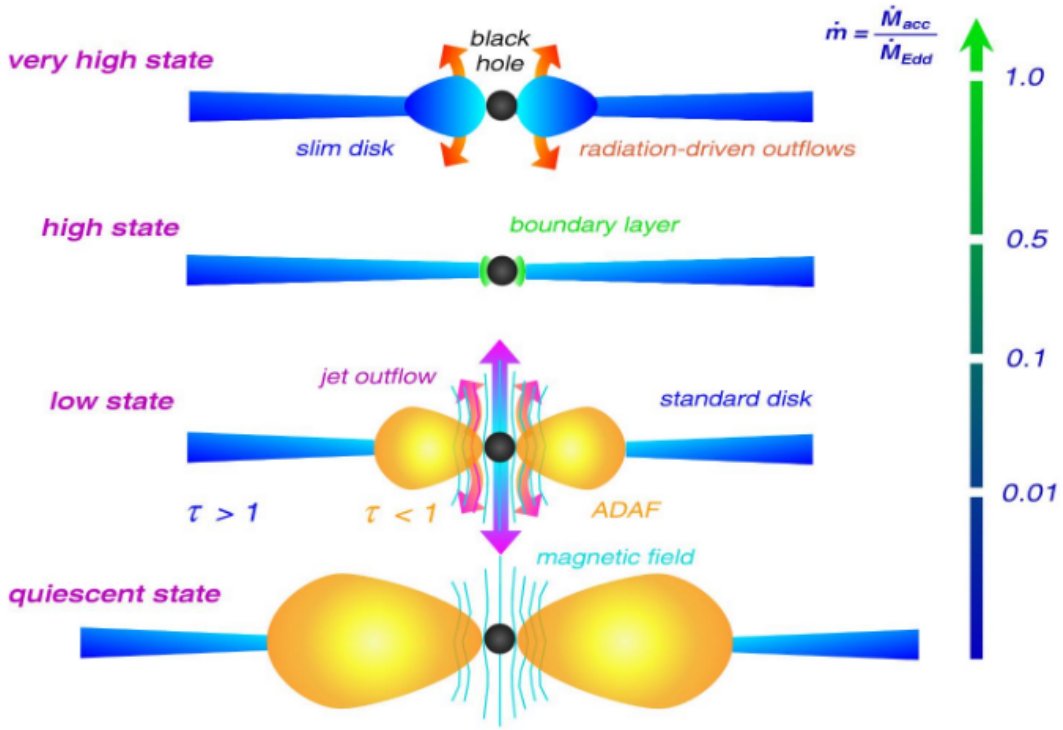

Figure 1.3: Schematic demonstrating the variation of gas structure surrounding the SMBH in an AGN for different strength accretion flows. The top two schematics represent the structure in radiatively efficient AGN, and the bottom two schematics show the gas structure in radiatively inefficient AGN. Taken directly from Müller (2004).

1.2.2 AGN and galaxy evolution

Observations demonstrate that the SMBH mass can correlate with host galaxy properties, such as bulge stellar velocity dispersion, mass, and luminosity (Ferrarese and Merritt 2000; Kormendy and Gebhardt 2001; Tremaine et al. 2002). Such a correlation suggests that the SMBH and galaxy may co-evolve, which is particularly surprising when considering the extreme difference in spatial scale between the parsec and sub-parsec scales for SMBH accretion and the kpc scale of the galaxy (Kormendy and Ho 2013). It has been suggested that SMBHs would be able to influence their host galaxy through efficient AGN feedback (Silk and Rees 1998), and observations have been able to directly observe the influence of AGN over large spatial scales (e.g the MS0735.6+7421 cluster shown in Figure 1.4 from McNamara and Nulsen 2007, one of the most powerful AGN in the Universe). In Figure 1.4, the radio emission from relativistic jets emitted from the SMBH are shown to be spatially co-incident with large cavities in the intracluster medium, demonstrating how AGN feedback can displace and heat gas that lies far outside the spatial extent of the host galaxy (McNamara and Nulsen 2007).

However, not all host galaxy properties (e.g. disks and pseudobulges) correlate with SMBH mass, which could indicate that co-evolution occurs at specific stages of galaxy evolution associated with bulge formation (see Section 1.3.1) but not during secular phases which form disks and pseudobulges (Kormendy and Ho 2013). Furthermore, it has been shown in semi-analytic modelling that the mass scaling relations can be obtained without explicitly coupling the growth of the SMBH and bulge (Jahnke and Macciò 2011), suggesting the correlation may arise from entirely non-causal origins.

If AGN are ubiquitous, i.e. every galaxy hosts a supermassive black hole with the potential to fuel AGN activity, then AGN activity could explain the transition of massive galaxies from the star forming to the passive population (Somerville et al. 2008). While the specific mechanisms by which AGN feedback may influence the host galaxy are still actively investigated, it is believed AGN could suppress star formation in galaxies via two broad scenarios: ejective or preventative feedback. In the ejective scenario, AGN remove gas from the host galaxy, for example through radiation pressure from the luminous accretion region (Sturm et al. 2011; Cicone et al. 2014; Ellison et al. 2021). Alternatively in the preventative scenario, AGN cut off the host galaxy from the source of gas needed to sustain star formation by

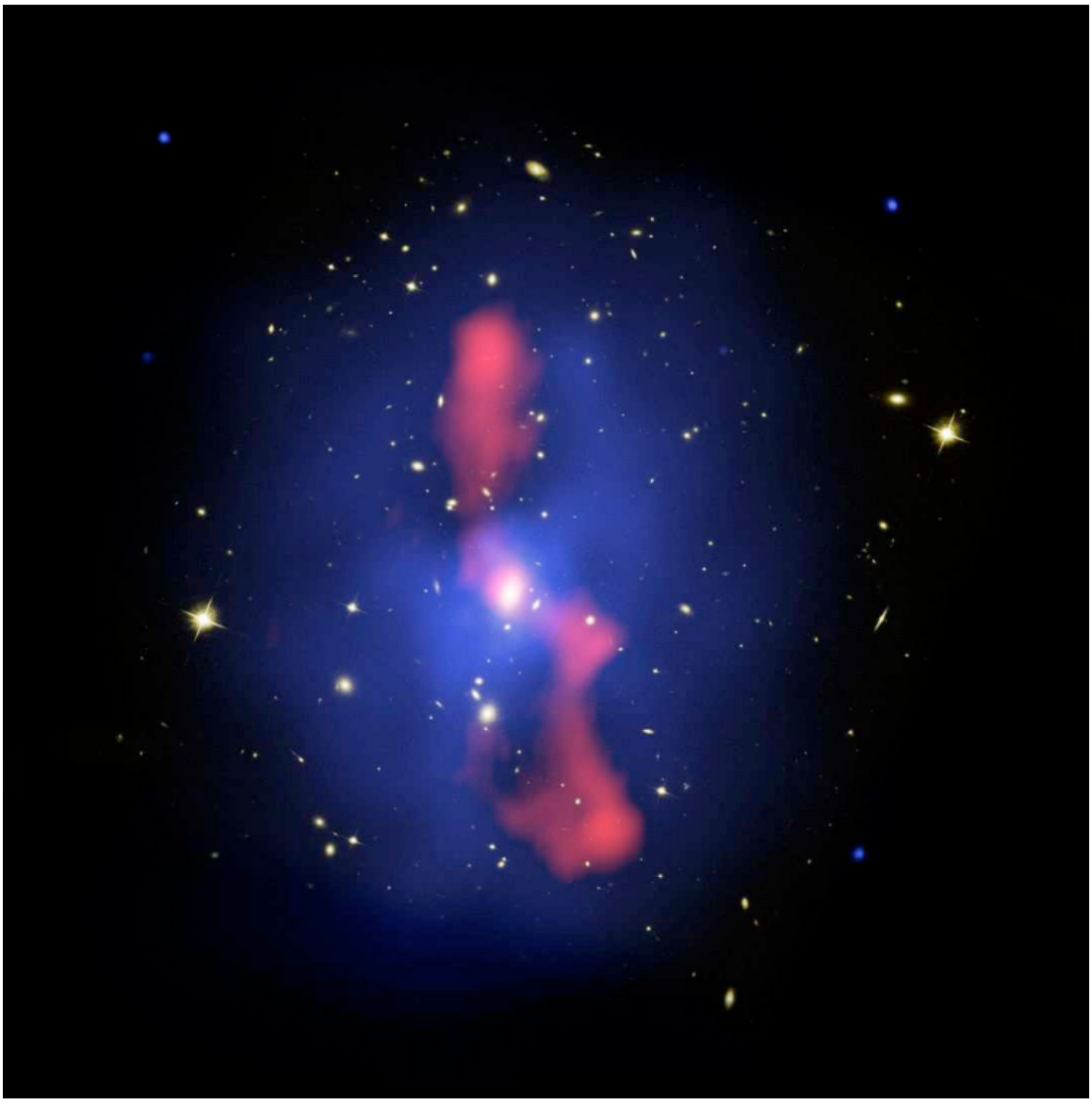

Figure 1.4: Hubble Space Telescope visual image of the MS0735.6+7421 cluster combined with the Chandra X-ray image of the X-ray emitting cluster medium (shown in blue) and the radio jet emission from the Very Large Array (shown in red). The image is taken directly from McNamara and Nulsen (2007).

heating the gas in the circumgalactic medium and suppressing the inflow of cooling gas (McNamara and Nulsen 2007; McCarthy et al. 2008).

1.3 Galaxy evolution: the role of mergers

In the standard model of cosmology, galaxies form from hierarchical merging, whereby massive galaxies are assembled over a history of mergers of smaller galaxies. Therefore, all galaxies have, at some point in the past, experienced a merger event, making mergers ubiquitous amongst the galaxy population.

1.3.1 Galaxy mergers and morphology

One way in which mergers may influence a galaxy's evolution is by facilitating morphological transformations. Observations have demonstrated the enhancement of irregular morphologies in interacting galaxies (Hernández-Toledo et al. 2005; Patton et al. 2005; Casteels et al. 2014; Patton et al. 2016). Figure 1.5 from Schweizer (1986) demonstrates the morphological features of interacting galaxies. These features, such as bridges and tails, have been shown to form due to the gravitational forces between galaxies during interactions and mergers (Toomre and Toomre 1972). Figure 1.6 demonstrates the morphological transformation undergone in a major merger event from a hydrodynamic simulation by Lotz et al. (2008). In the figure, the two undisturbed disk galaxies at $t = 0$ Gyrs undergo a significant interaction, forming numerous spiral features and tidal tails after first passage, demonstrating a very irregular morphology right before coalescence around $t = 1.66$ Gyrs, and post-coalescence features such as shells around $t = 1.66$.

In addition, simulations predict that the angular momentum of the particles in the disk can be redistributed, producing a post-coalescence morphology that is visually similar to elliptical (spheroidal) type galaxies (White 1978; Roos and Norman 1979; Villumsen 1982). It is therefore possible that mergers also play a role in assembling isotropic distributions of stellar material, forming bulges or elliptical galaxies.

1.3.2 Galaxy mergers and starbursts

Galaxy mergers are also linked to enhancements of star formation rate and central starburst galaxies, where numerous observational studies find star formation rate

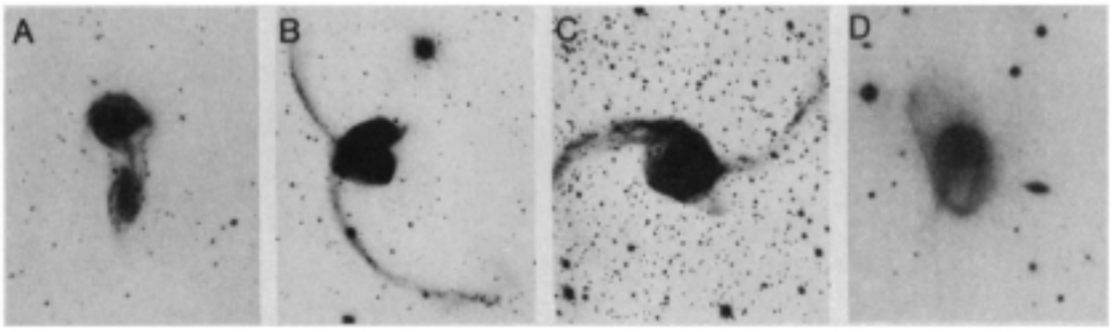

Figure 1.5: Observations of interacting galaxies are shown, for increasing stages of interaction from a to d (a: NGC 5426/5427, b: NGC 4038/4039, c: NGC 3256, d: NGC 3291). All images are taken directly from Schweizer (1986).

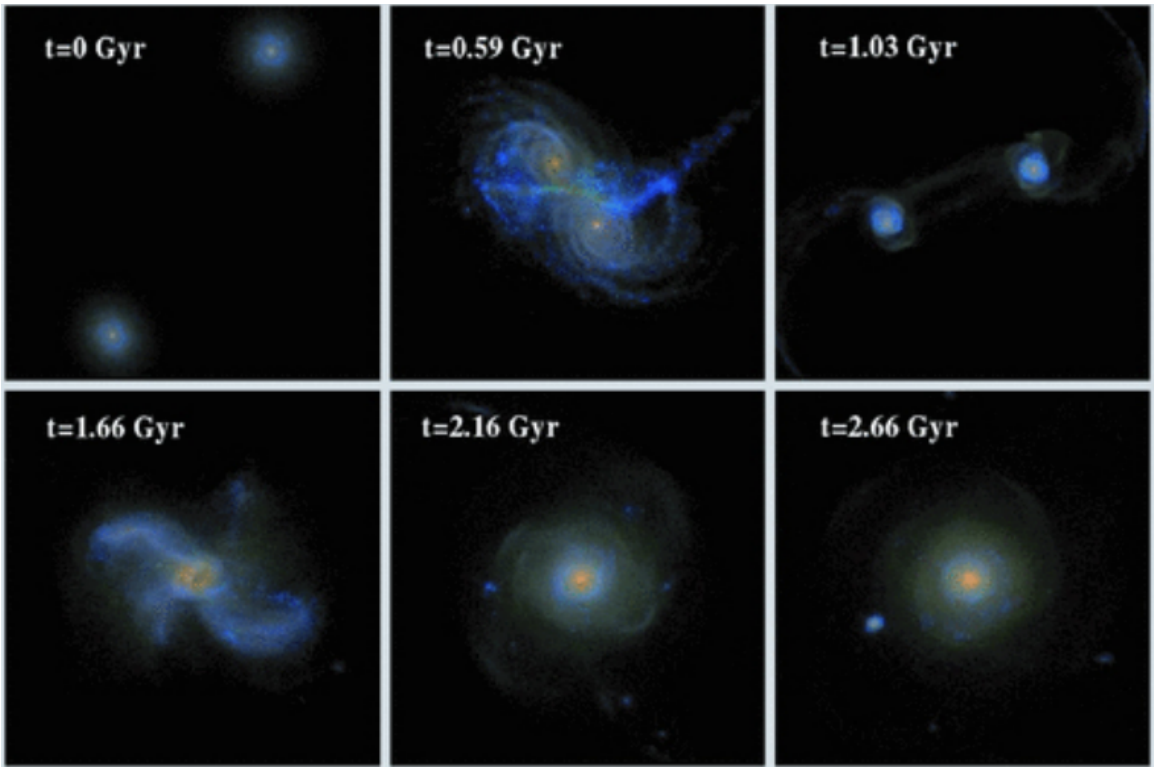

Figure 1.6: Morphological evolution of a major merger event, taken directly from Lotz et al. (2008).

enhancements in interacting (Barton et al. 2000; Woods et al. 2006; Woods and Geller 2007; Ellison et al. 2008; Woods et al. 2010; Scudder et al. 2012; Patton et al. 2013; Knapen et al. 2015; Cao et al. 2016) and post-merger (Ellison et al. 2008; Ellison et al. 2013; Thorp et al. 2019) galaxies.

Simulations investigating the merger-starburst connection demonstrate that for major mergers between gas rich disk type galaxies, merger induced asymmetric structures within the galaxies drain angular momentum from the gas in the disk, leading to gaseous inflows towards the nuclear region (Hernquist 1989; Barnes and Hernquist 1991; Blumenthal and Barnes 2018), which are then able to fuel strong bursts of star formation. Within a few hundred Myrs of the merger, the central starburst can affect the observed morphology of galaxies, due to the increase of light emitted from young stellar populations in the central regions of the galaxy (Conselice 2014). However, the long-term effect of the starburst on the galaxy's evolution is not well understood. Theoretical predictions and observations suggest the contribution of the starburst event to the total stellar mass of galaxies is minimal (Baugh et al. 2005; Rodighiero et al. 2011). However, it is possible that stellar feedback associated with the starburst could affect the host galaxy's star formation, either by ejecting or heating up the gas in the galaxy.

1.3.3 Galaxy mergers and AGN

If galaxy mergers can generate gaseous inflows capable of fueling central starbursts, could mergers also fuel an excess of accretion onto supermassive black holes? Such a scenario was posed in the observational study of ultraluminous infrared galaxies (ULIRGs) by Sanders et al. (1988). Merger induced bursts of AGN activity are further demonstrated in simulations of gas-rich major mergers by Di Matteo et al. (2005); Springel (2005). The theoretical framework for a merger-AGN connection was fully outlined in Hopkins et al. (2008), in which major mergers cause central starbursts and quasar activity, followed by the morphological transformation and rapid quenching of star formation in the post-merger galaxy, demonstrated in Figure 1.7.

The evolutionary pathway in Figure 1.7 suggests a relationship between galaxy mergers, quasar activity, and the quenched population of galaxies. However, in contrast to the overall consensus that interactions and mergers enhance the star formation rate of galaxies, observational studies do not overwhelmingly support a strong connection between AGN activity and interacting and/or merging systems. In fact,

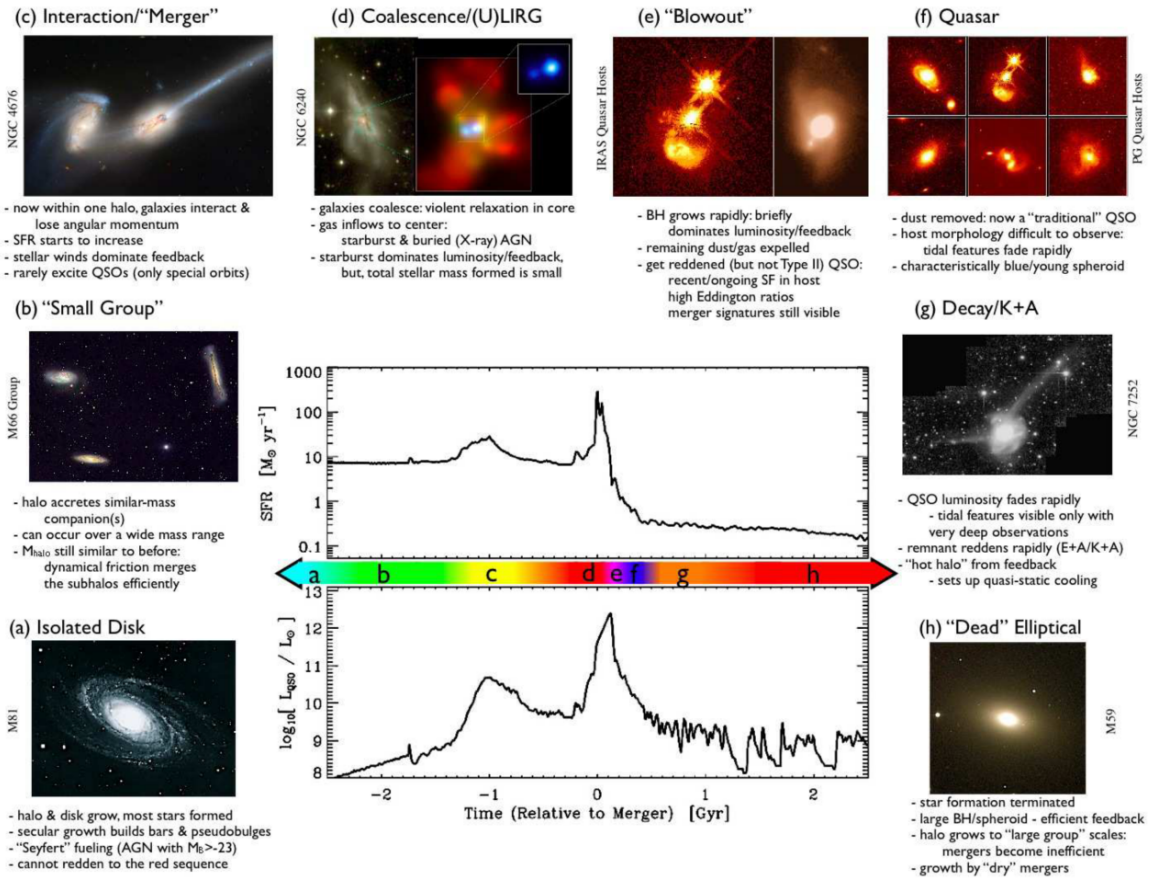

Figure 1.7: Evolutionary phases of a gas-rich major merger taken directly from Hopkins et al. (2008).

numerous observational studies do not find any connection between interacting galaxies and AGN activity (Cisternas et al. 2011; Schawinski et al. 2011; Kocevski et al. 2012; Böhm et al. 2013; Shah et al. 2020; Lambrides et al. 2021). On the other hand, many studies do find an excess of AGN in interacting pairs and post-mergers (Alonso et al. 2007; Ellison et al. 2011; Bessiere et al. 2012; Ellison et al. 2013; Hong et al. 2015; Kocevski et al. 2015; Hewlett et al. 2017; Marian et al. 2020).

A possible explanation for the tension in observational studies of the merger-AGN connection is that only some galaxy mergers will follow the evolutionary pathway proposed in Figure 1.7. It has been demonstrated in simulations that even in gas rich major mergers, the strength of gas inflows can vary depending on the properties of the merging galaxies (Mihos and Hernquist 1996) and the merger geometry (Di Matteo et al. 2007; Blumenthal and Barnes 2018). Furthermore, Capelo et al. (2015) study the accretion onto supermassive black holes in a suite of high resolution simulations of galaxy mergers and find that mass ratio is the most important factor in determining the strength of the enhancement in accretion rate, suggesting that minor mergers are not as likely to cause AGN activity.

There also exist possible complications within the observational studies of the AGN-merger connection. For example, since interacting and post-merger galaxies rely on visual identification, observational studies may be affected by the purity of the merger and isolated comparison samples. Bickley et al. (2021) demonstrate, using machine vision methods, that the purity of a post-merger identification technique is extremely important in order to recover population averaged signals such as star formation rate enhancement. It is also possible that the timescale over which AGN are identified and the timescale over which galaxy mergers are identified may not overlap. Depending on the merger selection technique, simulations suggest merger features will remain observable for as few as 200 Myrs post coalescence up to 1 Gyr after coalescence (Lotz et al. 2008). If observable merger features far outlive triggered AGN activity, co-incident merger and AGN identification may be rare, and the absence of an AGN detection in interacting or post-merger galaxies would not necessarily mean that there was no merger triggered AGN activity. Finally, observational studies of the merger-AGN connection rely on AGN detection techniques that may be strongly susceptible to AGN obscuration. AGN obscuration occurs when AGN emission is significantly absorbed or scattered by gas and dust (Hickox and Alexander 2018). The obscuration of AGN can impact the timescale over which merger and AGN features are simultaneously detectable, and may result in a false non-detection of

AGN activity.

Overall, observational results suggest that galaxy mergers can trigger AGN activity, as many studies find that AGN are more likely to appear in merging galaxies compared with an undisturbed control sample (Alonso et al. 2007; Ellison et al. 2011, 2013; Satyapal et al. 2014; Weston et al. 2017; Goulding et al. 2018; Ellison et al. 2019b; Gao et al. 2020). It is less clear whether galaxy mergers contribute significantly to the overall AGN population. For example, Ellison et al. (2019b) find that low redshift AGN (selected using optical and mid-IR selection) preferentially reside in disturbed systems, which is consistent with a number of other studies looking at the merger/disturbed fraction of AGN (Bessiere et al. 2012; Hong et al. 2015; Kocevski et al. 2015; Marian et al. 2020; Fan et al. 2016; Gao et al. 2020; Pierce et al. 2022). However, numerous studies disagree, finding no significant excess of disturbed or merging systems in AGN (Cisternas et al. 2011; Schawinski et al. 2011, 2012; Kocevski et al. 2012; Böhm et al. 2013; Villforth et al. 2014; Mechtley et al. 2016; Villforth et al. 2017; Marian et al. 2019; Lambrides et al. 2021). In addition, an important consideration in the contribution of mergers to the overall AGN population is the rarity of mergers in the Universe (Lotz et al. 2011). It is possible that mergers may efficiently trigger AGN activity, but are a sub-dominant contributor to the AGN population due to their rarity.

1.4 Cosmological simulations

In the last decade, significant advancements have been made in the field of large scale simulations of finite volume 'model universes'. In these cosmological scale simulations, which begin from the initial conditions of the cosmic microwave background, galaxies form and evolve within a dynamic large scale environment. Cosmological simulations thereby produce a diverse population of galaxies, with disky and spheroidal morphologies, star forming and quenched populations, and complex star formation and merger histories (Springel 2005; Vogelsberger et al. 2014a,b; Schaye et al. 2015; Nelson et al. 2017; Springel et al. 2017).

1.4.1 AGN-merger connection in cosmological simulations

Cosmological simulations provide a useful tool to address the challenges outlined above in studying the AGN-merger connection, producing a large sample of galaxy

mergers with a varied distribution of merger and galaxy properties such as mass ratio, orbital geometries, gas fractions, and environment. The advantages of a cosmological merger population are twofold. First, one is able to study how merger induced effects vary over a large parameter space. Second, the representative distributions obtained from cosmological simulations can provide insight on the cumulative impact of mergers on AGN activity. For example, minor mergers will contribute more, statistically, to a complete merger sample selected from a cosmological simulation. In addition, simulations in general allow for the merger and non-merger status of galaxies to be determined with certainty and avoid contamination.

However, cosmological simulations do also have some disadvantages compared with the binary merger simulation suites. Most notably, cosmological simulations sacrifice spatial and temporal resolution for the sake of a large simulation volume. Furthermore, binary merger simulations are better able to isolate the effects of different properties by running the exact same merger simulation varying only the parameter of interest. In comparison, each galaxy merger from a cosmological simulation is unique.

Cosmological simulations provide a very important component to the theoretical predictions for galaxy evolution: cosmological context. For example, the advantage of cosmological context is demonstrated in Hani et al. (2020), who investigate star formation rate enhancements in a sample of post-mergers from the IllustrisTNG cosmological simulation, and find that while major mergers drive stronger starbursts, the stellar mass contribution of the more common minor mergers equal the contribution of major mergers.

In addition, cosmological simulations are useful to study how common the evolutionary scheme proposed by Hopkins et al. (2008) in Figure 1.7 may be. In fact, Quai et al. (2021) investigate the connection between quenching and post-mergers in IllustrisTNG and find that while post-mergers are slightly more likely to quench, overall they rarely quench in the hundreds of Myrs immediately after coalescence. Put another way, mergers speed up the quenching process in the TNG cosmological simulation, but merger events on their own are not a major pathway towards quenching. A similar result is found in the SIMBA cosmological simulation (Rodríguez Montero et al. 2019), where it is predicted mergers induce starbursts but are unrelated to quenching.

The connection between quasars and major mergers in cosmological simulations has been investigated by Steinborn et al. (2018), for the Magneticum Pathfinder

simulation, and McAlpine et al. (2020), in the EAGLE simulation. Both studies conclude that the majority of high luminosity AGN are not connected to merger events, demonstrating that secular processes may be capable of significantly feeding SMBHs in cosmological simulations.

1.5 Thesis outline

The aim of the work presented in this thesis is to investigate the role of mergers in influencing AGN activity within a cosmological simulation. I am specifically investigating supermassive black hole accretion rates in post-merger galaxies. I aim to characterize how significantly supermassive black hole accretion rates are enhanced in the post-merger sample and understand how frequent or how rare accretion rate enhancements are in galaxy mergers. In Chapter 2, I summarize the details of the IllustrisTNG simulation, the simulation used in the majority of my research. In Chapter 2, I also summarize the algorithms used to identify galaxy mergers, find suitable non-merging galaxies for comparison, and outline the quantitative parameters used to measure the enhancement of supermassive black hole accretion rates. In Chapter 3, I present the results for IllustrisTNG. I demonstrate that for post-mergers in IllustrisTNG, on average, supermassive black hole accretion rates are enhanced, and I break down how the magnitude of the enhancement depends on galaxy and merger parameters, merger timescale, and the relationship with star formation rate enhancements. In Chapter 3, I also demonstrate the rarity of post-merger quasars, as well as the sub-dominant contribution to the overall AGN population in the simulation. In Chapter 4, I compare my results between the IllustrisTNG, Illustris, and EAGLE cosmological simulations, demonstrating that a statistically significant enhancement of supermassive black hole accretion rates is common between all three cosmological simulations, as well as demonstrating where the simulations produce different predictions. Overall, the goal of the work presented in this thesis is to investigate what the simulated AGN-merger connection looks like when considering the full spectrum of merger and galaxy properties and the additional context from a cosmological simulation.

Chapter 2

Identifying and Control Matching Galaxy Mergers from the IllustrisTNG Simulation

In the following chapter, I outline the methodology for the experiments presented in my thesis. For the majority of the research presented here, I focus on the IllustrisTNG simulation, which I summarize in detail in Section 2.1. For a summary of the Illustris and EAGLE simulations, I refer the reader to Section 4.1. In Section 2.2, I outline the methodology for identifying galaxy mergers from the TNG cosmological simulation. In Section 2.3, I outline the details of the control matching schemes and comparison samples used in my research and I define the quantitative parameter used to study SMBH accretion rate enhancements.

2.1 Summary of the IllustrisTNG simulation

In the research presented here, I use the IllustrisTNG galaxy formation simulation suite, hereafter TNG, which is a state-of-the-art cosmological magneto-hydrodynamic simulation (Nelson et al. 2017; Naiman et al. 2018; Marinacci et al. 2018; Pillepich et al. 2017a; Springel et al. 2017).

In TNG, the gravitational and hydrodynamic interactions are simulated using the AREPO code (Springel 2010). The gravitational interactions between matter are calculated using a Tree and Particle-Mesh, TreePM, algorithm. In general, in the TreePM method the short-range gravitational forces on a particle are directly

calculated between the particle and neighbouring individual or grouped particles, and the long-range forces are estimated using Fourier techniques applied to the long-range mass density field (Xu 1995; Springel 2005). For baryonic matter, AREPO solves the equations of hydrodynamics of on a moving unstructured mesh, generated using a Voronoi tessellation. The simulation volume is subdivided into cells such that the regions of space are associated to the cell of the nearest mesh-generating particle (Springel 2010). The Voronoi tessellation constructs a new mesh after each time-step of the simulation, the hydrodynamic equations are then solved over the newly generated mesh, and the velocity of the mesh-generating particle is updated according to the cell's flow (Springel 2010). Therefore, the moving unstructured mesh naturally adjusts the spatial resolution similarly to smoothed particle hydrodynamic techniques.

In addition to the hydrodynamics and gravity solvers, TNG has an extensive galaxy physics model that includes processes for the formation and evolution of galaxies. The physics models of galaxy formation simulations like TNG rely on coded prescriptions known as sub-grid models, to include unresolved processes such as stellar formation and feedback, black hole accretion and feedback, and more. The galaxy physics model of TNG builds upon the model of its predecessor, the Illustris simulation (Vogelsberger et al. 2014a,b; Genel et al. 2014; Sijacki et al. 2015), however TNG includes new and/or updated galactic scale stellar feedback, stellar population evolution and chemical enrichment, primordial and metal-line gas cooling and heating, and multi-mode black hole feedback(Pillepich et al. 2017b). Most relevant to the work presented here are the supermassive black hole formation, accretion, and feedback sub-grid models, which I will summarize following Weinberger et al. (2016).

Supermassive black holes are seeded with a mass of $M_{BH} = 8 \times 10^5\,\mathrm{h}^{-1}\mathrm{M}_\odot$ at the centre of halos that meet a threshold mass of $5 \times 10^{10}\,\mathrm{h}^{-1}\mathrm{M}_\odot$. The black holes can then grow via two channels, either accreting gas from the region surrounding the black hole or by merging with other black holes.

SMBH accretion is calculated using a Bondi-Hoyle-Lyttleton subgrid model,

$$\dot{M}_{Bondi} = \frac{4\pi G^2 M_{BH}^2 \rho}{c_s^3} \tag{2.1}$$

where G is the gravitational constant, M_{BH} is the black hole mass, and ρ and c_s are the density and sound speed sampled in a kernel-weighted sphere centred on the SMBH, labelled the accretion region. The SMBH accretion rate is capped by

the Eddington rate. The Eddington rate is a theoretical limit corresponding to an accretion rate that would produce an SMBH luminosity where the radiation pressure from the emission equalizes the gravitational collapse of material onto the SMBH. The formula for the Eddington rate is as follows,

$$\dot{M}_{Edd} = \frac{4\pi G M_{BH} m_p}{\epsilon_r \sigma_T c} \tag{2.2}$$

where m_p is the proton mass, ϵ_r is the radiative accretion efficiency, σ_T is the Thompson cross-section, and c is the vacuum speed of light.

SMBHs are merged when the black holes are within the accretion regions of one-another. Furthermore, in order to prevent the wandering of SMBHs away from the halo centre, SMBHs are fixed to the local gravitational potential minima, which has the added effect of promptly merging SMBHs when their host galaxies merge.

TNG uses a dual feedback mode model, where SMBHs will use different feedback prescriptions depending on the SMBH accretion rate. At high accretion rates the SMBH will use the radiative mode feedback model, and at low accretion rates it will use the kinetic mode feedback model. The classification of high vs. low accretion is made by calculating the ratio of the Bondi accretion rate to the Eddington accretion rate, where a high accretion rate is defined as $\dot{M}_{Bondi} \geq \chi \dot{M}_{Edd}$ and χ is defined as,

$$\chi = min\left[\chi_0 \left(\frac{M_{BH}}{10^8 M_\odot}\right)^\beta, 0.1\right]. \tag{2.3}$$

The maximum $\chi = 0.1$ follows observational constraints set by X-ray binaries Dunn et al. (2010), whereas the parameters χ_0 and β are simulation parameters which were tuned to 0.002 and 2 respectively in order to well replicate observations such as SMBH scaling relations and the cosmic star formation rate history. Equation 2.3 therefore preferentially promotes low accretion states in high SMBH mass systems, where $\chi(M_{BH}) = 0.1$ at $\sim 10^{8.85} M_\odot$.

For SMBHs with high accretion rates, the simulation uses a radiative feedback prescription, where a fraction of the accreted mass energy is injected as thermal energy into the region surrounding the black hole. At low accretion rates, once again a fraction of the accreted mass energy is injected into the surrounding BH region, however the energy injected is in the form of kinetic energy in randomized directions away from the black hole.

In the work presented here, we use the TNG100-1 simulation run, the intermediate

volume and resolution run of the fiducial IllustrisTNG galaxy formation model, which has a $(110.7\,\mathrm{Mpc})^3$ volume, a baryonic resolution of $1.4 \times 10^6\,\mathrm{M}_\odot$, and a dark matter resolution of $7.5 \times 10^6\,\mathrm{M}_\odot$ (Pillepich et al. 2017b; Weinberger et al. 2016).

2.2 Identifying galaxies and mergers in IllustrisTNG

In the work presented here, I utilize a sample of post-merger galaxies from the TNG simulation that was inherited from previous work done by Dr. Maan Hani, published in Hani et al. (2020). The merger mass ratio determination was further improved upon by Dr. Salvatore Quai. For completeness, I will describe the details of the merger selection processes here, with credit to Drs. Hani and Quai as well as Dr. Dave Patton who provided calculations of several parameters for characterizing galactic environment.

Before selecting for galaxy mergers in the TNG simulation, a number of selection criteria are first applied to the total galaxy sample selected from TNG, from which post-merger galaxies are identified.

First, galaxies at redshift>1 are excluded from the sample because the increased frequency of mergers and interactions exacerbate issues such as numerical stripping and subhalo switching (Rodriguez-Gomez et al. 2015) making robust merger identification more difficult. Numerical stripping occurs when the subhalo algorithm[1] has a difficult time differentiating the particles between subhalos, which often occurs when subhalos are in close spatial proximity. The result is that the mass of the subhalo is 'stripped', such that the mass reported in the subhalo catalogues are lower due to algorithmic error rather than true physical reasons. Similarly, subhalo switching occurs when the algorithm which reconstructs the history of a subhalo, i.e. links subhalos between snapshots[2] in the simulation, has difficulty identifying the correct progenitor or descendants subhalos. The switching results in a subhalo history where the object followed in time 'switches' to a different object. Numerical stripping and subhalo switching are particularly common in galaxy interactions where galaxies are in close proximity and there can be exchanges of simulation particles between subhalos.

To ensure the selected galaxies are well resolved, a minimum stellar mass criterion

[1] The subhalo algorithm identifies over densities of matter, and determines the constituent particles to assign to the identified object, i.e. subhalo.

[2] Snapshots refer to the sequence of outputs of data from the simulation that occur at periodic time intervals.

of at least $10^{10}\,M_{\odot}$, or $\sim$ 10000 particles, is applied. More specifically, the minimum stellar mass ensures that, for a minimum mass ratio of 1:10, the progenitors of the merging galaxy will have at least $\sim$ 1000 stellar particles, which is considered sufficiently well resolved.

In addition to redshift and stellar mass, an additional environmental constraint is applied to remove galaxies susceptible to numerical stripping due to close overlap with neighbouring subhalos. Following the procedure of Patton et al. (2020), each subhalo is assigned a calculated environmental parameter r_{sep},

$$r_{sep} = \frac{r}{R_{1/2}^{host} + R_{1/2}^{comp}} \tag{2.4}$$

where r is the 3D separation of the galaxies, and $R_{1/2}^{host}$ and $R_{1/2}^{comp}$ are the stellar half mass radii of the host and companion. Patton et al. (2020) demonstrated that TNG galaxies with $r_{sep} \lesssim 2$ had stripped stellar mass. Therefore, the TNG galaxy sample only includes galaxies with $r_{sep} > 2$.

Once appropriate candidate galaxies from TNG have been identified, galaxy mergers are identified using the merger-trees created by the SUBLINK algorithm (Rodriguez-Gomez et al. 2015). SUBLINK associates each subhalo in TNG with the progenitor and/or descendant subhalos. Galaxy mergers are identified by selecting nodes within the merger trees, where nodes occur when particles assigned into distinct subhalos at a given snapshot are subsequently assigned into the same subhalo in the following snapshots. To calculate the mass ratio of the merger, the following steps are applied, once again, as a precaution against numerical stripping and subhalo switching. First, the stellar mass ratio of the merger is calculated, using the stellar mass within twice the stellar half-mass radius, for the snapshots leading up to coalescence of the subhalos (up to a maximum of 10 snapshots). Next, the maximum and minimum mass ratios are excluded, which will remove extreme outliers due to subhalo switching or significant numerical stripping. Finally, the mass ratio and the mass ratio error is calculated using the average and standard deviation of the remaining mass ratio measurements. Note that for the work presented here, mergers are defined as a coalescence of subhalos with a stellar mass ratio within $0.1 < \mu \leq 1$, and more minor mergers, $\mu < 0.1$, are excluded from the post-merger sample.

In the work presented here I define post-merger galaxies as galaxy mergers that have coalesced in the previous snapshot, which corresponds to a merger event in the window of time between snapshots (within $\sim$ 160 Myrs). Selecting galaxies imme-

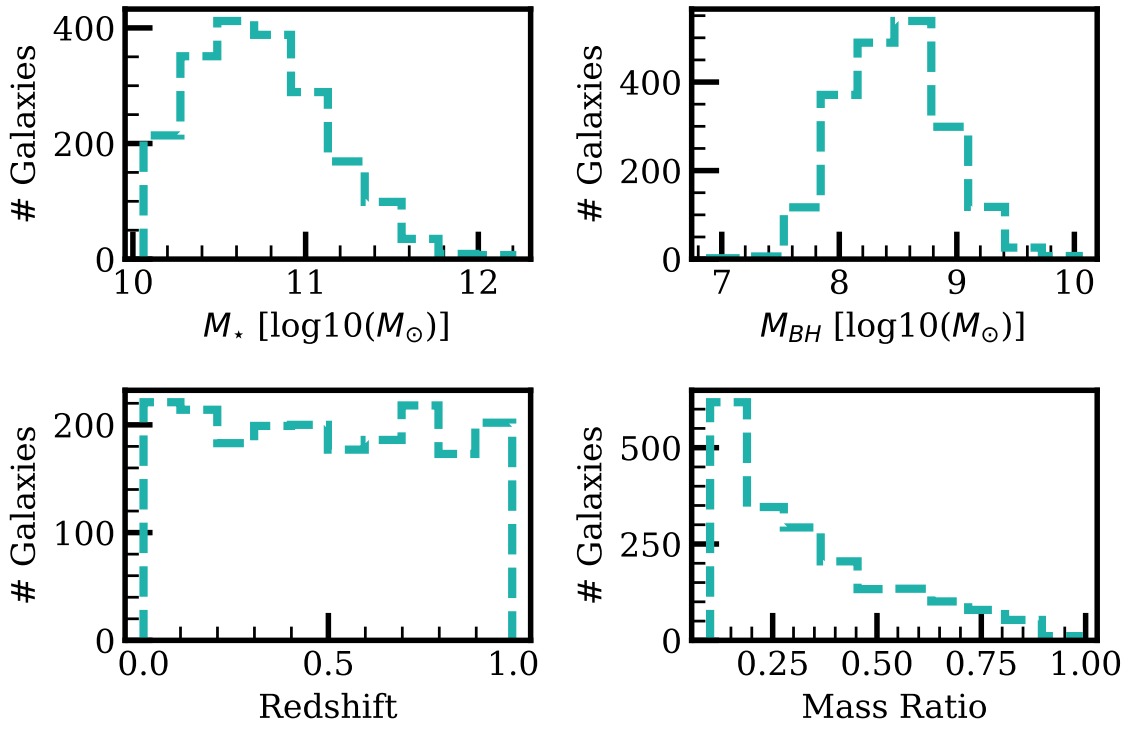

Figure 2.1: Distribution of the total post-merger sample in stellar mass, SMBH mass, redshift, and mass ratio.

diately after coalescence, and applying the galaxy selection criteria outlined above, yields a total sample of 1973 post-merger galaxies from TNG100-1. The stellar mass, SMBH mass, redshift and mass ratio distributions of the total post-merger sample are shown in the dashed teal line in Figure 2.1.

2.3 Post-mergers, non-mergers, and control matching algorithms

In Section 2.2, I have outlined the selection process for the total post-merger population from TNG100-1. However, ultimately my goal is to study the SMBH accretion rates of post-merger galaxies, specifically whether the SMBH accretion rates of the post-merger sample differs from comparative galaxies of similar characteristics. To this end, in addition to the post-mergers, I define a sample of non-mergers whose properties are representative of the post-mergers. I construct a non-merger sample in order to generate a comparative population that has the same underlying distribution as the post-merger sample, and in order to contextualize how the underlying stochasticity of SMBH accretion rates affect the measurement of accretion rate enhancements.

The representative non-merger sample is constructed as follows. For each of the 1973 post-mergers, I identify one non-merging galaxy that is selected to be the single best match in redshift, stellar mass, gas mass, environment, and feedback mode (see Section 2.3.1 for details on the necessity of feedback mode matching) that has not undergone a merger of mass ratio $\mu > 0.1$ within the last two Gyrs. The environment is quantified using two parameters from Patton et al. (2020): r_1 and N_2. r_1 is the 3D distance to the nearest neighbour with a mass above $10^9\,M_\odot$ within two Mpc of the galaxy centre. N_2 is the number of neighbours within two Mpc of the galaxy centre. The single best match is selected as an exact match in redshift and feedback mode, and the best simultaneous match of stellar mass, gas mass, r_1 and N_2 following the statistical weighting scheme of Patton et al. (2016). I therefore begin with a sample of 1973 post-mergers and 1973 non-mergers.

In order to quantify the difference between a given physical property (e.g. SMBH accretion rate) of an individual galaxy and the typical expected value for galaxies of similar properties, I use a control matching algorithm to identify a sample of comparative controls for each individual galaxy in the post-merger and non-merger

sample. The pool of possible control galaxies consists of all galaxies from TNG meeting the criteria outlined in Section 2.2, that have not undergone a merger of mass ratio $\mu > 0.1$ within the last two Gyrs. Note that when control matching the non-mergers, I exclude galaxies that have already been assigned into the non-merger sample from the control pool, such that no galaxy can be control matched to itself.

I begin by down-selecting the pool of potential control galaxies by imposing two cuts (which are effectively broad matching constraints). First, I require that the controls for a given galaxy are drawn from the same simulation snapshot, which corresponds to matching in redshift. Second, I require that the controls for a given galaxy are in the same instantaneous feedback mode as the post-merger (or non-merger), using the feedback mode classification outlined in Section 2.1. The necessity for feedback mode matching will be further discussed in Section 2.3.1.

In addition to snapshot (redshift) and feedback mode, the control galaxies for each post-merger and non-merger are matched on several further properties. First, the control sample is limited to galaxies whose stellar mass is matched to within ± 0.05 dex. The environment is again quantified using r_1 and N_2. The matched control sample is limited to galaxies within $\pm 10\%$ of r_1 and N_2. In addition, I also limit the control sample to galaxies with a gas mass within ± 0.1 dex. I allow all of the error tolerances to grow, 0.01 dex in stellar mass, 0.1 dex in gas mass, and 10% in r_1 and N_2, up to four times until at least five matched control galaxies are found. If fewer than five control galaxies are found, then the post-merger is excluded from the sample. On average, galaxies have to grow their error tolerances twice to meet the required number of controls, and 410 post-merger galaxies (and 451 non-merger galaxies) did not meet the control requirements within permitted error tolerances after the maximum number of grows and were hence rejected from our sample. Therefore, the final matched sample consists of 1563 matched post-merger galaxies and 1522 non-merger galaxies, with an average of 10 matched controls each. Table 2.1 outlines the matching tolerances for the fiducial matching model used in the work presented here.

The properties of the final post-merger and non-merger samples are shown in the solid teal and dashed yellow lines in Figure 2.2, where the total post-merger distribution is once again shown in the dotted teal line. In general, Figure 2.2 demonstrates the comparability between the total post-merger population and matched post-merger and non-merger samples. However, Figure 2.2 also highlights two significant biases in the control matching methodology. First, the control matching algorithm more

	$\Delta M_\star$ [dex]	ΔM_{gas} [dex]	Δr_1 [%]	N_2 [%]	redshift	feedback
base	0.05	0.1	10	10	exact	exact
grow	0.01	0.1	10	10	0	0

Table 2.1: The fiducial matching criteria for TNG post-mergers and non-mergers. The base error tolerance is shown in the top row, and the increase in error tolerance (up to four times) is shown in the second row.

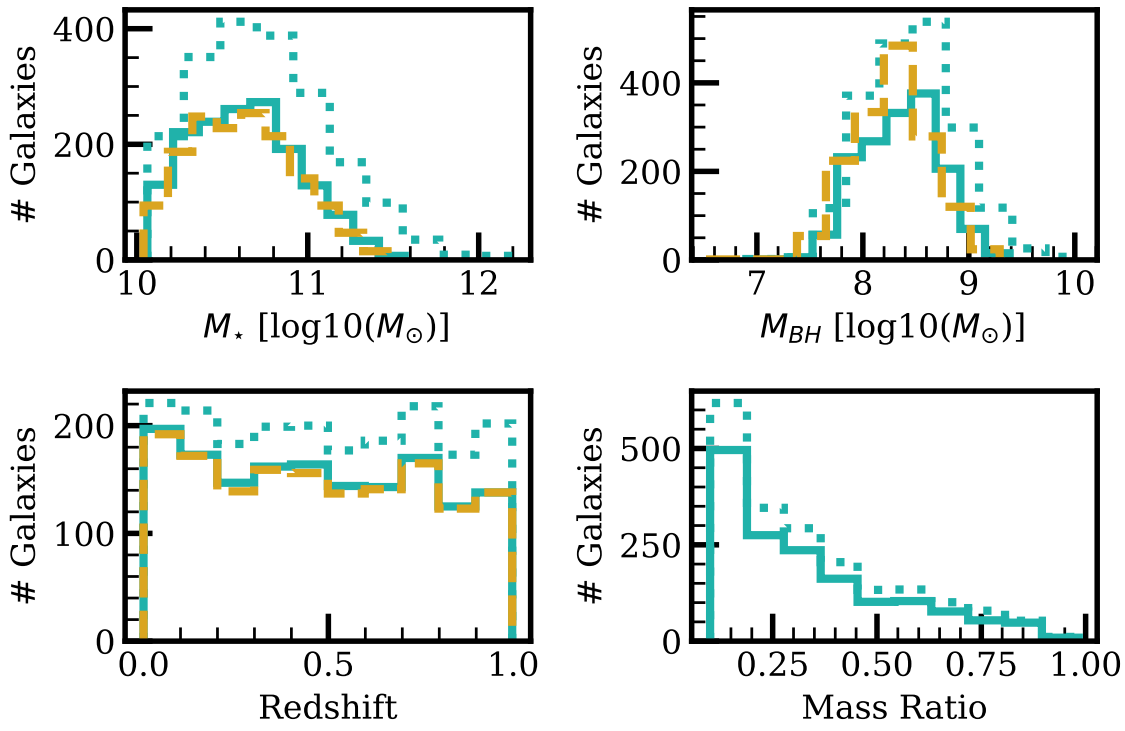

Figure 2.2: Distribution of the total post-merger (dotted teal), matched post-merger (solid teal), and matched non-merger (dashed yellow) samples in stellar mass, SMBH mass, redshift, and mass ratio.

commonly matches post-mergers with lower stellar masses. Such a selection bias is expected in the range beyond $\sim 10^{11} M_{\odot}$, since there are fewer control galaxies at higher masses and therefore the algorithm will more commonly fail to find 5 or more suitable controls. In fact, investigation of the ~ 400 unmatched post-mergers reveals the majority are of stellar mass in excess of $10^{11} M_{\odot}$. However, there is a persistent low stellar mass bias when comparing post-mergers of similar abundance in the total post-merger sample (for example, post-mergers within the dotted histogram around bins of $\sim 10^{10} M_{\odot}$ and $\sim 10^{11} M_{\odot}$ in stellar mass). Investigation into the stellar mass bias determined that the inefficiency of matching higher stellar mass post-mergers is primarily driven by the introduction of gas mass matching. More specifically, the bias is due to the broad tail of lower gas masses that occupy high stellar mass galaxies. Matching in gas mass therefore selects fewer control options within the gas mass error tolerance, compared with the control options for low stellar mass and high gas mass galaxies, and there is an increased chance that the higher stellar mass galaxy will be unmatched. The second bias highlighted in Figure 2.2 concerns the SMBH mass of the post-merger and non-merger galaxies. Figure 2.2 suggests that post-mergers may be biased towards higher SMBH masses. The concerns and effects of the SMBH mass offset is explored in detail in Section 4.4.

Figure 2.3 shows the distribution of stellar mass, gas mass, r_1, and N_2 for the post-merger galaxies, shown in the teal line, and the matched control galaxies, shown in dashed pink line. In Figure 2.3, the distributions trace one another closely, demonstrating the success of the control matching methodology in identifying galaxies with similar properties to the post-merger sample. Although not shown in Figure 2.3, I note that the non-merger sample and its controls exhibit similarly closely matched properties.

Once the control matching procedure is complete, I calculate the relative SMBH accretion rate enhancement, $\Delta \dot{M}_{BH}$, for each post-merger and non-merger galaxy as

$$\Delta \dot{M}_{BH} = log_{10}(\dot{M}_{BH}) - median[log_{10}(\dot{M}_{BHControls})]. \tag{2.5}$$

Therefore, $\Delta \dot{M}_{BH}$ quantifies the relative enhancement or suppression of each galaxy's SMBH accretion rate relative to the 'typical' accretion rate for a galaxy of the same properties.

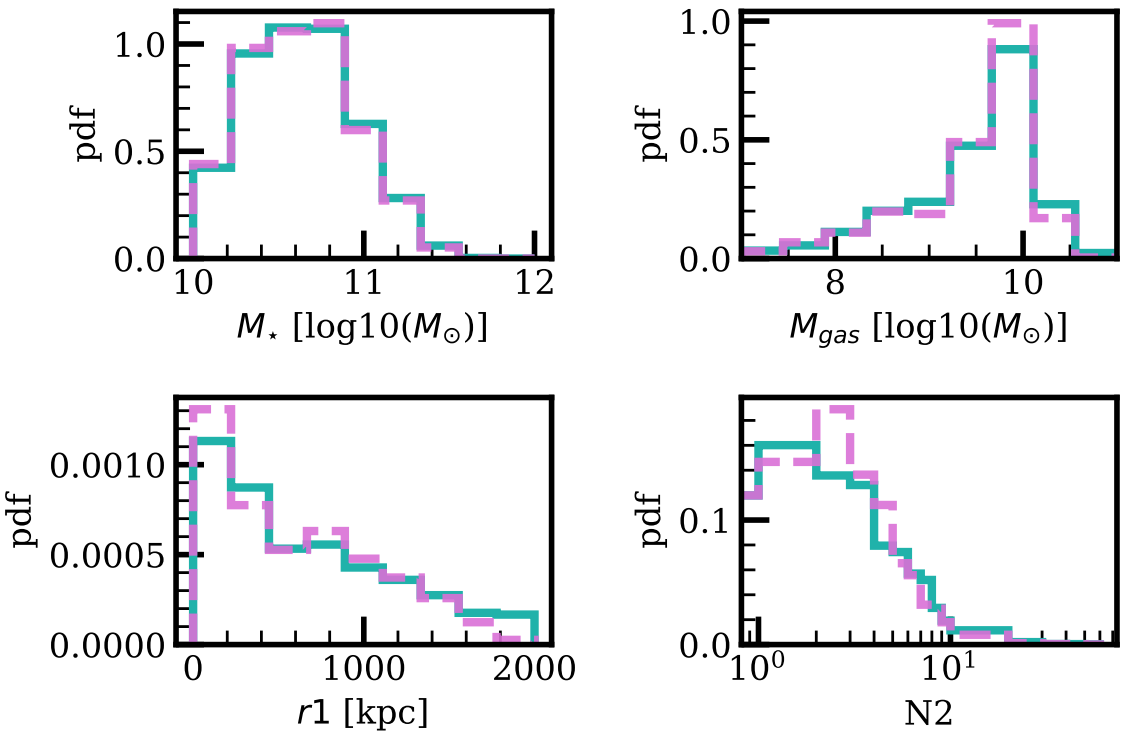

Figure 2.3: Distribution of the parameters matched in the control matching algorithm: stellar mass, gas mass, distance to nearest neighbour within two Mpc, and number of neighbours within two Mpc. Post-mergers are represented with the teal line, and the controls are represented with the dashed pink line.

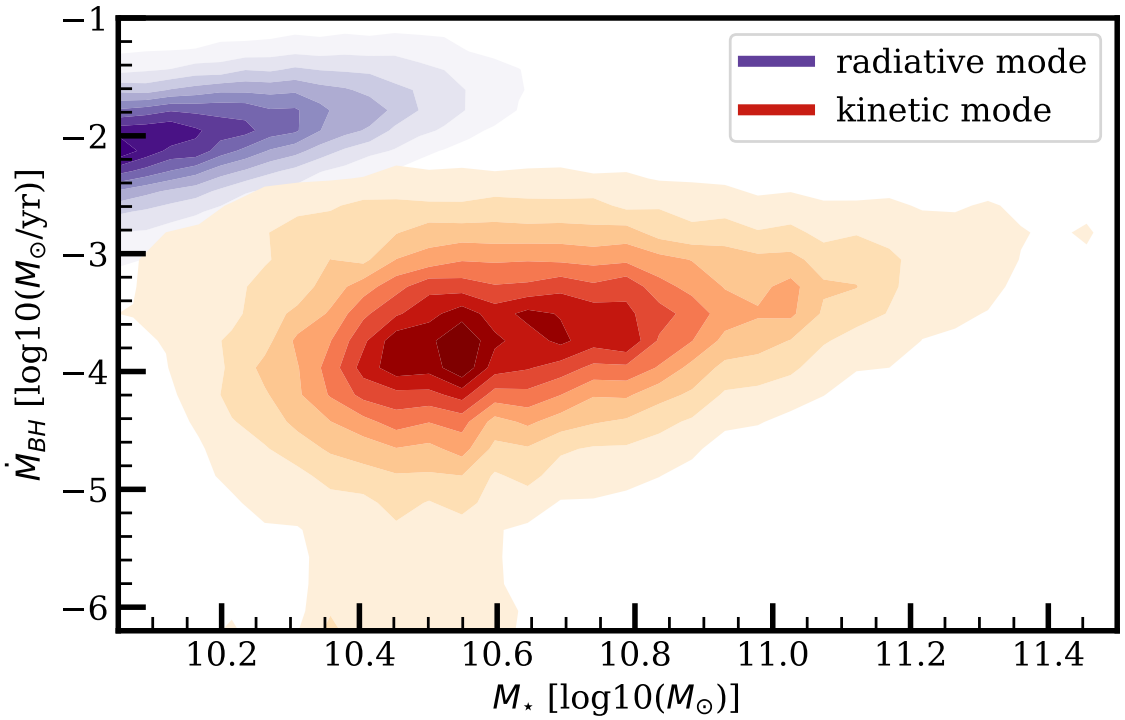

Figure 2.4: Density distribution of black hole accretion rates as a function of stellar mass for the total sample of galaxies from TNG 100-1. The dark blue contours represent the sample in radiative mode feedback and the orange contours represent the sample in kinetic mode feedback.

2.3.1 Control matching tests: the necessity of feedback mode matching in TNG

The fiducial matching scheme adopted for the work presented in this thesis diverges from the matching criteria used in previous works which investigate mergers in TNG by Patton et al. (2020), Hani et al. (2020), and Quai et al. (2021). In particular, the fiducial model introduces a unique matching criterion: AGN feedback mode matching.

Feedback mode matching is introduced due to the rapid transition from high to low accretion states that occurs in TNG when galaxies undergo kinetic AGN feedback. In particular, Figure 2.4 demonstrates the strong bimodal distribution of SMBH accretion rates (shown on the y-axis) in the TNG galaxy sample, where galaxies in radiative feedback mode are shown in blue and galaxies in kinetic feedback mode are shown in red, and the galaxy stellar mass is shown on the x-axis. Figure 2.4 demonstrates that the SMBH accretion rate is strongly sensitive to the prescription

for AGN feedback in TNG. Such an effect can present a challenge when studying the merger induced enhancement of SMBH accretion using $\Delta\dot{M}_{BH}$.

For example, consider a post-merger galaxy occupying the stellar mass range of $\sim 10^{10.5} M_{\odot}$ which has been undergoing radiative mode feedback. The control matches to such a post-merger galaxy would be preferentially selected from the population undergoing kinetic mode feedback where there are statistically more galaxies in this regime, and consequently the enhancement parameter $\Delta\dot{M}_{BH}$ would be very large. However, it may be inaccurate to interpret such a result as a merger driven enhancement in SMBH accretion rate, particularly if the merger event did not strongly influence the determination of the AGN feedback mode of the post-merger galaxy.

The incidence of post-mergers and controls matched across high and low accretion states is demonstrated in Figure 2.5. In Figure 2.5, all the panels show the SMBH accretion rate vs SMBH mass for matched TNG100-1 galaxies that have had a merger event within redshift $0 < z < 1$, shown as light blue (radiative mode galaxies) or light red (kinetic mode galaxies) points. For each successfully matched galaxy, the median SMBH mass and accretion rate of the identified controls is plotted as a dark blue/red point. The left hand panels use the control matching criteria of Section 2.3 but excluding feedback type, whereas the right hand panels show the full fiducial matching scheme with feedback type matching. When no feedback type matching is applied (left side panels), a significant number of controls are selected which occupy accretion rates offset by ~ 2 dex from the average accretion rate of the post-mergers. In comparison, for the matching scheme including feedback mode, we see that there is no longer a significant number of controls that have median accretion rates significantly offset from the post-merger population. I therefore include feedback type in the control matching criteria for all TNG experiments unless specifically stated otherwise.

The enforcement of an AGN feedback mode matching criteria results in two notable constraints to the work presented in this thesis. Firstly, the feedback matching criteria limits the scope of the work presented here to merger driven enhancements within the high and low accretion states, but not between accretion states. Therefore, merger induced enhancements which may result in a transition from low to high accretion states will be either discarded from the post-merger sample (if suitable controls cannot be found) or the enhancement strength will be suppressed in the calculation of $\Delta\dot{M}_{BH}$ (if controls are selected from within the same feedback type). Furthermore, such a limitation will preferentially affect higher mass post-mergers as they are predominantly in the low accretion state and kinetic feedback mode, and therefore able to

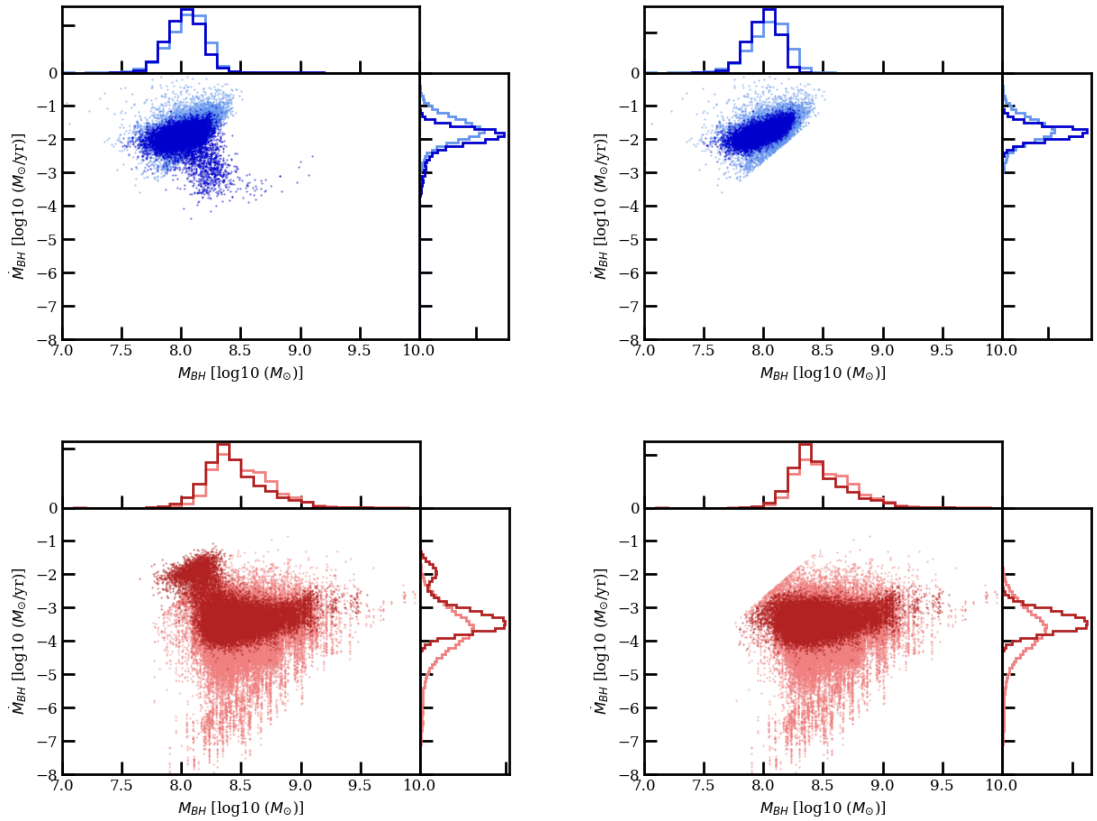

Figure 2.5: The distribution of SMBH mass and accretion rate for all TNG100-1 galaxies within redshift $0 < z < 1$ (light blue/red) and the median SMBH mass and accretion rate of matched controls (dark blue/red). The population in radiative mode feedback is shown in blue and kinetic mode feedback shown in red. The left hand plots show the comparison of galaxies and controls when AGN feedback mode matching is not included, and the right hand plots show the comparison when AGN feedback mode matching is included.

transition to the high accretion state due to a merger driven accretion enhancement.

2.4 Chapter summary

To summarize, in the research presented here I utilize a sample of post-merger galaxies identified from the IllustrisTNG cosmological galaxy formation simulation, specifically the TNG100-1 run of the TNG simulation suite. Post-mergers are identified using merger-trees, whereby the post-merger sample consists of galaxies that have coalesced within the last $\sim$ 160 Myrs. For each post-merger from TNG100-1, I identify control

galaxies that have not undergone a merger event with the past 2 Gyrs that are matched to post-mergers on stellar mass, gas mass, environment, redshift, and AGN feedback mode. I then calculate the relative enhancement or suppression of the SMBH accretion rate, $\Delta\dot{M}_{BH}$, defined in Eq. 2.5. For direct comparison, I also select a representative population of non-mergers that match the characteristics of the post-merger sample, for which I also calculate $\Delta\dot{M}_{BH}$. The final sample of matched post-merger galaxies studied in the following chapter consists of 1563 galaxies, with 1522 non-merger comparisons.

Chapter 3

Supermassive Black Hole Accretion Rate Enhancements in IllustrisTNG Post-Merger Galaxies

In the following chapter, I study in detail the enhancement of SMBH accretion rate in TNG post-mergers. Applying the methodology of the previous section, I investigate the distribution of SMBH accretion rate enhancements in the post-merger sample in Section 3.1. In Sections 3.1.1 and 3.1.2, I break down the SMBH accretion rate enhancements in terms of host galaxy properties and look at the timescale for a population averaged signal of enhancement. In Section 3.2, I look at the connection between SMBH accretion and star formation rate enhancements, as a population average (Section 3.2.1) and on a galaxy by galaxy basis (Section 3.2.2). Finally, in Section 3.3, I investigate the incidence of high accretion rate events in post-mergers (Section 3.3.1) and the contribution of mergers to the overall AGN population (Section 3.3.2).

3.1 SMBH accretion rate enhancements in the IllustrisTNG post-mergers

Recall from Section 2.3 that for every galaxy in the post-merger and non-merger samples, I calculate the relative SMBH accretion rate enhancement or suppression $\Delta\dot{M}_{BH}$. The first result of my research concerns the distribution of $\Delta\dot{M}_{BH}$ shown in Figure 3.1. The distribution of the post-merger sample is shown in the teal line,

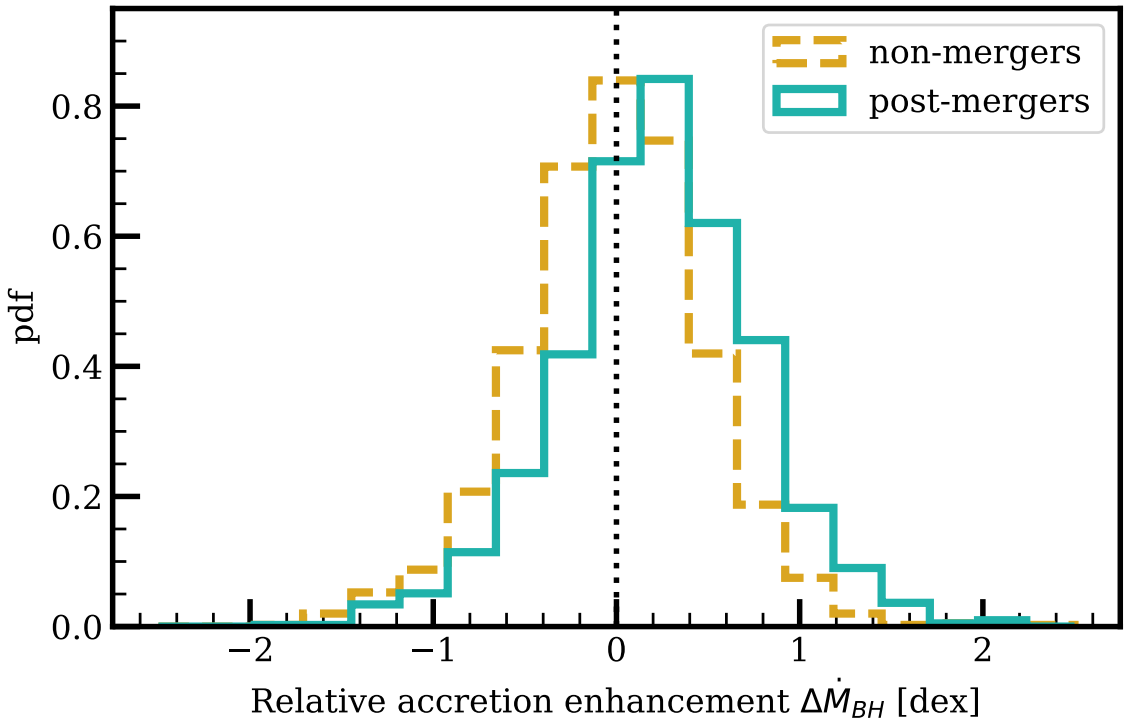

Figure 3.1: Histogram of accretion rate enhancements for the post-merger population and non-merger population. Post-mergers are represented with the teal line, and non-mergers are represented with the dashed yellow line. The median enhancement of the post-merger sample is 0.23 dex.

and the non-merger sample is shown in the yellow dashed line. The non-merger population peaks at 0 dex, consistent with no enhancement, as expected from its construction. Nonetheless, the non-merger distribution provides a useful reference to characterize the 'natural' stochasticity of SMBH accretion rates. In fact, both populations show a similar distribution of $\Delta\dot{M}_{BH}$, ranging from 100 times enhanced to 100 times suppressed accretion rates relative to controls, demonstrating the variability on a galaxy by galaxy basis. In contrast to the non-mergers, the post-merger sample peaks at a positive accretion rate enhancement, with a median enhancement of 0.23 dex, corresponding to an enhancement of $\sim 70\%$. Figure 3.1 therefore demonstrates a key result of my research, that mergers in TNG, on average, have an elevated accretion rate in the post-merger phase.

3.1.1 SMBH accretion rate enhancements and host galaxy properties

Figure 3.1 also demonstrates that not all post-mergers have accretion rate enhancements. In particular, I wish to test which galaxy parameters, if any, are most important in producing SMBH accretion rate enhancements and if any parameters correlate with the strength of the enhancements.

Figure 3.2 shows the SMBH accretion rate enhancement of the post-merger and non-merger samples as a function of redshift. The full distribution of the post-merger sample is shown in the background density plot, and the foreground points are the median accretion enhancement for the post-merger sample (teal circles) and non-merger sample (yellow squares) within equally spaced bins of redshift. The errorbars represent the standard error on the median within each bin. The median accretion rate enhancement of the post-merger sample is consistently above 0 across the redshift range. I present both the median enhancement points and the background distribution to emphasize that while there is a bias for positive median $\Delta\dot{M}_{BH}$ in post-mergers, not all post-mergers show accretion rate enhancements. Overall, neither sample (post-mergers nor non-mergers) show any significant dependence on redshift, indicating that the merger process elevates accretion rates out to at least $z = 1$ (the limit of our sample selection).

I find a similarly consistent result looking at the dependence of SMBH accretion rate enhancements on stellar mass, shown in Figure 3.3. As expected, the non-merger sample has accretion rate enhancements consistent with zero at all stellar masses. In

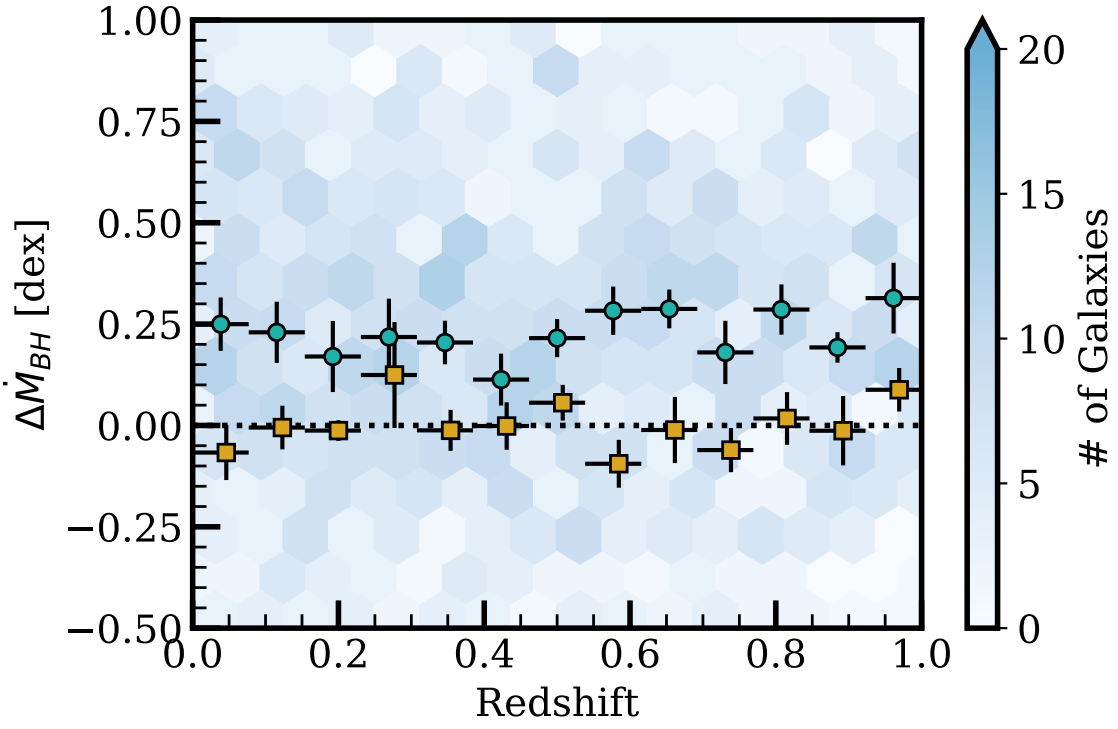

Figure 3.2: Accretion rate enhancements of post-merger galaxies for different redshifts. The background density plot shows the distribution of $\Delta\dot{M}_{BH}$ for the post-merger sample, and the foreground points represent the median value at that redshift. The teal circles are the median post-merger $\Delta\dot{M}_{BH}$ and the yellow squares are the median non-merger $\Delta\dot{M}_{BH}$. The error on the x-axis represents the bin width for each data point, and the error on the y-axis is the standard error on the median for that redshift bin.

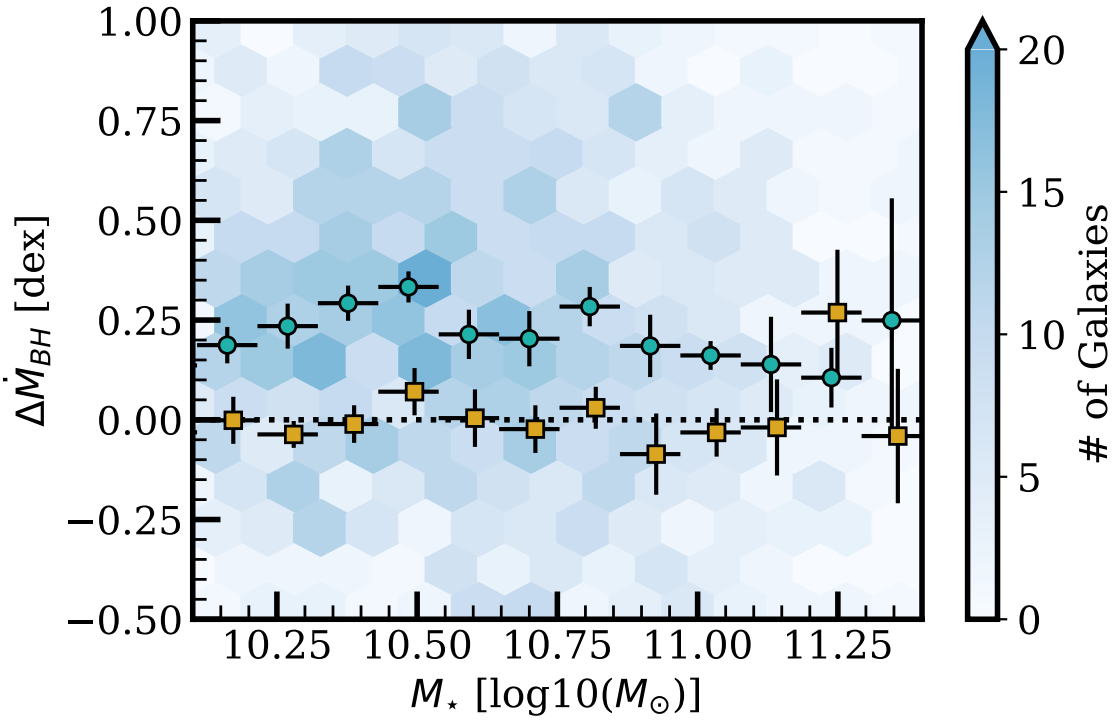

Figure 3.3: Accretion rate enhancements of post-merger galaxies for different stellar masses. The background density plot shows the distribution of $\Delta\dot{M}_{BH}$ for the post-merger sample, and the foreground points represent the median value at that stellar mass. The teal circles are the median post-merger $\Delta\dot{M}_{BH}$ and the yellow squares are the median non-merger $\Delta\dot{M}_{BH}$. The error on the x-axis represents the bin width for each data point, and the error on the y-axis is the standard error on the median for that stellar mass bin.

contrast, for the post-mergers, I find that the median accretion rate enhancement is consistently above zero for all of the stellar mass domain. I therefore find that the SMBH accretion rates are consistently enhanced, on average, at all stellar masses within our control matched sample. However, I note that the control matched sample is incomplete in the higher stellar mass regime exceeding $\sim 10^{11} M_{\odot}$ (recall Section 2.3).

Figure 3.4 shows the accretion rate enhancements as a function of the gas mass (top panel) and gas fraction (bottom panel) of the post-merger or non-merger samples. In the top panel, I find that for a gas mass less than $\sim 10^{9} M_{\odot}$, the median enhancements of the post-merger sample are not significantly distinct from the non-merger sample, with the exception of the two lowest gas mass points at $\sim 10^{8.1-8.4} M_{\odot}$. However in the regime of $> 10^{9} \mathrm{M}_{\odot}$, post-mergers consistently show enhancements in SMBH accretion rate, suggesting that post-mergers of a lower gas mass are less likely to have enhanced accretion rates. In addition, at gas masses above $10^{9} \mathrm{M}_{\odot}$, non-merger galaxies do not show enhanced accretion rates, demonstrating that the presence of a large amount of gas does not guarantee higher than average accretion rates.

I find a qualitatively consistent result looking at the gas fraction, shown in the bottom panel of Figure 3.4. Post-mergers with a lower gas fraction have low to no relative accretion enhancements. Once again, there is some evidence for an exception to this trend at the lowest gas fraction. However, I caution that the poor statistics at lower gas mass and gas fraction make the median data point more susceptible to the variability of $\Delta \dot{M}_{BH}$ on a galaxy by galaxy basis. Therefore, Figure 3.4 suggests that the presence of a significant amount of gas is an essential, but insufficient criterion to produce accretion rate enhancements. Instead, it is essential that the merger generates a mechanism for driving an excess of gas towards the central SMBH whence it can accrete.

Finally, Figure 3.5 shows $\Delta \dot{M}_{BH}$ for post-merger galaxies of different merger mass ratios. I note that in this plot, I only include galaxies with a merger mass ratio error (defined in Chapter 2) of $\sigma_{\mu} \leq 0.1$, which excludes 130 galaxies from the sample of 1563 post-mergers. By visual inspection, I do not find a strong relationship between the strength of the accretion rate enhancement and the merger mass ratio. In fact, the majority of enhancements are consistent, within error, with the overall sample accretion rate enhancement of 0.23 dex. I further confirm weak correlation with a statistical Pearson correlation test, which yields a correlation coefficient of $\sim$0.1.

The lack of correlation between $\Delta \dot{M}_{BH}$ and mass ratio is somewhat contradictory

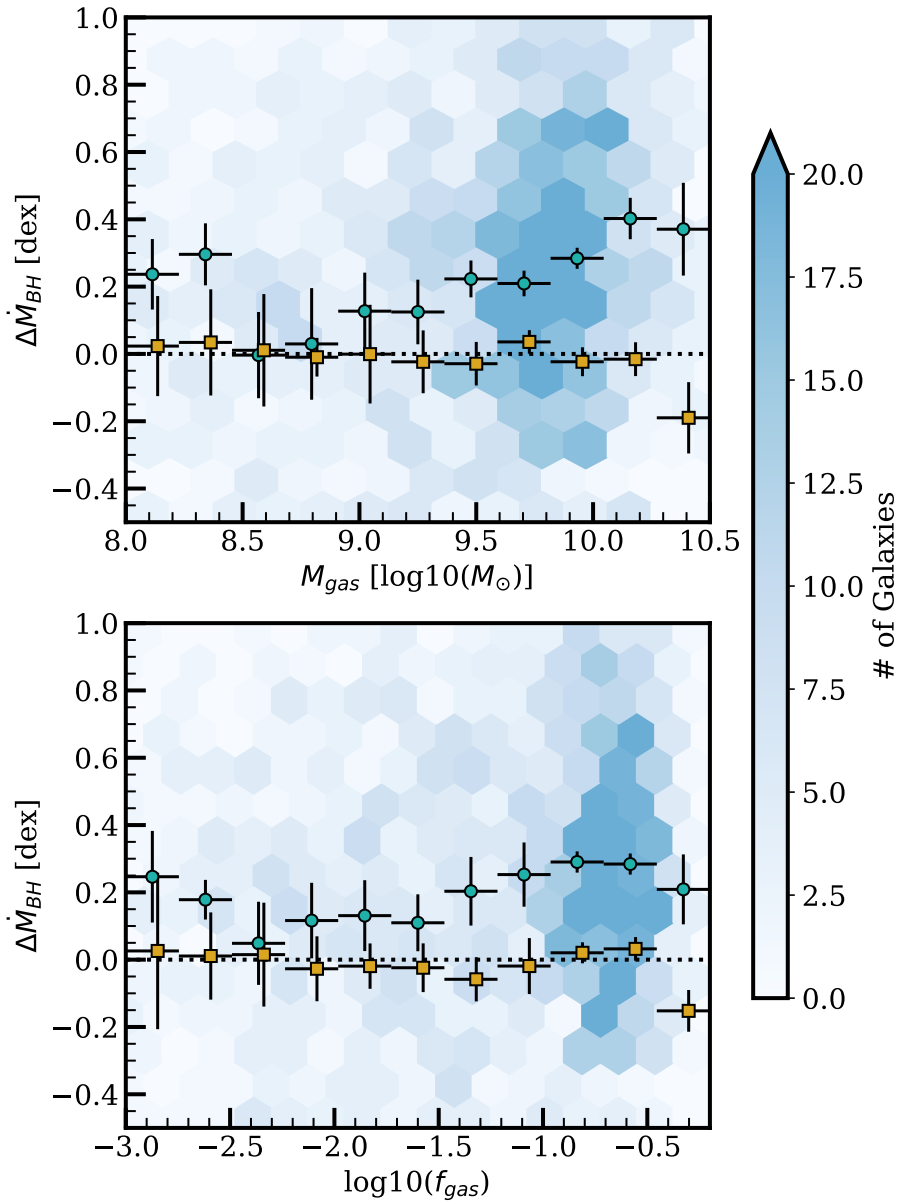

Figure 3.4: Accretion rate enhancements of post-merger galaxies for different M_{gas} (shown in top panel) and gas fractions (shown in bottom panel). The gas mass is the sum of all gas particles within twice the stellar half-mass radius. The gas fraction is the ratio of the gas mass to the baryon mass (gas mass + stellar mass) within twice the stellar half-mass radius. The background density plot shows the distribution of $\Delta\dot{M}_{BH}$ for the post-merger sample, and the foreground points represent the median value at that M_{gas} of gas fraction. The teal circles are the median post-merger $\Delta\dot{M}_{BH}$ and the yellow squares are the median non-merger $\Delta\dot{M}_{BH}$. The error on the x-axis represents the bin width for each data point, and the error on the y-axis is the standard error on the median for that M_{gas} or gas fraction bin.

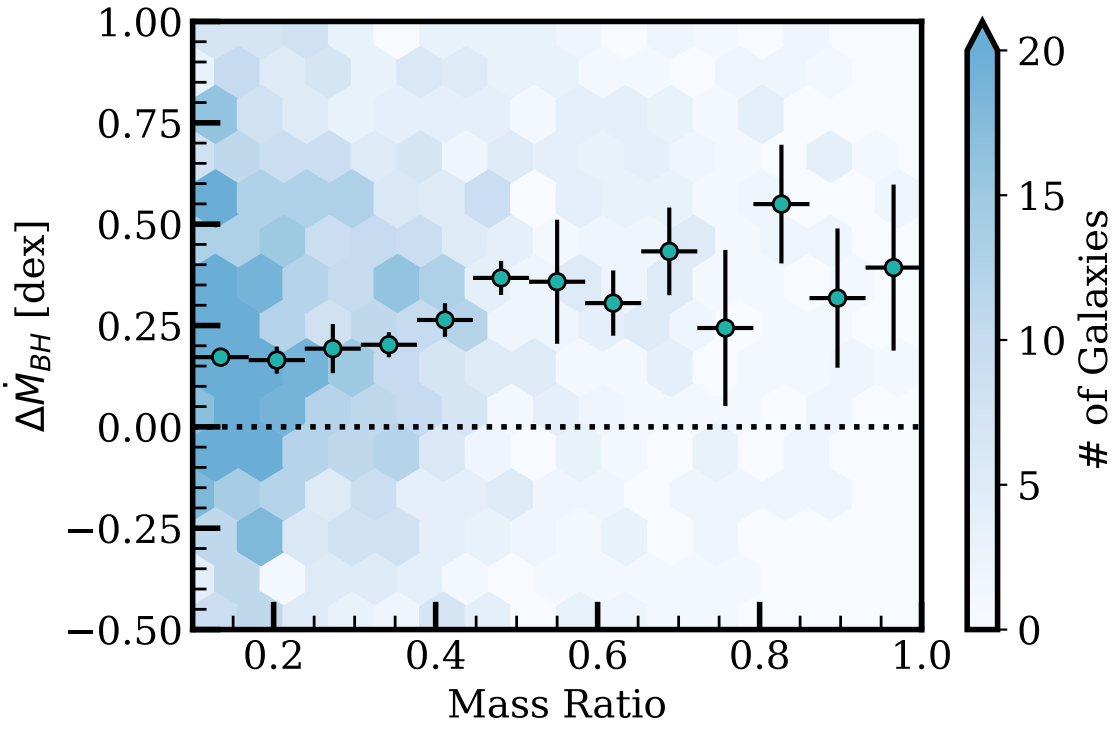

Figure 3.5: Accretion rate enhancements of post-merger galaxies for different merger mass ratio. The background density plot shows the distribution of $\Delta\dot{M}_{BH}$ for the post-merger sample, and the foreground points represent the median value at that mass ratio. The error on the x-axis represents the bin width for each data point, and the error on the y-axis is the standard error on the median for that mass ratio bin.

to previous simulation results. For example, Capelo et al. (2015) find mass ratio to be the most important factor influencing SMBH accretion rate in a suite of high resolution binary merger simulations. However, there are notable differences between the experiments of Capelo et al. (2015) and the work presented here. First of all, in the suite of ideal binary mergers used in Capelo et al. (2015), one is able to isolate the effect of varying the merger mass ratio while keeping other merger parameters such as the orbital geometry and gas fraction constant. In contrast, my results looks at a population averaged enhancement and is therefore subject to the variable conditions of every individual merger. In addition, Capelo et al. (2015) comment on the role of resolution in their result, and that some of the torques generated in the galaxy interaction require high resolution simulations in order to be resolved. Finally, my result should not be interpreted as mass ratio having zero role in regulating gas inflows. Instead, Figure 3.5 demonstrates that, once the full demographic of merger properties is sampled, mass ratio is not a dominant factor in predicting the strength of a SMBH accretion rate enhancement.

3.1.2 Timescale of population averaged SMBH accretion rate enhancements

I have thus far demonstrated that post-merger galaxies show, on average, enhanced accretion rates when compared to matched controls, a result which is in agreement with previous theoretical studies that demonstrate merger driven gas inflows (Di Matteo et al. 2005; Springel et al. 2005; Hopkins et al. 2008). However, the timescales of enhanced SMBH accretion rates are crucial to understanding the influence of the merger beyond the immediate post-merger phase, and the role of merger induced accretion rate enhancements on a galaxy's evolution.

To study the timescales of accretion rate enhancements, I perform an experiment following the procedure of Hani et al. (2020) (which studied the population averaged timescales of SFR enhancements). I calculate a $\Delta\dot{M}_{BH}$ for post-merger galaxies in the snapshots following coalescence. Specifically, I re-select control galaxies for my post-merger in the subsequent snapshots, following the same matching criteria as Chapter 2. Therefore, a galaxy at snapshot N will not be matched to the same controls in the subsequent snapshot N+1 if the controls fall out of the acceptable matching criteria and tolerances specified in Chapter 2.

Figure 3.6 shows the evolution of SMBH accretion rate enhancements in post-

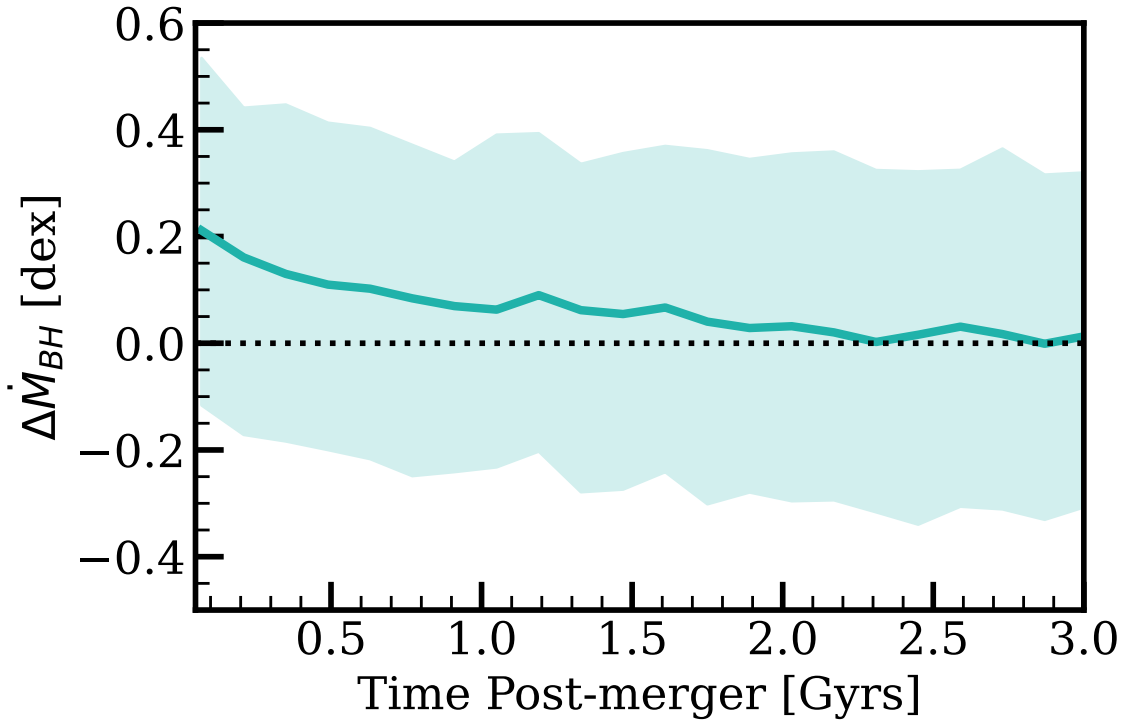

Figure 3.6: Running median of the accretion rate enhancement, shown in teal. The error of the shaded region represents the 25th and 75th percentiles associated with the median for the time post-merger bin.

mergers for increasing time post-merger. The median SMBH accretion rate enhancement is shown in the teal line, where the shaded region represents the 25th and 75th percentiles. I find that, on average, SMBH accretion rate enhancements persist for up to two Gyrs post-merger. A long-lived accretion rate enhancement may seem to be in contradiction with the short lived (tens-hundreds of Myrs) high accretion rate events observed in previous simulation studies (Di Matteo et al. 2005; Springel et al. 2005; Hopkins et al. 2008). However I emphasise that the relative enhancement variable $\Delta\dot{M}_{BH}$ is subtly different from an enhanced absolute accretion rate. Figure 3.6 demonstrates that post-mergers sustain a population-averaged enhanced accretion rate relative to matched controls, which does not necessarily correspond to a long lived high accretion rate event in an individual galaxy. A long-lived population average suggests that the dynamical disturbance that leads to higher than normal feeding of the SMBHs persists for up to ~ 2 Gyrs in TNG100-1.

In conclusion, I find that the overall population of post-mergers show a significant averaged signal of enhanced SMBH accretion rates. I find that the enhancement in

SMBH accretion rates is persistent across the entire redshift and stellar mass range of the post-merger sample, but is dependent on a presence of a sufficient amount of gas in the post-merger galaxy. I also find there is no significant trend between the relative strength of the SMBH accretion rate enhancement and the merger mass ratio, suggesting that major mergers, on their own, are not much more likely to produce stronger relative enhancements of SMBH accretion rates than the more common minor mergers.

3.2 Co-incidence of SMBH accretion rate and star formation rate enhancements

In Section 3.1 I focused exclusively on the SMBH accretion enhancements of post-merger galaxies. However, I am also interested in investigating the temporal correlation, or lack there-of, between star formation rate enhancements and SMBH accretion rate enhancements. Numerous observational studies have looked for a starburst-AGN connection, motivated by the possible causal connection associated with gas inflows. However, few find evidence for a connection between AGN and high star formation rate outside of the most luminous systems Rowan-Robinson (1995); Schweitzer et al. (2006); Lutz et al. (2010); Shao et al. (2010); Santini et al. (2012); Rosario et al. (2013). Some simulation studies explain the lack of connection as a consequence of the high variability in AGN activity on short timescales (Hickox et al. 2014; Volonteri et al. 2015b). In the context of my research, I am interested in whether there is evidence for a starburst-AGN connection in the cosmological post-merger sample, and whether host galaxy properties affect the correlation between star formation and SMBH accretion rate enhancements. To this end, I also calculate star formation rate enhancements for the post-merger sample,

$$\Delta SFR = log_{10}(SFR) - median[log_{10}(SFR_{Controls})], \tag{3.1}$$

where the star formation rate is the sum of star formation rates for all cells within twice the stellar half-mass radius. The calculation of ΔSFR uses the same matching criteria as outlined in Chapter 2, with one additional matching criterion following the procedure of Hani et al. (2020). As was demonstrated in Hani et al. (2020), it is important that galaxies be matched within a classification of star forming or passive

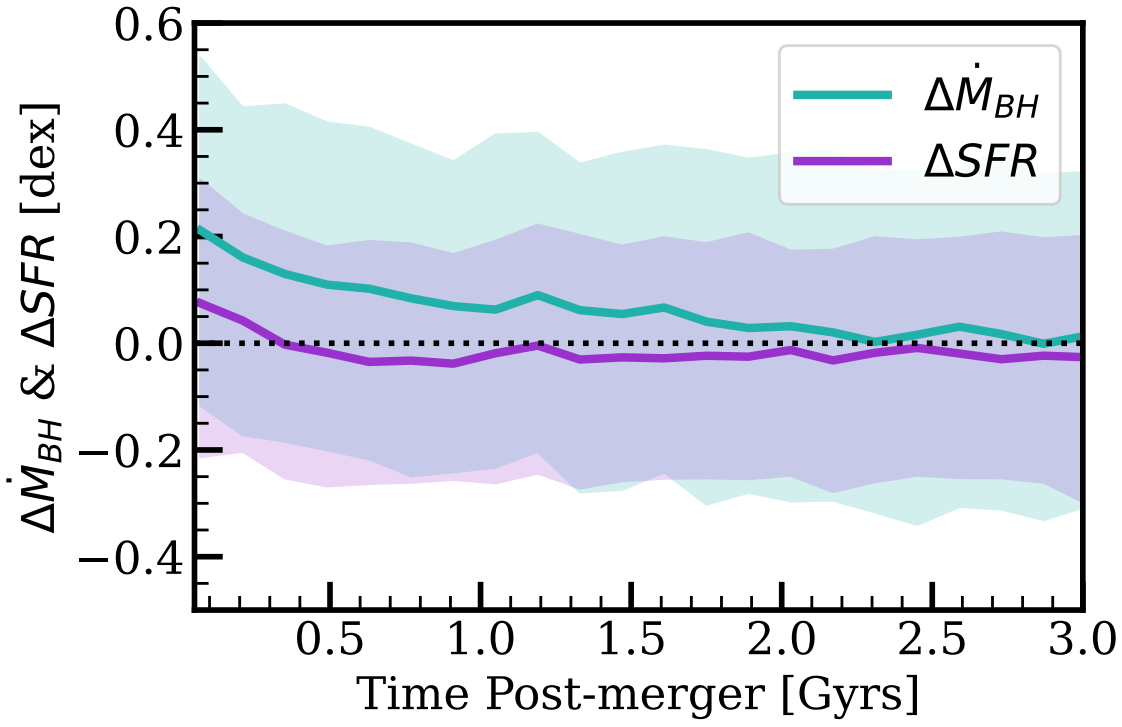

Figure 3.7: Running median of the accretion rate enhancement (teal) and star formation rate enhancement (purple) over the time post-merger. The error of the shaded region represents the 25th and 75th percentiles associated with the median for the time post-merger bin.

in order to avoid (spuriously) large/small values of ΔSFR, similar to the necessity for feedback type matching when calculating $\Delta\dot{M}_{BH}$. Passive galaxies are defined as galaxies which lie more than 2σ below the star forming main sequence, where I calculate the star forming main sequence by applying a linear fit to TNG100-1 galaxies with stellar mass between $10^{9-10.2}M_{\odot}$ and between redshift 0 to 1, and extrapolate the linear fit to higher stellar masses following the procedure of (Donnari et al. 2019). In this way, post-merger star-forming galaxies are matched to star-forming controls and passive post-mergers are matched to passive controls.

Figure 3.7 shows the evolution of star formation rate enhancements with increasing time post-merger in the purple line, where once again the shaded region represents the 25th and 75th percentiles. I recover the result of Hani et al. (2020), who find that, on average, post-merger galaxies demonstrated star formation rate enhancements, and that the enhancements persisted for up to ~ 500 Myrs after the merger, consistent with previous simulation studies (Di Matteo et al. 2008) and observational

estimates (Wild et al. 2010). I note that the magnitude of the enhancement in the work presented here is lower than the fiducial model of Hani et al. (2020), which may be attributed to the difference in matching schemes, most specifically the inclusion of gas mass matching which is demonstrated in Hani et al. (2020) to reduce the magnitude of SFR enhancements.

Comparing the averaged star formation and SMBH accretion rate enhancements, I find that SMBH accretion rate enhancements are significantly longer lived than star formation rate enhancements. In fact, the $\sim$ 1.5-2 Gyr long relative enhancement of SMBH accretion rate may be consistent with the results of Volonteri et al. (2015a), who find that the SMBH accretion rates of merger remnants can remain sufficiently high such that the luminosity of the AGN is dominant over the stellar luminosity up to 1.5 Gyrs after the merger.

3.2.1 SMBH accretion and star formation rate enhancements in radiative vs. kinetic mode feedback galaxies

In Figure 3.7, I present the population averaged behaviour of $\Delta\dot{M}_{BH}$ and ΔSFR in the post-merger sample. However, not all galaxies show positive SMBH accretion rate or SFR enhancements (recall Figure 3.1). In particular, the results of Section 3.1.1 suggest that gas poorer galaxies do not exhibit, on average, accretion rate enhancements. I therefore regenerate Figure 3.7, where I split the post-merger population based on the instantaneous feedback mode, which separates the post-mergers with high absolute accretion rates (radiative mode) from low absolute accretion rates (kinetic mode). In addition, the feedback mode separation also broadly separates lower mass, gas rich galaxies (radiative mode) from higher mass, gas poor galaxies (kinetic mode).

Figure 3.8 shows SMBH accretion rate enhancements and SFR enhancements, separated into the radiative mode, shown in blue, and kinetic mode, shown in red. In the top panel, which shows the SMBH accretion rate enhancements, I find that both populations show, on average, positive accretion rate enhancements within two Gyrs of coalescence. The radiative mode feedback population has a higher peak accretion rate enhancement right after coalescence of $\sim$ 0.3 dex compared with an enhancement of $\sim$0.2 dex in the kinetic mode feedback population. The lower median accretion rate enhancements in kinetic mode feedback galaxies is consistent with Section 3.1.1, demonstrating that accretion rate enhancements are lower in higher mass gas poor

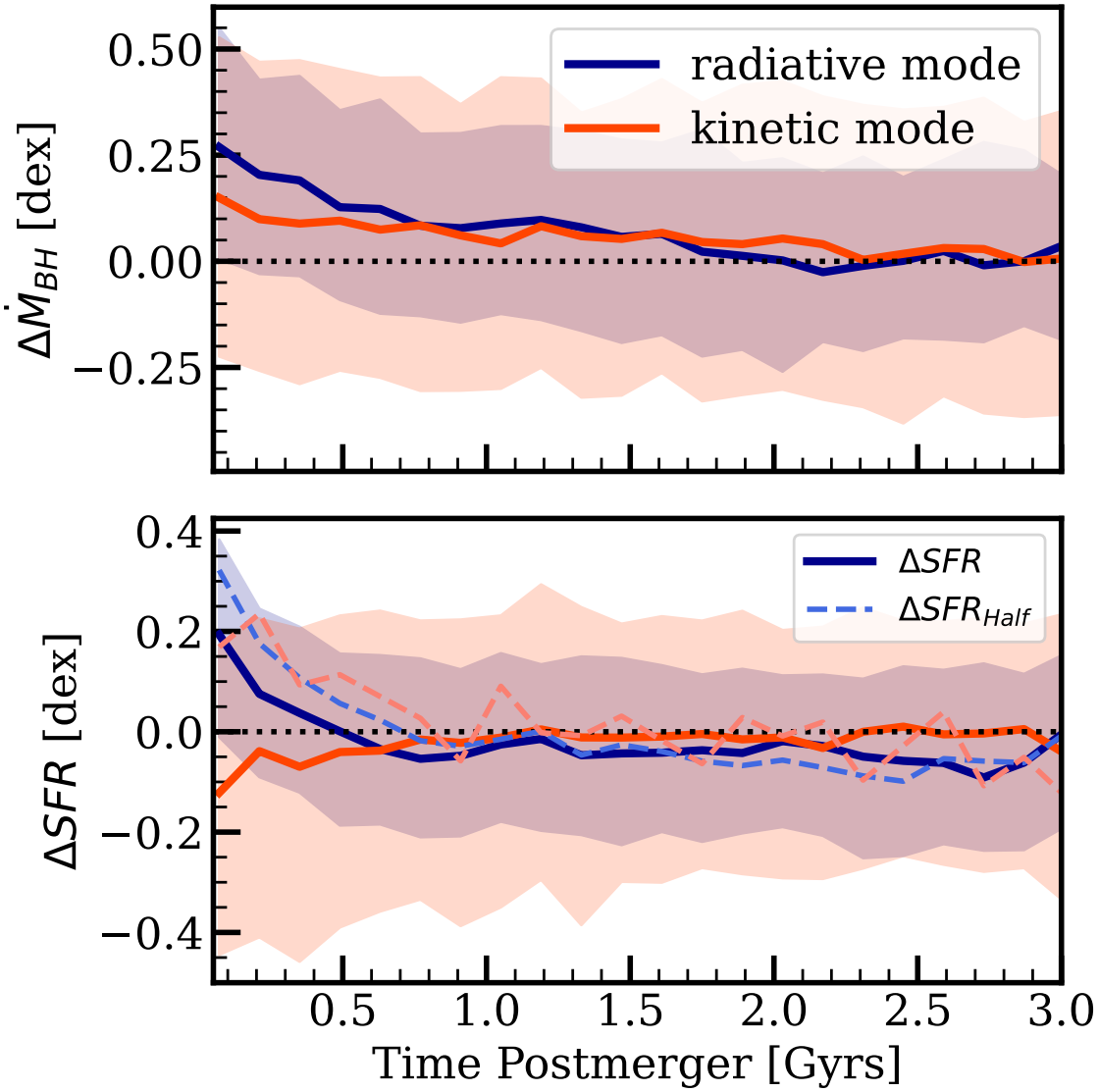

Figure 3.8: Running median of the accretion rate enhancement (top panel) and the star formation rate enhancement (bottom panel) over the time post-merger. The dark blue line represents the population in radiative mode feedback, and the orange points represent the population in kinetic mode feedback. The solid lines show the star formation rate measured within twice the stellar half-mass radius. The dashed lines represent the star formation rate enhancement calculated in a smaller aperture of one stellar half-mass radius. The error on the y-axis represents the 25th and 75th percentiles associated with the median $\Delta\dot{M}_{BH}$ and ΔSFR for the time post-merger bin.

galaxies.

The bottom panel of Figure 3.8 shows the star formation rate enhancement separated by feedback mode. In addition to the solid lines, which show the star formation rate enhancement calculated within twice the stellar half-mass radius, I also calculate ΔSFR within one stellar half-mass radius, shown in the dashed line. I include a second radius in order to compare the behaviour of the star formation rates on a global and central scale.

Starting with the solid lines in Figure 3.8, I find that the two feedback modes show different behaviour in the first 500 Myrs post-merger. Radiative mode feedback galaxies show star formation rate enhancements for $\sim$ 500 Myrs after the merger, demonstrating that galaxies in radiative mode feedback, on average, have both accretion rate and star formation rate enhancements within the first few hundred Myrs. In contrast, kinetic mode feedback galaxies show a relative star formation suppression for 500 Myrs after the merger. Therefore, despite an increased supply of gas, resulting in enhanced SMBH accretion rates, kinetic mode post-mergers display lower than average rates of star formation within $\sim$ 500 Myrs of coalescence. The suppression of star formation rate in galaxies with kinetic mode feedback is likely influenced by the relationship between star formation quenching and kinetic mode feedback in TNG (Davies et al. 2020; Luo et al. 2020; Terrazas et al. 2020; Nelson et al. 2021; Piotrowska et al. 2021). I will discuss the implications of this result within the context of galaxy quenching in more detail in Chapter 5.

Returning to Figure 3.8, I now focus on the dashed lines, which represent the star formation rate enhancement calculated within one stellar half-mass radius, $\Delta SFR_{\rm half}$. In particular, $\Delta SFR_{\rm half}$ allows me to explore a possible explanation for the difference in timescales between $\Delta \dot{M}_{BH}$ and ΔSFR. It is important to note that the enhancement in accretion rate is measured in the accretion region, within the cells in the immediate vicinity of the black hole particle. In contrast, the star formation rate used to calculate ΔSFR is measured globally within twice the stellar half-mass radius. It is possible that the star formation rate enhancement is 'diluted' when sampling the global star formation rate, resulting in shorter lived lifetimes. Comparing the solid lines, ΔSFR, with the dashed lines, $\Delta SFR_{\rm half}$, demonstrates how a more centralized aperture, although still much larger in spatial extent than the BH accretion region, affects the lifetimes of the star formation rate enhancements. For the radiative feedback mode galaxies, we see that the SFR enhancement peak is higher, reaching almost 0.4 dex. We also see that the enhancement is slightly longer

lived. In the kinetic mode galaxies, we see that the star formation rate is slightly enhanced within the ∼500 Myr window, demonstrating relative star formation rate enhancements within a more centralized aperture, despite a suppressed global star formation rate. The different behaviour in the global vs. central star formation rate enhancements may reflect the way that the global star formation rate reacts to the cumulative energy input from AGN feedback Terrazas et al. (2020), whereas the central star formation rate is enhanced due to the enhanced central gas densities associated with the merger.

3.2.2 Co-incidence of SMBH accretion and star formation rate enhancements on a galaxy by galaxy basis

I have thus far demonstrated that, on average, there is a co-incidence of SMBH accretion and star formation rate enhancements within the first few hundred Myrs of coalescence. However, I can also test the co-incidence of enhancements on a galaxy by galaxy basis. In order to compare $\Delta\dot{M}_{BH}$ and ΔSFR on a galaxy by galaxy basis, I re-calculate $\Delta\dot{M}_{BH}$ and ΔSFR using a single matching criteria, modifying the fiducial matching scheme to include the star forming vs passive classification discussed previously. To be specific, for each post-merger, I identify a set of suitable controls matched in redshift, stellar mass, feedback mode, environment, gas mass, and star forming or passive classification and calculate $\Delta\dot{M}_{BH}$ and ΔSFR relative to the same set of controls.

Figure 3.9 shows the distribution of $\Delta\dot{M}_{BH}$ and ΔSFR in three time bins, motivated by the result of Figure 3.7. The percentages of galaxies occupying each quadrant is shown in Figure 3.9; a high occupation fraction in the top right quadrant would be indicative of an excess of simultaneous enhancements. I find that within 200 Myrs of the merger, 42% of post-mergers have both an SMBH accretion rate and SFR enhancement, corresponding to a bias for post-mergers to occupy the top right quadrant. However, despite a bias for the top right quadrant, the majority of post-mergers (the remaining 58%) occupy the other three quadrants, demonstrating that the star formation and SMBH accretion rate processes are not generally synchronized in post-mergers. For each panel, I perform a Pearson correlation test, with the correlation coefficient quoted in the light blue textbox. The correlation coefficient is strongest within 200 Myrs of the merger and decreases with each subsequent time bin. However, even in the shortest time-since-merger interval, the correlation between SFR

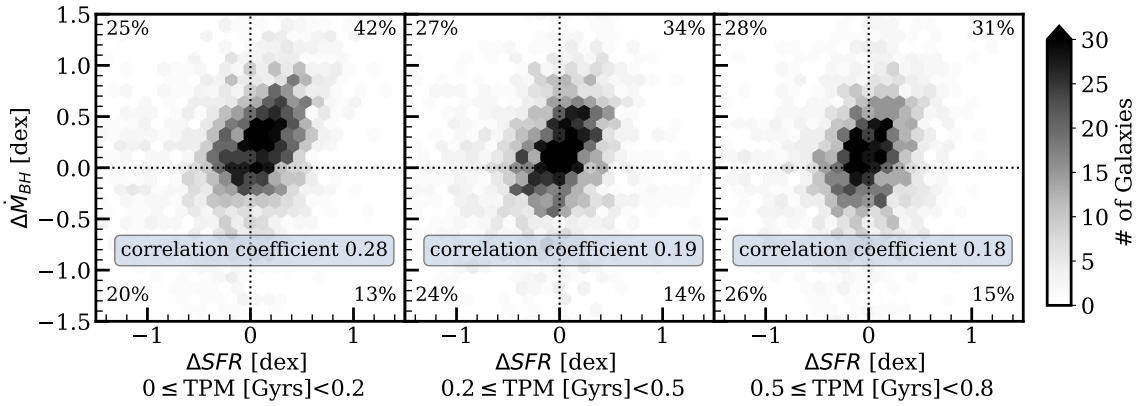

Figure 3.9: Accretion rate enhancements vs star formation rate enhancements, where each panel represents bins of time post-merger (TPM in Gyrs), since the most recent 1:10 mass ratio merger. The percentages represent the number of galaxies within each quadrant relative to the total number of galaxies in the panel. The Pearson correlation coefficient is shown in the light blue text box.

and SMBH accretion rate enhancements is modest (correlation coefficient = 0.28). I therefore demonstrate that the synchronicity or correlation between SFR and SMBH accretion rate enhancements is affected by the timescale on which the galaxy is observed. I also demonstrate that a significant correlation between $\Delta\dot{M}_{BH}$ and ΔSFR is only present in the first few hundred Myrs post-merger, consistent with the timescale of temporally correlated SFR and SMBH accretion rates in Volonteri et al. (2015b). Finally, I find that even within 200 Myrs of coalescence, the majority of post-mergers do not have synchronized ΔSFR and $\Delta\dot{M}_{BH}$.

Considering how the majority of post-mergers do not demonstrate synchronicity in SFR and SMBH accretion rate enhancements, I now test the effect of gas mass and mass ratio on the synchronicity of $\Delta\dot{M}_{BH}$ and ΔSFR within 200 Myrs of the merger. Figure 3.10 shows the distribution mergers within 200 Myrs of coalescence in $\Delta\dot{M}_{BH}$ and ΔSFR space, separated into bins of mass ratio and gas mass. The panels are organized such that gas mass is increasing from top to bottom and mass ratio is increasing from left to right. I note that the separation between major and minor mergers (μ=0.5) is based on common practice from literature, whereas the separation between 'gas poor' and 'gas rich' ($M_{gas} = 10^{9.75}\ M_{\odot}$) was chosen such that it roughly separates the post-merger population in half.

The post-mergers in the bottom row of panels, corresponding to a gas mass $10^{9.75-11} M_{\odot}$, demonstrate that the majority of gas-rich post-mergers have both positive $\Delta\dot{M}_{BH}$ and ΔSFR (i.e. over 50% are in the top right quadrant). However, the correlation coefficient is lowest in the 'minor' mergers. In fact, comparing the bottom left panel (gas-rich 'minor' mergers) to the bottom right panel (gas-rich major mergers), I find that gas-rich major mergers are more likely to have synchronicity (51% compared with 76%). I also find that overall, gas rich major mergers are more likely to produce SMBH accretion rate enhancements (68% have a positive $\Delta\dot{M}_{BH}$ compared with 89%).

The panels of the top row, corresponding to gas mass $10^{7-9.75} M_{\odot}$, show a slight bias for galaxies to occupy the left-side quadrants, corresponding to suppressed star formation rates (compared with controls). A star formation rate suppression in lower gas mass post-mergers is consistent with the results of Section 3.1.1 as well as the results of Figure 3.8. I emphasize that the gas mass used in the work presented here is that of the galaxy post-coalescence, an important distinction when comparing my results with previous work such as Di Matteo et al. (2007) and Scudder et al. (2015). Specifically, Di Matteo et al. (2007) do not find a strong dependence of star formation

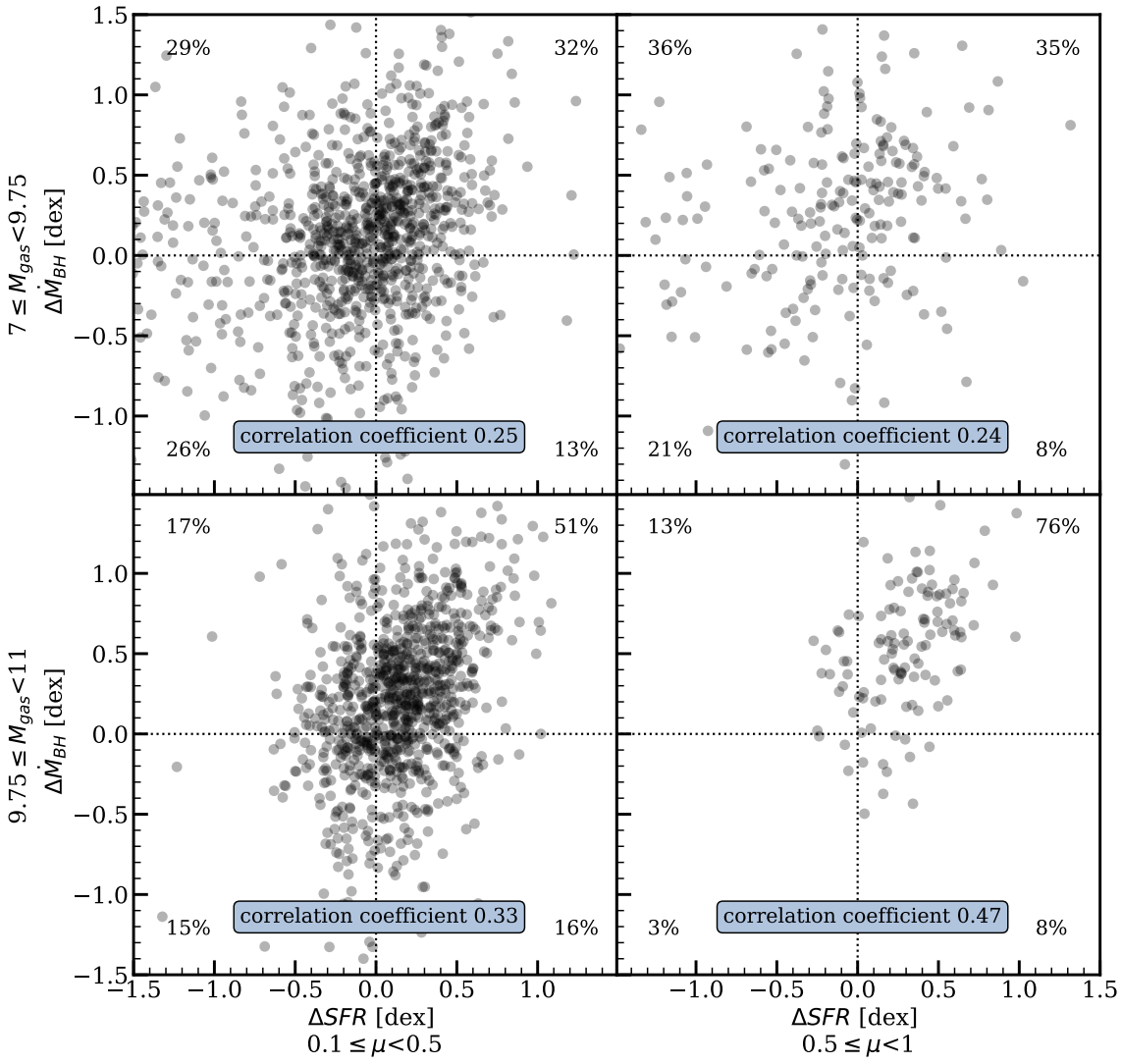

Figure 3.10: Accretion rate enhancement vs star formation rate enhancement for galaxies within 200 Myrs of a 1:10 mass ratio merger. The plots are organized by increasing gas mass, in units $log_{10}M_{\odot}$, from top to bottom and increasing mass ratio from left to right. The percentages represent the number of galaxies within each quadrant relative to the total number of galaxies in each panel. The Pearson correlation coefficient is shown in the light blue text box for each quadrant

rate enhancement on the initial gas mass (i.e. the amount of gas available just before coalescence), while Scudder et al. (2015) find that galaxies with the lowest initial gas fraction have the highest SFR enhancements due to interactions. The results of my work demonstrate that star formation rate enhancements are less likely in post-mergers with a low post-coalescence gas mass. The dependence of ΔSFR on gas mass may be explained, in part, by the correlation between SFR and gas fraction (as was demonstrated in Scudder et al. 2015 and Hani et al. 2020). However, I find lower SMBH accretion rate enhancements and star formation rate enhancements in gas poor post-mergers despite matching explicitly on gas mass. Returning to the top right panel of Figure 3.10, I find that the bias for negative ΔSFR is present even in the highest mass ratio mergers, suggesting that even major mergers are not likely to have star formation rate enhancements if they have a low gas mass.

Overall, Figure 3.10 demonstrates that the strongest bias for synchronicity and the strongest correlation (coefficient=0.47) occurs in gas-rich major mergers.

In summary, in this section I have investigated the co-incidence of SMBH accretion and star formation rate enhancements both as a population average and on a galaxy by galaxy basis. I find that the population averaged enhancements only overlap within the first few hundred Myrs of coalescence. Furthermore, I find that the co-incidence of positive $\Delta \dot{M}_{BH}$ and ΔSFR is only present, on average, in galaxies instantaneously undergoing radiative mode feedback. However this result is affected by the aperture in which the star formation rate is calculated. On a galaxy by galaxy basis, I find the majority of post-mergers do not have synchronized enhancements in SMBH accretion rate and star formation rate. I also find the strongest co-incidence of positive $\Delta \dot{M}_{BH}$ and ΔSFR and the strongest correlation between the two enhancements in gas rich major mergers.

3.3 Consequences for the AGN-Merger connection

Recall from Section 1.3.3 that there exists significant debate amongst observational literature regarding the triggering of AGN in galaxy mergers, and the importance of galaxy mergers in contributing to the overall population of AGN. In the following section, I present two experiments designed to tackle the following questions about the AGN-merger connection in TNG: what fraction of mergers 'trigger' an AGN and what fraction of AGN have had a recent merger?

3.3.1 What fraction of mergers 'trigger' an AGN?

In my first experiment, I am interested in quantifying what fraction of all post-mergers will have a high accretion rate event within 500 Myrs of coalescence. For reference, I compare the fraction of mergers that experience a high accretion rate event within 500 Myrs of coalescence to the fraction of non-mergers that similarly experience a high accretion rate event within a 500 Myr long observation window. To begin, I define an enhancement fraction, f_{enhanced}, as the number of galaxies that have a SMBH accretion rate at or above a cutoff $\dot{M}_{BH}^{cutoff}$ divided by the total number of galaxies in the sample. Figure 3.11 shows the fraction of enhanced galaxies for the post-merger and non-merger samples. The top panel shows the enhancement fraction as a function of $\dot{M}_{BH}^{cutoff}$, for the post-merger samples shown in the solid line and the non-merger samples shown in the dashed line. The bottom panel shows the ratio of the post-merger to non-merger fractions, or the fractional excess of post-mergers to non-mergers that achieve an accretion rate exceeding $\dot{M}_{BH}^{cutoff}$ within 500 Myrs. The accretion rate in units of bolometric luminosity is shown along the top axis, where I calculate L_{bol} as 10% of the accretion mass energy, or $0.1\dot{M}_{BH}c^2$, as 10% is a commonly used scaling factor for the radiative efficiency of AGN (Weinberger et al. 2016).

The top panel of Figure 3.11 demonstrates that $\sim$ 60% of post-merger galaxies have accretion rates exceeding $L_{bol} > 10^{43} erg/s$ within 500 Myrs of the merger. However, I find that 50% of non-merger galaxies also have an AGN phase of $L_{bol} > 10^{43} erg/s$, demonstrating that accretion rate events exceeding $L_{bol} > 10^{43} erg/s$ are common in both samples, though slightly more common in the post-mergers. Although the absolute fraction of galaxies with an AGN phase decreases with increasing luminosity (as expected), I find that there is a growing excess in the fraction of post-mergers that undergo an AGN phase for higher AGN luminosities. Therefore, although fewer than 10% of post-mergers will achieve accretion rates exceeding $L_{bol} > 10^{45} erg/s$, four times more AGN appear in the post-merger sample than the non-merger sample. Overall, I find that post-mergers are more likely to have an AGN phase than a non-mergers with an increasing excess as a function of luminosity, which is consistent with results from the Magneticum Pathfinder simulation (Steinborn et al. 2018) and the EAGLE simulation (McAlpine et al. 2020), as well as complimentary to Bhowmick et al. (2020) who find that high luminosity AGN are more likely to appear in environments with a higher density of SMBHs in IllustrisTNG.

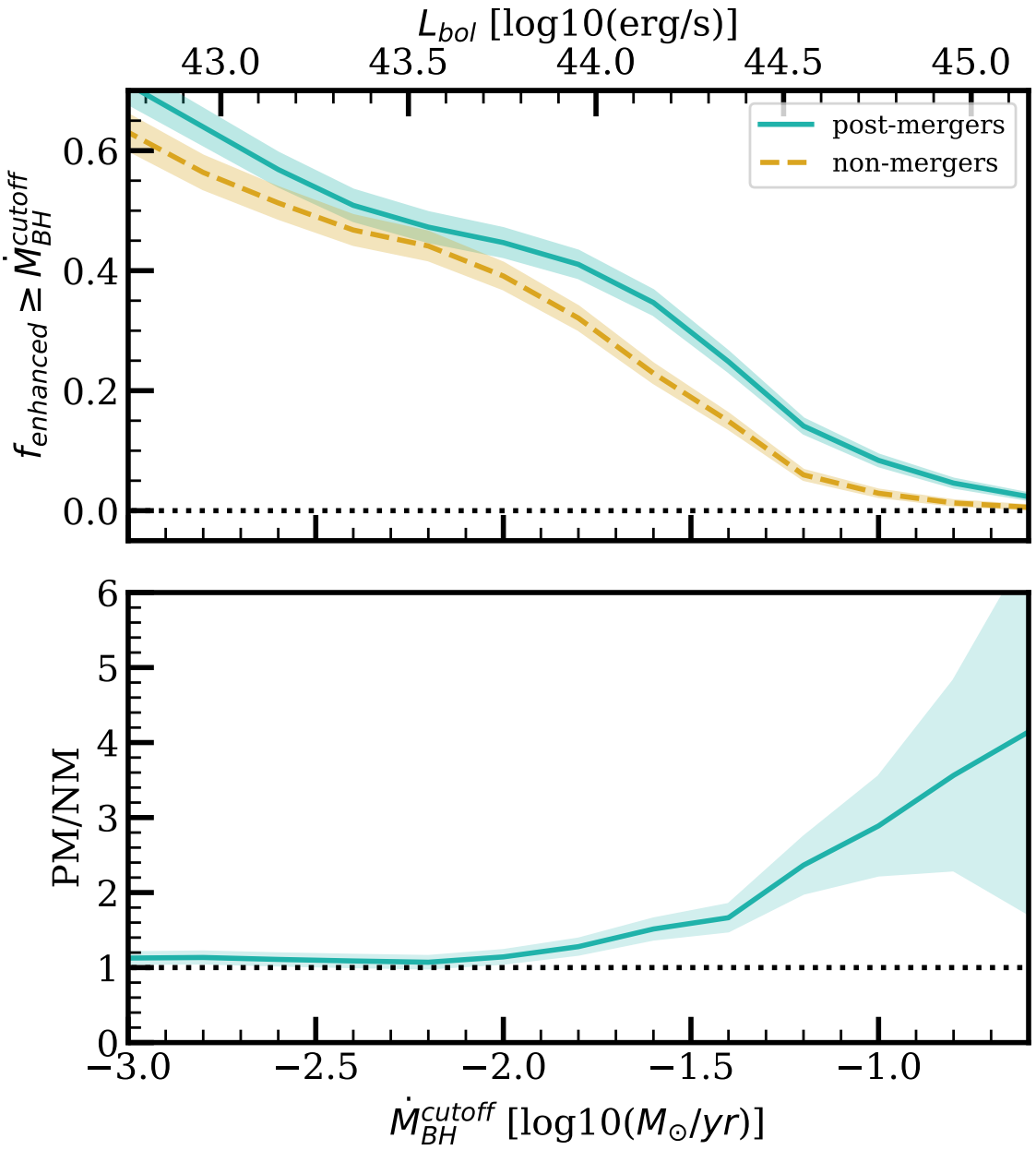

Figure 3.11: Shown on the top panels is the fraction of galaxies that have a SMBH accretion rate at or higher than $\dot{M}_{BH}^{cutoff}$ within a period of 500 Myrs, relative to the total number of galaxies. The teal line corresponds to the post-merger sample and the yellow dashed line is the non-merger sample, as defined in Section 2.3. The top x-axis of the Figure shows the corresponding AGN luminosity, calculated as $L_{bol} = 0.1\dot{M}_{BH}c^2$. The bottom panel shows the ratio of the fraction of post-merger galaxies to non-merger galaxies. This is the fractional excess of post-mergers that have an accretion rate at or higher than the cutoff relative to the non-merger sample. The error in the shaded region is the Poisson error reflecting the number of galaxies.

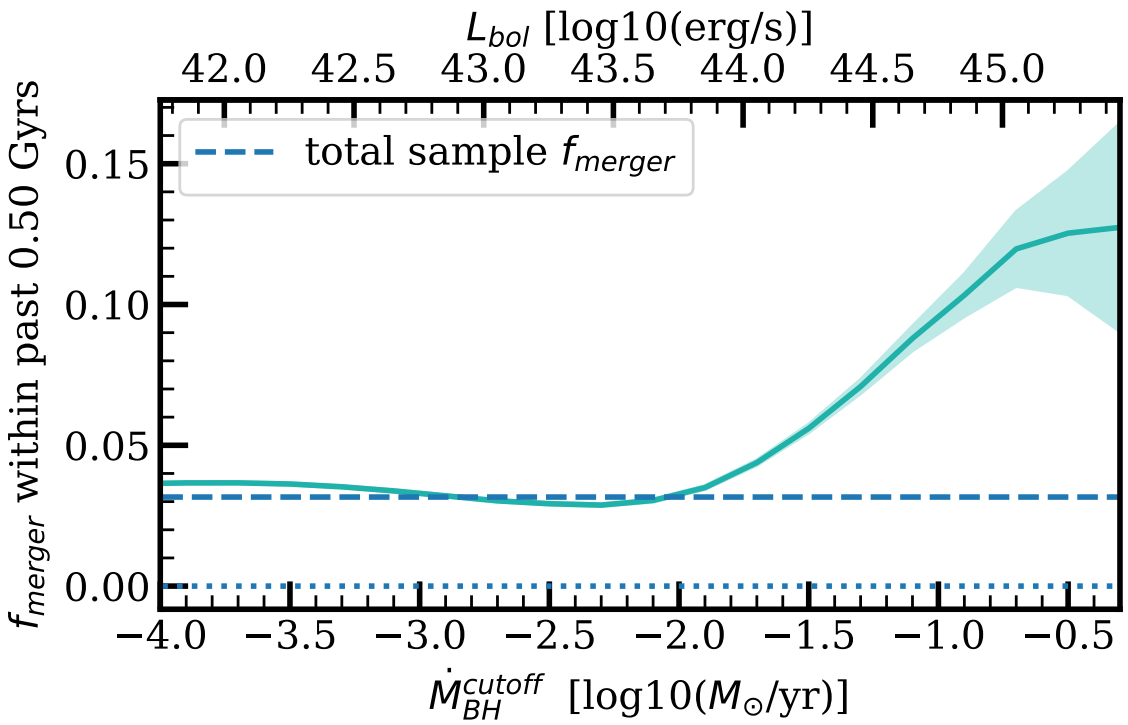

Figure 3.12: The teal line shows the fraction of galaxies that have had a merger of mass ratio greater than 1:10 within 500 Myrs. The x-axis defines the sample used to calculate the merger fraction from left to right, where only galaxies with a black hole accretion rate of at least $\dot{M}_{BH}^{cutoff}$ are included in the calculation of the merger fraction. The top x-axis shows the corresponding AGN luminosity, calculated as $L_{bol} = 0.1\dot{M}_{BH}c^2$. The error in the shaded region is the Poisson error reflecting the number of galaxies. The horizontal dashed line represents the overall merger fraction of the sample, ∼3%, for all galaxies in IllustrisTNG with stellar mass of at least $10^{10}M_\odot$ and a redshift < 1.

3.3.2 What fraction of AGN are recent mergers?

In my second experiment, I consider what fraction of galaxies with high accretion rates are recent mergers. In Figure 3.11, I demonstrated that galaxies in the post-merger sample are more likely to have an AGN phase than those in the non-merger sample. However, post-mergers are rare in both IllustrisTNG and the observed universe and thus may not be the major pathway to AGN triggering. Therefore, in this experiment I aim to quantify the contribution of recent mergers to the total AGN population in the simulation.

To investigate the merger fraction of AGN, I first define an 'AGN sample' by selecting all galaxies that have a SMBH accretion rate at or above $\dot{M}_{BH}^{cutoff}$. In this

experiment, the merger fraction is defined as the fraction of galaxies that have had a merger, of a mass ratio of at least 1:10, in the last 500 Myrs. Figure 3.12 shows the merger fraction as a function of the cutoff accretion rate. The x-axis defines the AGN sample, which will consist of all galaxies with accretion rates at or exceeding $\dot{M}_{BH}^{cutoff}$ (and meeting the selection criteria outlined in Chapter 2, i.e $M_\star > 10^{10} M_\odot$ and $z < 1$). Once again, I show the equivalent bolometric luminosity along the top axis, calculated as $L_{bol} = 0.1 \dot{M}_{BH} c^2$. In Figure 3.12, I find that the merger fraction increases as a function of accretion rate (or, equivalently, luminosity). The horizontal dashed line represents the total merger fraction for all the selected galaxies from IllustrisTNG up to redshift 1, $\sim 3\%$. We see that the merger fraction of the AGN sample exceeds the total f_{merger} around $L_{bol} \sim 10^{44} erg/s$. Therefore, there is no significant luminosity dependence of the merger fraction for $L_{bol} \lesssim 10^{44} erg/s$. At the highest accretion rates, the merger fraction peaks at approximately 13%.

Although there is a luminosity dependence on the merger fraction for $L_{bol} \gtrsim 10^{44} erg/s$, I find that recent mergers never dominate the AGN sample. This result is once again consistent with the results of Steinborn et al. (2018) and McAlpine et al. (2020) for the Magneticum Pathfinder and EAGLE simulations. Our result would also agree with the observational findings of Villforth et al. (2014, 2017), who do not find a dominant presence of mergers in high luminosity AGN, but is in contrast to observations which find the majority of high luminosity AGN are recent mergers Bennert et al. (2008); Treister et al. (2012); Glikman et al. (2015).

Although I find that in IllustrisTNG, recent mergers do not dominate the AGN population even at high luminosities, I cannot exclude the possibility that galaxies with recent pair interactions could contribute to a fraction of the remaining ∼90% of galaxies at or above 10^{45} erg/s. There may also be minor mergers that are not accounted for in the merger fraction. However, the result of Figure 3.12 also supports a scenario where secular processes play a significant role in fueling even the highest luminosity AGN (at least in the redshift regime 0-1). I therefore conclude that post-mergers contribute more significantly to the population of high luminosity AGN, but they are non-dominant over the entire luminosity range presented here.

Chapter 4

SMBH Accretion Rate Enhancements in the Illustris and EAGLE Simulations

In the research presented in Chapter 3, I focused on an in depth analysis of post-mergers from the IllustrisTNG cosmological simulation. However, IllustrisTNG is only one of a number of modern state-of-the-art cosmological scale galaxy formation simulations which may or may not demonstrate enhanced SMBH accretion rates in post-mergers. One might expect post-mergers to behave the same between cosmological simulations, as there are often many similarities in the galaxy physics models, and the simulations are tuned to reproduce specific benchmarks of galaxy realism, such as morphological diversity and a star forming and quenched population. However, there are also important differences, particularly in the subgrid recipes for SMBH accretion and feedback, that can lead to significant differences between simulations. For example, different simulations may produce both a star forming and quenched galaxy population, but may disagree as to whether it is the inner or outer stellar regions which quench first and the associated timescales for quenching in different types of galaxies (Starkenburg et al. 2019; Walters et al. 2022). In addition, many cosmological simulations with different AGN models can produce both similarities and differences. In fact, Habouzit et al. (2022) demonstrate that many simulations produce significant differences in the low-redshift AGN luminosity functions, despite broadly comparable SMBH mass-stellar mass relations (Habouzit et al. 2021).

In order to investigate how the results of my research vary between cosmological

simulations, I investigate two other cosmological scale galaxy formation simulations: Illustris (Vogelsberger et al. 2014a,b; Genel et al. 2014; Sijacki et al. 2015) and EAGLE (Schaye et al. 2015; McAlpine et al. 2016). Illustris is the predecessor of the TNG simulation, however there exist key differences between the two simulations, including differences in the SMBH accretion and AGN feedback models. EAGLE is also an excellent simulation for comparison, as EAGLE uses an AGN feedback model different from the models of both Illustris and TNG. It is important to note that the AGN feedback model is not the only difference between the cosmological simulations. However, there are also many similarities in the galaxy physics models of Illustris, TNG, and EAGLE, allowing for some interpretation of how the SMBH accretion and AGN feedback models may influence the results of my work. A summary of the Illustris and EAGLE simulations is presented in Section 4.1.

In the following chapter, I will repeat the main experiments of Chapter 3 using the Illustris and EAGLE simulations. In Section 4.2, I discuss new methodology introduced to study the accretion rates in Illustris and EAGLE, as well as demonstrate that the results for TNG post-mergers are robust to such changes in the methodology. The results of the main experiments on Illustris and EAGLE are presented in Section 4.3. The purpose of the comparison is primarily to determine whether the major findings of Chapter 3 are reproduced between the three simulations or unique to TNG. I also aim to identify the differences in the post-merger and AGN connection in Illustris and EAGLE compared with TNG, and discuss what might be responsible for such differences. In addition, in Section 4.4, I also discuss how the inclusion of SMBH mass matching impacts the results of TNG, Illustris, and EAGLE.

4.1 Summary of the EAGLE and Illustris simulations

In the following section, I briefly review the details of the Illustris and EAGLE simulations, focusing primarily on the differences in the SMBH seeding, accretion, and feedback models.

For the following section, I use the Illustris-1 run of the Illustris simulation (Vogelsberger et al. 2014a,b; Genel et al. 2014; Sijacki et al. 2015) and the L100N1504 run of the EAGLE (Schaye et al. 2015), which have a similar volume and resolution as the TNG100-1 simulation used in Chapter 3. The volume and resolutions for each

	TNG100-1	**Illustris-1**	**EAGLE L100N1504**
Volume	$(110.7\,\mathrm{Mpc})^3$	$(106.5\,\mathrm{Mpc})^3$	$(100\,\mathrm{Mpc})^3$
Dark matter	$7.5 \times 10^6\,\mathrm{M}_\odot$	$6.26 \times 10^6\,\mathrm{M}_\odot$	$9.7 \times 10^6\,\mathrm{M}_\odot$
Baryonic matter	$1.4 \times 10^6\,\mathrm{M}_\odot$	$1.26 \times 10^6\,\mathrm{M}_\odot$	$1.81 \times 10^6\,\mathrm{M}_\odot$
Seeded halo mass	$5 \times 10^{10}\,\mathrm{h}^{-1}\mathrm{M}_\odot$	$7.1 \times 10^{10}\,\mathrm{h}^{-1}\mathrm{M}_\odot$	$1 \times 10^{10}\,\mathrm{h}^{-1}\mathrm{M}_\odot$
SMBH seed mass	$8 \times 10^5\,\mathrm{h}^{-1}\mathrm{M}_\odot$	$1.42 \times 10^5\,\mathrm{h}^{-1}\mathrm{M}_\odot$	$1 \times 10^5\,\mathrm{h}^{-1}\mathrm{M}_\odot$

Table 4.1: Comparison of simulation volume, resolution, and SMBH seeding mass parameters for TNG, Illustris, and EAGLE

simulation run are shown in Table 4.1. Illustris and TNG have a similar interval of time between snapshots of $\sim$ 150 Myrs. In EAGLE, I use the more frequently sampled 'snipshots' which have a time interval around $\sim$ 60 Myrs. Therefore the post-mergers from Illustris and TNG will have coalesced within the last $\sim$ 150 Myrs and post-mergers from EAGLE coalesced within the last $\sim$ 60 Myrs. In addition, all three simulations seed SMBHs at the centre of halos that meet a minimum mass threshold, with slight variations is the specific halo mass threshold and seed mass shown in Table 4.1.

4.1.1 SMBH accretion rate models

All three simulations use a Bondi-Hoyle-Lyttleton subgrid model to calculate SMBH accretion rates (see Eq. 2.1), where the maximum allowed accretion rate is capped by the Eddington rate (see Eq. 2.2). However, Illustris and EAGLE both apply different modifications to the Bondi rate.

In Illustris, the Bondi accretion rate is enhanced with a boost factor of $\alpha = 100$ which is argued to be necessary to compensate for unresolved gas cloud structure in the interstellar medium (ISM) (Sijacki et al. 2015). The boost factor is dropped in the TNG simulation suite which instead seeds SMBH particles at a higher seed mass, as there exists somewhat of a degeneracy between the inclusion of an accretion boosting factor and the SMBH seed mass (Weinberger et al. 2016). In addition, Illustris implements a pressure-criterion based suppression of accretion rates when the gas surrounding the black hole is sufficiently low density (Sijacki et al. 2015), as the boosting factor may lead to an overestimated SMBH accretion rate in a low density ISM (Vogelsberger et al. 2013).

In EAGLE, the Bondi accretion rate is multiplied by a factor, that is the ratio

of the Bondi and the viscous time-scales, as outlined in Rosas-Guevara et al. (2015). The modification applied in EAGLE suppresses the Bondi accretion rate when the accreting gas contains sufficiently high angular momentum. The modified Bondi accretion is parameterized using the critical ratio between the rotational speed and the sound speed of the gas accreting onto the SMBH (Rosas-Guevara et al. 2015; Schaye et al. 2015).

4.1.2 SMBH mergers

In Illustris, SMBHs are merged when they are within a sufficient distance of one another, which corresponds to the smoothing length in Illustris (Sijacki et al. 2015). The procedure of SMBH merging in Illustris is, in practice, very similar to TNG, which also merge SMBH particles when they are close together irrespective of the relative velocities (see Section 2.1). In fact, the effective differences between simulations that arises from the choice for the threshold SMBH merging distance is minimized by the fact SMBH particles are re-positioned (in all three simulations) to the local gravitational potential minima, which results in the placement of SMBH particles within close proximity and prompt merging Bahé et al. (2022).

EAGLE applies a similar requirement for SMBHs to be within close proximity in order to merger, specifically a distance that is the minimum between the accretion sampled region or three times the smoothing length (Schaye et al. 2015). However, EAGLE has an additional criterion on the relative SMBH velocities, requiring the relative velocities of the SMBH particles to be lower than the circular velocity at a separation of the smoothing length (Schaye et al. 2015). According to Schaye et al. (2015), the additional relative velocity criterion reduces the likelihood that the SMBHs will merge during the initial stages of the merger.

4.1.3 AGN feedback models

Finally, I will briefly describe the main differences in the AGN feedback models of TNG, Illustris, and EAGLE.

Recall from Section 2.1 that TNG uses a bimodal feedback model, with continuous thermal mode feedback used for SMBHs with high accretion rates and kinetic mode feedback used for SMBHs with low accretion rates, where the distinction between high and low accretion rates is determined by Eq. 2.3.

Illustris similarly uses a multi-mode AGN feedback model depending on the ratio of the Bondi accretion rate to the Eddington rate. At high accretion rates, defined by $\dot{M}_{BH}/\dot{M}_{Edd} > 0.05$, Illustris uses the same radiative mode as TNG, releasing a portion of the mass energy accreted by the SMBH continuously as thermal energy in the direct vicinity of the SMBH (Sijacki et al. 2015). In addition, for high accretion rates, Illustris also implements an AGN feedback model where the cooling rates of low density gas in the vicinity of the highly accreting SMBH are modified to account for heating due to the quasar's radiation field (Sijacki et al. 2015). At low accretion rates, $\dot{M}_{BH}/\dot{M}_{Edd} < 0.05$, Illustris inflates 'bubbles' of hot gas where thermal energy (corresponding to a fraction of the accretion rate of the SMBH) is injected within the bubble (Sijacki et al. 2015).

In EAGLE, only one type of AGN feedback is used, where thermal energy is injected into the vicinity of the SMBH to heat up the gas. However, importantly, energy is not injected continuously. Rather, SMBHs have a reservoir of thermal energy that is stored until there is enough energy to sufficiently heat the surrounding gas (Schaye et al. 2015). As discussed in Schaye et al. (2015), the nature of the AGN feedback implemented through the stochastic thermal model depends strongly on the threshold temperature that defines the AGN feedback reservoir. If the energy reservoir is large, the AGN feedback events will be more energetic but less frequent, and alternatively a smaller energy reservoir results in less effective but more frequent AGN activity.

4.1.4 SMBH mass vs. stellar mass and SMBH accretion rate

In the previous sections, I have outlined some similarities and differences between the TNG, Illustris, and EAGLE galaxy physics models. However, each of the different simulations choices, as well as differences not discussed in the previous sections, can affect the characteristics of the SMBH population in non-trivial ways. In Figures 4.1 and 4.2, I compare the overall SMBH mass, stellar mass, and SMBH accretion rates for the total sample of galaxies (meeting the criteria of stellar mass $> 10^{10} M_{\odot}$ and redshift $0 \leq z \leq 1$) in EAGLE, Illustris, and TNG to demonstrate some of the differences in the SMBH population.

Figure 4.1 shows the SMBH mass vs stellar mass in the three simulations, EAGLE in purple, Illustris in blue, and TNG in green. Figure 4.1 demonstrates how, despite many broad similarities in the subgrid models for SMBH seeding, merging,

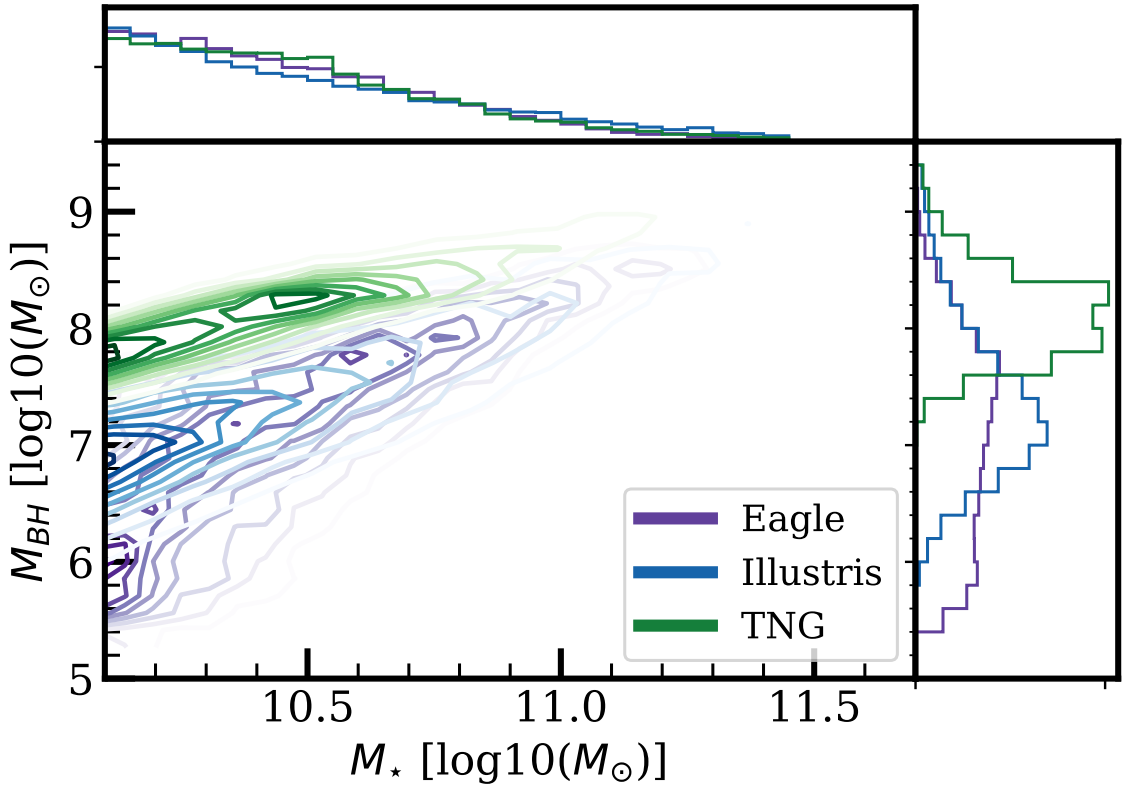

Figure 4.1: Comparison of the SMBH mass with stellar mass of galaxies from TNG (Green), EAGLE (Purple), and Illustris (Blue), for a galaxy sample from redshift range $0 \leq z \leq 1$ and stellar mass of at least $10^{10} M_\odot$.

and accretion, there are significant differences in the SMBH masses that populate the same stellar mass range between the three simulations. Notably, the TNG simulation has the narrowest range in SMBH mass, compared with Illustris and EAGLE. The large SMBH masses are primarily due to a combination of the higher seed mass, rapid early growth of SMBHs in TNG, and slow growth in large SMBH masses due to the SMBH mass dependent criterion for AGN feedback mode (Weinberger et al. 2016). In comparison, Illustris and EAGLE demonstrate a wider variety of SMBH masses within the selected stellar mass range, with the widest range of SMBH mass in EAGLE and a larger population of low mass SMBHs.

Figure 4.2 demonstrates the differences in the distributions of SMBH mass and accretion rate. In contrast to the significant differences in the distribution of SMBH mass, the range of SMBH accretion rates of the three simulations are fairly comparable. The similarity in range of SMBH accretion rate is perhaps unsurprising when

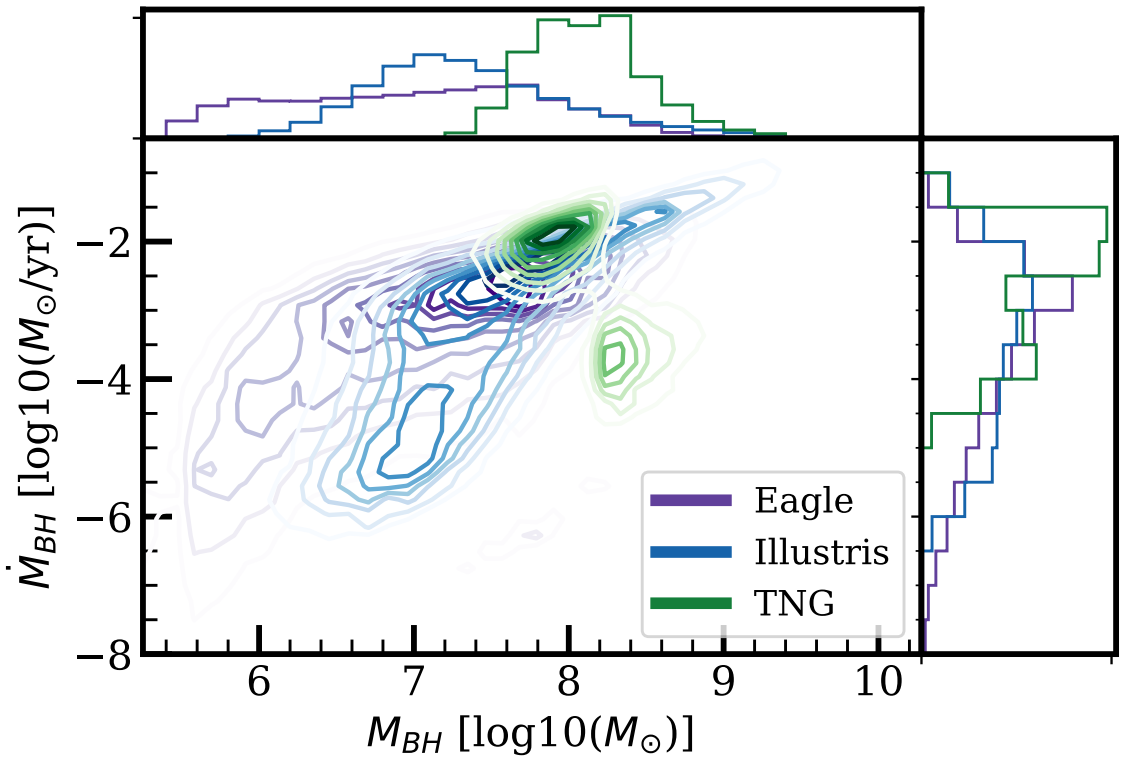

Figure 4.2: Comparison of the average SMBH growth rate of galaxies with SMBH mass with from TNG (Green), EAGLE (Purple), and Illustris (Blue), for a galaxy sample from redshift range $0 \leq z \leq 1$ and stellar mass of at least $10^{10} M_\odot$.

considering the stochasticity. That is, a single galaxy can demonstrate large fluctuations in SMBH accretion rates from one snapshot to another, and therefore the full range of SMBH accretion rates is well sampled. However, In Figure 4.2, there is a significant difference in the general trend between SMBH mass and accretion rate. Once again this can be explained due to the SMBH mass dependence in the TNG AGN feedback mode, such that most high mass SMBHs will use kinetic mode AGN feedback which effectively regulates SMBH accretion and reduces accretion rates using isotropic injections of kinetic energy into surrounding particles (recall the transition shown in Figure 2.4). In contrast, the connection between feedback mode and SMBH mass is weaker in Illustris, and the highest SMBH accretion rates are actually found in the highest SMBH masses. EAGLE demonstrates a similar trend to Illustris, though the positive correlation between SMBH mass and accretion rate is not as strong.

Overall, despite applying the same selection criteria for galaxies within all three simulations, Figures 4.1 and 4.2 demonstrate the significant differences in the SMBH

populations.

4.2 Instantaneous accretion rates vs. averaged SMBH growth rates

In Chapter 3, I used the instantaneous SMBH accretion rates in the analysis of TNG post-mergers. However, for the EAGLE simulation, I did not have access to reliable instantaneous SMBH accretion rates. In order to use a consistent accretion rate between simulations, I make use of the reliable SMBH mass trees to calculate the averaged SMBH growth rate between snapshots (or snipshots),

$$\dot{M}_{BH}^{ave} = \frac{M_{BH}^{\text{snap N+1}} - M_{BH}^{\text{snap N}}}{t^{\text{snap N+1}} - t^{\text{snap N}}}. \tag{4.1}$$

I note that using an average SMBH growth rate provides the advantage that $\dot{M}_{BH}^{ave}$ will be able to capture a short lived period of significant SMBH growth within the $\sim$ 50-150 Myr window of time between snapshots in the cosmological simulations. The disadvantage is that the averaged accretion rates are less compatible with observations, which can only observe AGN luminosity at the time of observation.

When calculating the average accretion rate over a snapshot, I exclude snapshots where there is an increase of SMBH mass due to mergers of SMBHs. I emphasize that I flag for SMBH mergers, and subsequently remove the snapshots where galaxies are undergoing an SMBH merger from my overall sample. I exclude SMBH mergers because I am interested in the enhancement of accretion rate of SMBHs, and therefore do not want to include SMBH growth from SMBH mergers in my sample of post-merger accretion rates. To identify mergers of SMBHs, I algorithmically flag discontinuities in the SMBH mass growth. I identify cases where there is a sudden growth in SMBH mass over one snapshot, i.e. a percentage change in SMBH mass $\Delta M_{BH}/M_{BH}$ over one snapshot which is statistically higher than the changes in SMBH mass in adjacent snapshots. In order to identify sudden jumps in SMBH mass, I calculate the average percentage change, $\Delta M_{BH}/M_{BH}$, and standard deviation in the preceding 5 snapshots and following 5 snapshots. I identify a SMBH merger when the change in SMBH mass, $\Delta M_{BH}/M_{BH}$, is at least 2σ above the average of the preceding and following snapshots. Figure 4.3 demonstrates the merger identification on an example galaxy from TNG, where two SMBH mergers are detected.

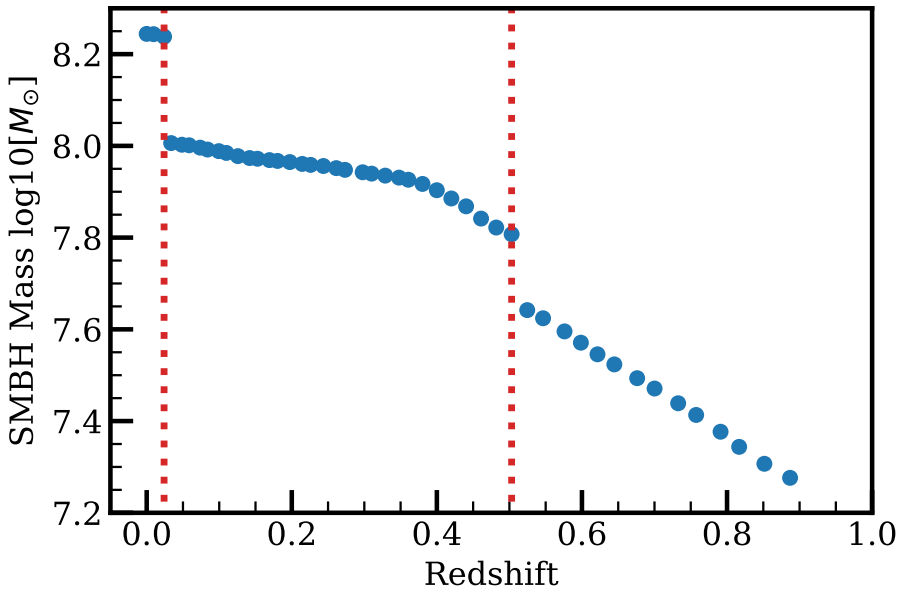

Figure 4.3: Example SMBH mass for one galaxy in TNG, with SMBH mass on the y-axis and redshift on the x-axis. SMBH mergers are identified at locations marked with a vertical red dotted line.

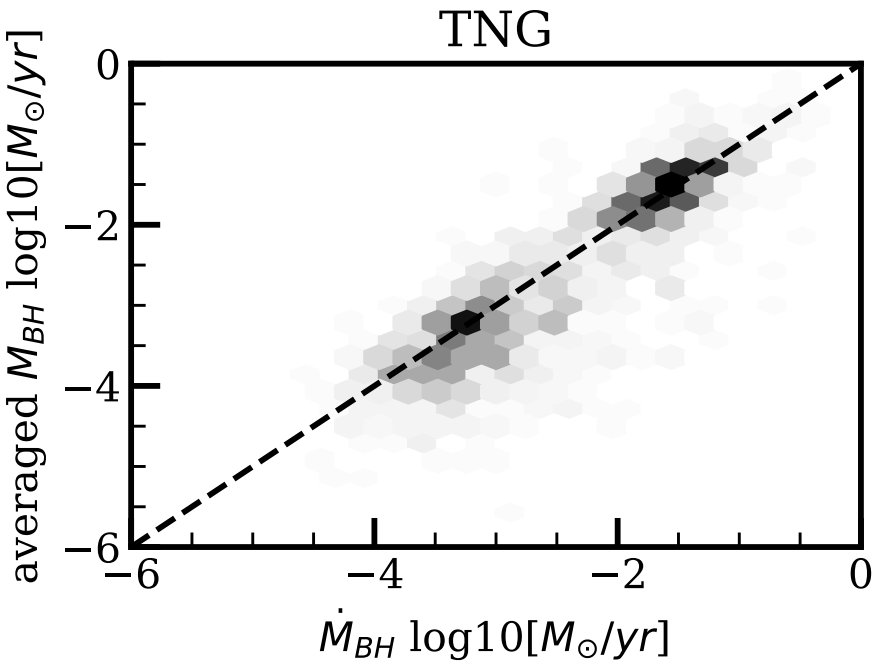

Figure 4.4: Comparison of the averaged SMBH growth rate (y-axis) with the instantaneous SMBH accretion rate (x-axis) on a galaxy by galaxy basis for TNG. The diagonal line corresponds to the one-to-one line.

In Figures 4.4 and 4.5, I demonstrate the compatibility between the instantaneous SMBH accretion rates and the average SMBH growth rates in TNG. Figure 4.4 shows a direct comparison of averaged SMBH growth rate and instantaneous accretion rate for galaxies in TNG. I find that there is broad agreement on a galaxy by galaxy basis. Figure 4.5 shows two main results from Chapter 3, the overall enhancement of post-merger accretion rates (top) and the long-lived timescale of accretion rate enhancements (bottom). For both experiments, I use the same control matching methodology, outlined in Section 2.3, and show the instantaneous accretion rate in the dash dotted black line and the averaged accretion rate in the green solid line. In the top panel of Figure 4.5, I find that the median $\Delta\dot{M}_{BH}$ of the post-merger sample is approximately 0.29 dex using the averaged accretion rates, compared with 0.23 dex for the instantaneous accretion rates. I suspect that the post-mergers have higher averaged accretion rates enhancements because the average accretion rate will capture any period of high SMBH accretion that occurs over the 50-150 Myr time window, whereas an instantaneous accretion rate will only be enhanced if it is observed at a moment of high accretion. Furthermore, the averaged accretion rates have reduced scatter, which is expected. In the bottom panel of Figure 4.5, I find that both approaches recover a comparable timescale for population averaged accretion rate enhancements, approximately 2 Gyrs. I therefore demonstrate the compatibility of the main results of the work presented here between instantaneous and averaged SMBH accretion rates in TNG, and therefore proceed with the analysis of Illustris and EAGLE simulations.

4.3 SMBH accretion rate enhancements in EAGLE and Illustris

To begin, I will define the post-merger and non-merger samples for EAGLE and Illustris following the same methodology as Chapter 2. I note that the post-merger identification from Illustris, which follows the same process outlined in Section 2.2, was inherited from previous work done by Dr. Maan Hani and Dr. Salvatore Quai, and the environmental control variables r_1 and N_2 were provided by Dr. Dave Patton. The post-merger sample and environmental variables from the EAGLE simulations were provided by Dr. Stuart McAlpine. The merger selection process and control matching follow the procedure of Chapter 2, so I refer the reader back to the relevant

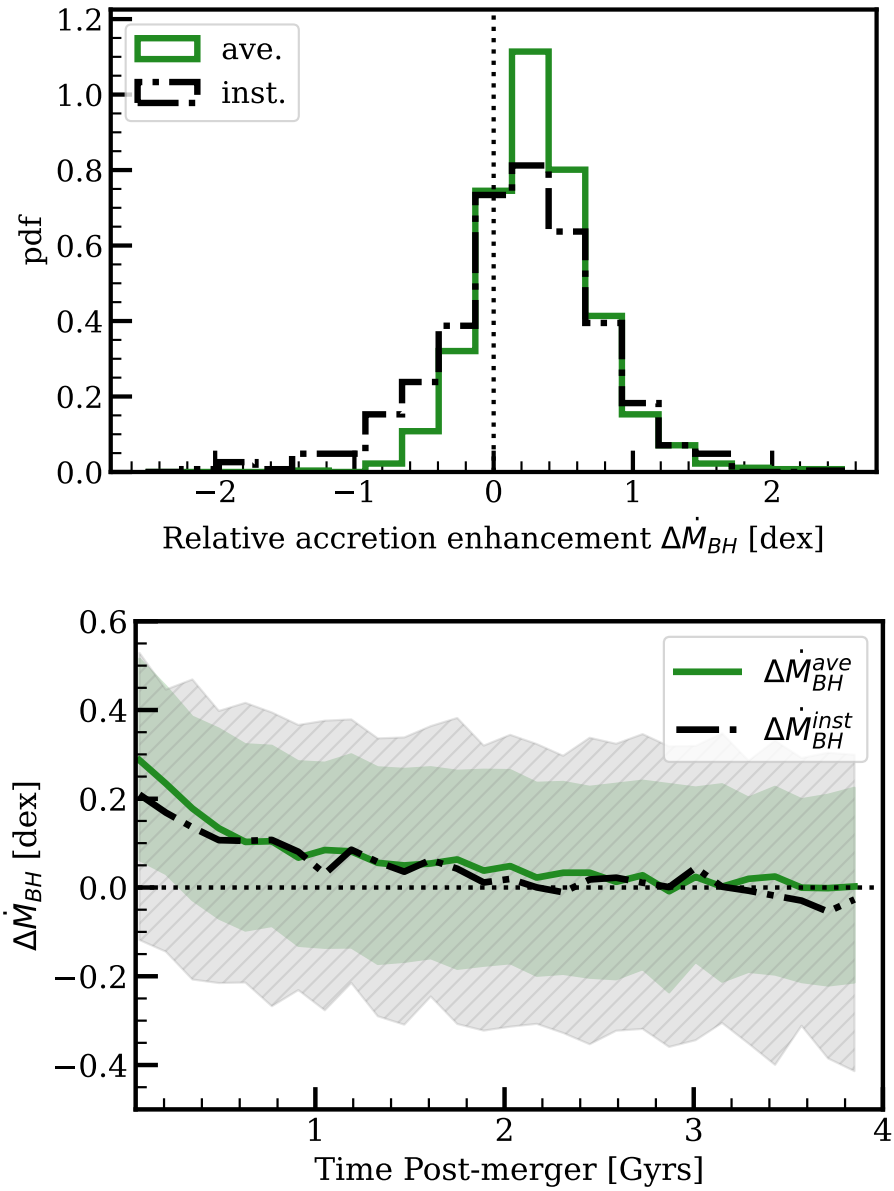

Figure 4.5: Comparison of the averaged SMBH growth rate (solid green line) with the instantaneous accretion rates (dash dot black line) for TNG. The top panel shows the histogram of relative accretion rate enhancements in the post-merger sample. The bottom panel shows the running median of the accretion rate enhancements as a function of time post-merger, where the 25th and 75th percentiles are shown in the green and grey shaded regions. In both panels, the trends seen using the instantaneous accretion rates are recovered using average accretion rates, and the scatter is reduced.

sections, Sections 2.2 and 2.3, for reference. I apply one difference to the methodology of Section 2.3, where I no longer require galaxies to be matched in feedback type for Illustris and EAGLE. As mentioned in Section 4.1.3, there is only one feedback type in EAGLE, eliminating any feedback type matching scheme. Furthermore, unlike TNG, the feedback modes in Illustris, radiative and 'bubble' mode, do not correspond to a strong bimodal distribution of accretion rate, and therefore feedback type matching is deemed unnecessary.

4.3.1 Control matched post-mergers and non-mergers in Illustris and EAGLE

In Illustris, I begin with a sample of 1215 candidate post-mergers meeting the selection criteria of Section 2.2. Removing galaxies that underwent an SMBH merger in the same snapshot, I end up with 1001 candidate post-mergers. Finally, applying the control matching scheme outlined in Section 2.3 removes 76 post-mergers where a suitable number of controls cannot be identified, for a final sample of 925 post-mergers. On average, post-mergers in Illustris find ~ 11 suitable controls and grow their error tolerances 2 times.

Similarly, in EAGLE, I begin with a sample of 2198 candidate post-mergers. Applying the SMBH merger identification algorithm, I further reduce the sample of candidate post-mergers to 2044. Control matching removes 300 post-mergers, for a final sample of 1744 post-mergers. Post-mergers in EAGLE find ~ 10 suitable controls, and grow their error tolerances 3 times.

Figure 4.6 shows the population characteristics for Illustris (left) and EAGLE (right). The overall post-merger population is shown in the dotted lines, and the successfully matched post-merger population is shown in the solid lines. I select two samples of non-mergers (see Section 2.3) for comparison with both Illustris and EAGLE, shown in yellow dashed lines. As in the case of TNG, I note that there is evidence in Illustris of a bias for the post-mergers to host larger SMBHs compared with the non-mergers. In Section 4.4, I discuss how matching explicitly in SMBH mass affects the results presented here. SMBH mass aside, Figure 4.6 demonstrates the overall compatibility of the post-merger and non-merger samples.

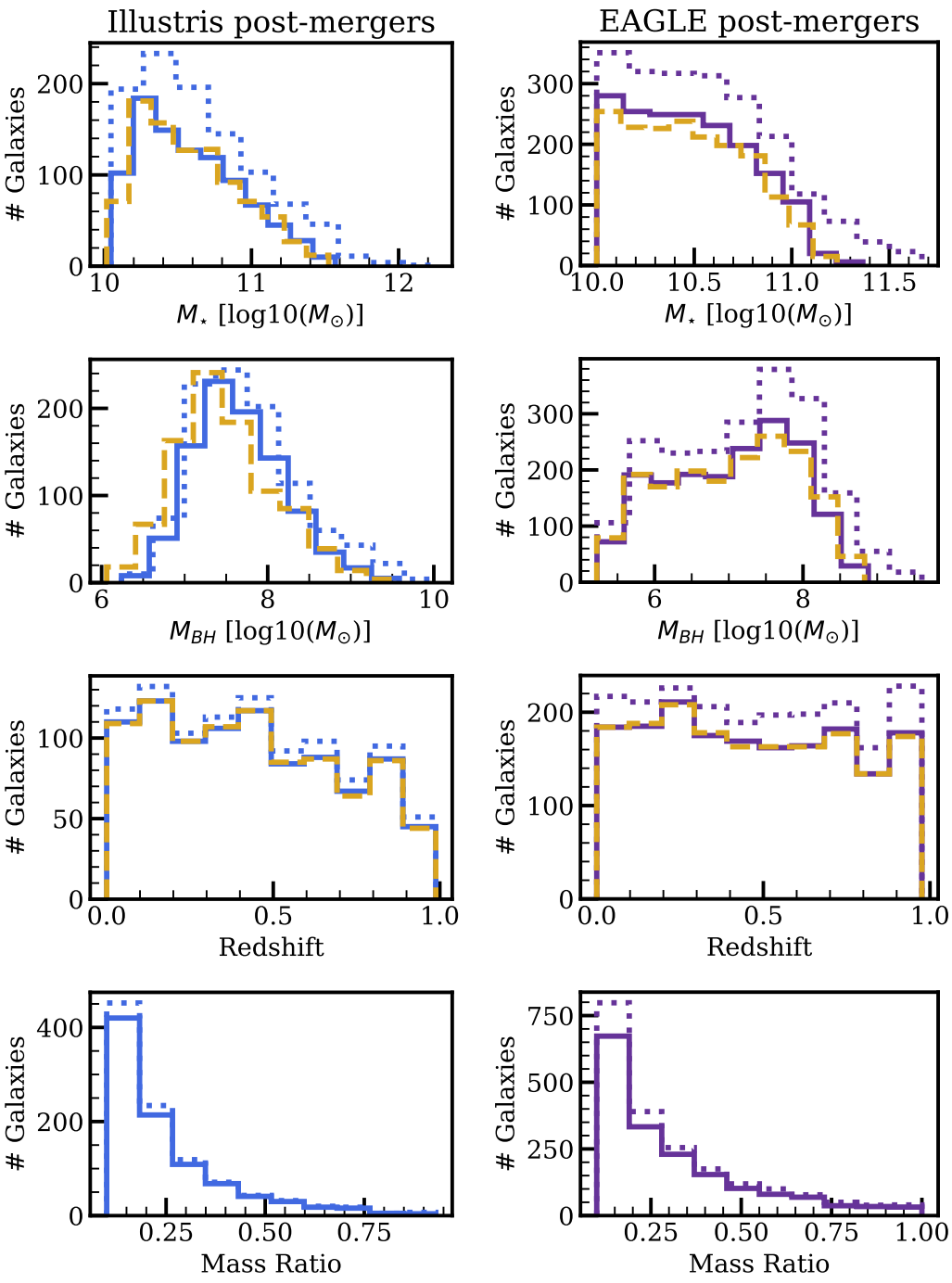

Figure 4.6: Distribution of the total post-merger, matched post-merger, and matched non-merger samples in stellar mass, SMBH mass, redshift, and mass ratio for the Illustris (left) and EAGLE (right) simulations. The dotted line shows the distribution of all the post-mergers. The solid line shows the distribution of the successfully control matched post-mergers. The dashed yellow line shows the successfully control matched non-mergers.

4.3.2 SMBH accretion rate enhancements in Illustris and EAGLE post-mergers

In Figure 4.7, I present a histogram of the accretion rate enhancements, $\Delta\dot{M}_{BH}$, in Illustris (top) and EAGLE (bottom). Both post-merger samples are compared with the distribution of $\Delta\dot{M}_{BH}$ for the respective non-merger samples shown in the yellow dashed lines.

In the top panel of Figure 4.7, I find that Illustris post-mergers have highly enhanced SMBH accretion rates, a median enhancement of 0.69 dex. In addition, the shape of the distribution of the Illustris post-mergers is different from the non-merger sample, with a tail towards larger enhancements. Therefore, in Illustris, post-mergers have on average relatively higher accretion rates compared with controls, and post-mergers are very likely to have enhanced SMBH accretion rates (84% of post-mergers have enhancements).

In the bottom panel of Figure 4.7, I find that post-mergers in EAGLE also demonstrate enhanced SMBH accretion rates, with a median enhancement of 0.31 dex. The median enhancement in EAGLE is very similar to the median enhancement from TNG, which was $\sim$0.29 dex for the averaged SMBH accretion rates. However, post-mergers in EAGLE are less likely overall to have a positive enhancement compared with TNG, where only 62% of EAGLE post-mergers demonstrate positive $\Delta\dot{M}_{BH}$.

Comparing the results of Illustris and EAGLE with TNG, I demonstrate that all three cosmological simulations qualitatively agree; post-mergers have, on average, relatively enhanced accretion rates. The quantitative differences suggest that Illustris has the strongest enhancement of SMBH accretion rates from the merger, and that EAGLE produces comparable results to TNG. One possible explanation for the large enhancement in Illustris, compared with TNG and EAGLE, is that the AGN feedback model may be less effective at regulating SMBH accretion rate. Vogelsberger et al. (2014b) comment that the feedback mode responsible for quenching in Illustris, the 'bubble' mode feedback, does not provide sufficient effective feedback which leads to a slight overabundance of massive and star forming galaxies.

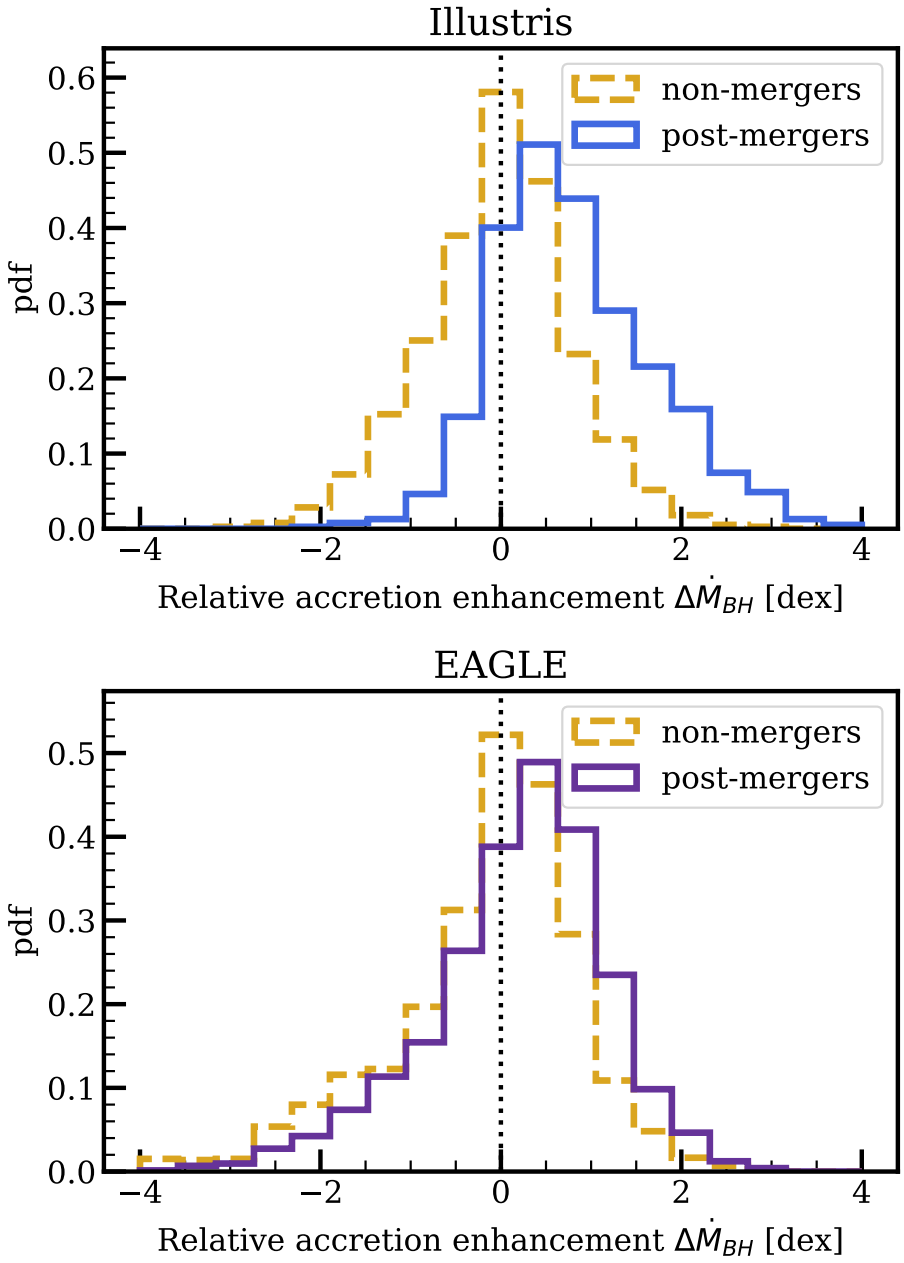

Figure 4.7: Histogram of accretion rate enhancements for the post-merger population and non-merger populations in Illustris (top) and EAGLE (bottom). Post-mergers are represented with the solid line, and non-mergers are represented with the dashed yellow line.

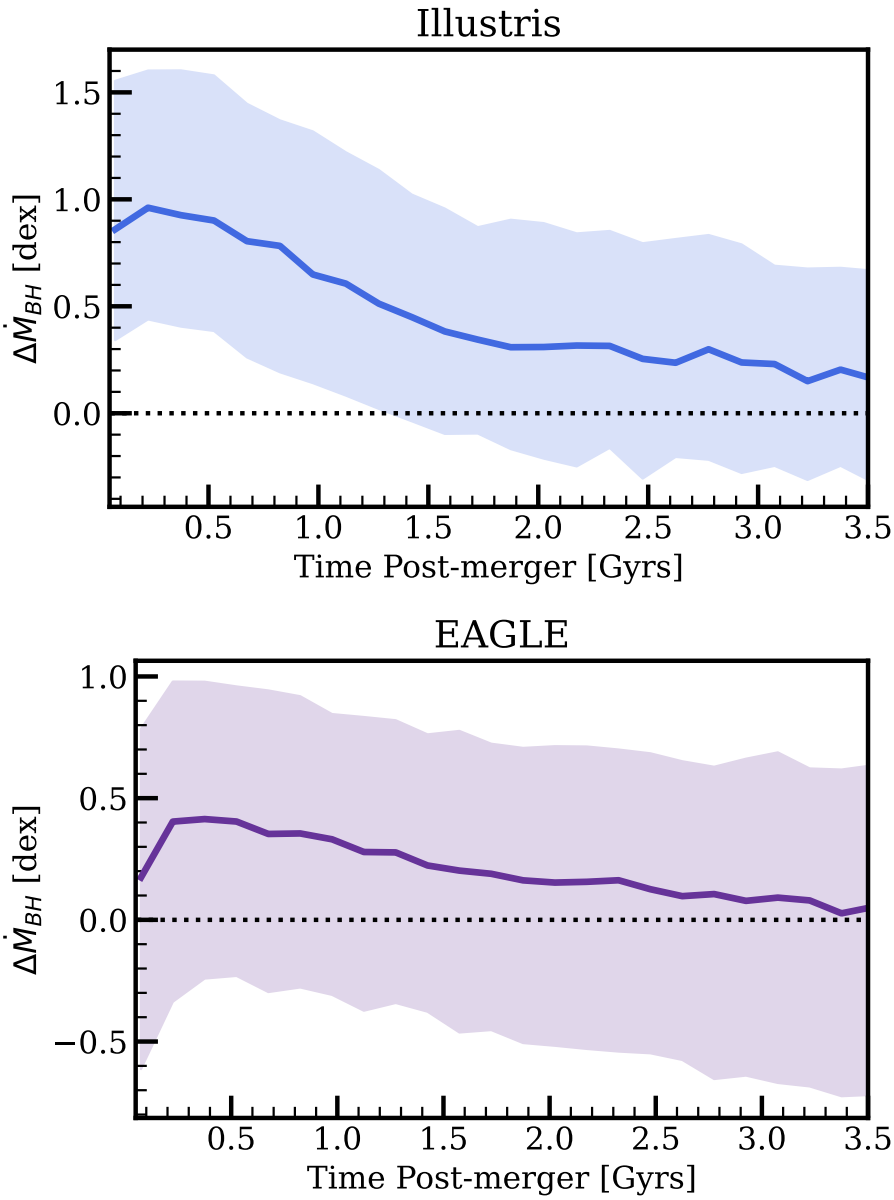

Figure 4.8: Running median of the SMBH accretion rate enhancements as a function of time post-merger. The error of the shaded region represents the 25th and 75th percentiles associated with the median at that time post-merger.

4.3.3 Timescale of population averaged SMBH accretion rate enhancements in Illustris and EAGLE

In Figure 4.8, I present the time evolution of the accretion rate enhancements for Illustris (top) and EAGLE (bottom). Following the experimental set-up discussed in Chapter 3, I re-match post-mergers in the snapshots after the merger and re-calculate $\Delta\dot{M}_{BH}$.

For Illustris, shown in the top panel of Figure 4.8, I find that the accretion rates for post-mergers are enhanced at levels exceeding $\Delta\dot{M}_{BH} > 0.2$ dex for approximately 2 Gyrs, the timescale for population averaged enhancements in TNG. However, the accretion rate of Illustris post-mergers never 'return' to accretion rates comparable to controls galaxies of the same stellar mass, gas mass, and environment. It is possible that the behaviour in Illustris is a result of post-mergers with larger SMBH masses than their matched controls (recall Figure 4.6). Since the accretion rate is proportional to the SMBH mass, a bias of higher SMBH mass in post-mergers would result in higher accretion rates. In Section 4.4, I explicitly investigate such a scenario and apply SMBH mass matching to the fiducial matching scheme.

In EAGLE, shown in the bottom panel of Figure 4.8, I observe a similar behaviour. Population averaged SMBH accretion rate enhancements are long lived, up to 3 Gyrs after the merger. The timescale is slightly longer compared with the 2 Gyr timescale for TNG. I speculate that the longer timescale in EAGLE may have to do with AGN feedback modes once again. Recall from Figure 4.2 that in TNG the accretion rates of SMBHs with kinetic mode feedback are typically orders of magnitude lower than the radiative mode feedback. I propose that in TNG, once a post-merger has an SMBH accretion rate sufficiently low (or SMBH mass sufficiently high), the onset of strong kinetic mode feedback efficiently and quickly evacuates the gas in the region surrounding the SMBH. In EAGLE, the effective AGN feedback works intermittently, and therefore the enhancement to the central gas density may be more slowly disrupted by recurring AGN feedback events.

To summarize, Figure 4.8 demonstrates that SMBH accretion rate enhancements are long lasting in TNG, Illustris, and EAGLE. However, Figure 4.8 also demonstrates differences between the simulations in the evolution of the population averaged enhancement over time post-merger. I refer the reader to Section 4.4.2, where the differences between TNG, Illustris, and EAGLE are discussed in further detail and with the added context of the effects of SMBH mass matching.

4.3.4 What fraction of mergers 'trigger' an AGN in Illustris and EAGLE?

Finally, I repeat the experiment from Section 3.3.2, which investigates the incidence of AGN events in the post-merger sample, using the post-merger samples from Illustris and EAGLE. Figure 4.9 shows the results of the experiment, where the fraction of post-mergers that undergo an AGN phase within 500 Myrs of the merger is shown on the top panels, and the fractional excess is shown on the bottom panel.

In Illustris, shown in Figure 4.9 in blue, I find a fractional excess of AGN events in the post-mergers over nearly the entire accretion rate range, with a maximum excess of ~ 2. An excess of post-mergers at most SMBH accretion rates is compatible with the result of Figure 4.7, which found that post-mergers are very likely to have enhanced accretion rates (~ 80 % have accretion rate enhancements). Furthermore, the AGN fractional excess in Illustris demonstrates a luminosity dependence beginning around $L_{bol} \sim 10^{41}$ erg/s. Therefore, Illustris post-mergers are more likely to experience a high accretion rate event, which yields a luminosity dependent post-merger excess, with at most 2 times as many post-mergers to non-mergers.

I find a similar excess of high accretion rate events in post-mergers in EAGLE, shown in Figure 4.9 in purple. However, unlike Illustris, the difference in the percentage of post-mergers that experience high accretion rate events compared with non-mergers is less significant at lower accretion rates. Recall from Figure 4.7, in EAGLE, despite a population averaged enhancement, post-mergers were only slightly more likely to have an enhanced accretion rate compared with controls (~ 60 %). Therefore EAGLE post-mergers only show a modest fractional excess over the majority of the SMBH accretion rate range. However, similar to Illustris and TNG, EAGLE post-mergers demonstrate a significant luminosity dependence in the fractional excess, beginning around $L_{bol} \sim 10^{42}$ erg/s. For the highest luminoisities ($L_{bol} > 10^{44}$ erg/s), there are as many as 2-4 times more post-mergers than non-mergers. The fractional excess of AGN I find in post-mergers from EAGLE is similar to the result of McAlpine et al. (2020) who conduct a similar experiment looking at the excess of AGN in mergers and pairs in EAGLE. I find a slightly higher excess of AGN in post-mergers, which may be attributed to different methodology. I observe the post-mergers for 500 Myrs after the merger event and count any instance of $\dot{M}_{BH} > \dot{M}_{BH}^{cutoff}$ as an 'AGN event', whereas McAlpine et al. (2020) define an AGN as a bolometric luminosity in excess of $L_{bol} > 10^{43}$ erg/s.

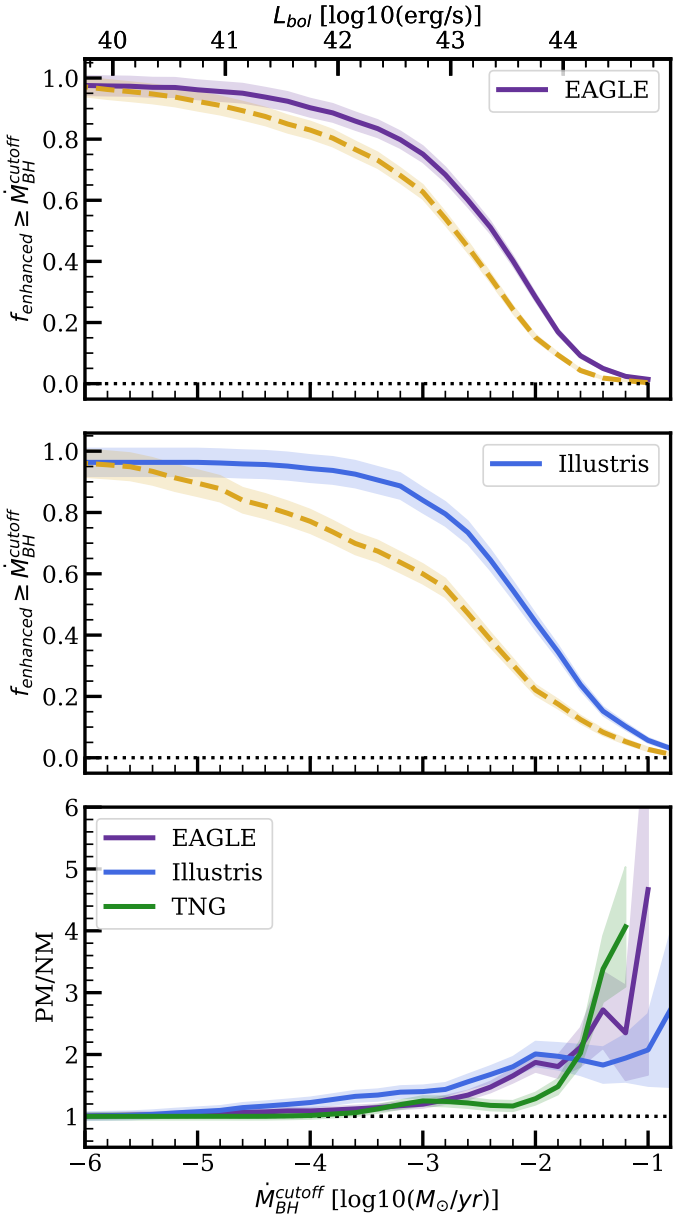

Figure 4.9: The top and middle panels show the fraction of galaxies that have an SMBH accretion rate at or higher than $\dot{M}_{BH}^{cutoff}$ within a period of 500 Myrs, relative to the total number of galaxies, for Illustris (top) and EAGLE (middle). The solid line corresponds to the post-merger sample and the yellow dashed line is the non-merger sample, as defined in Section 2.3. The top x-axis of the Figure shows the corresponding AGN luminosity. The bottom panel shows the ratio of the fraction of post-merger galaxies to non-merger galaxies for Illustris (blue), EAGLE (purple), and TNG (green). This is the fractional excess of post-mergers that have an accretion rate at or higher than the cutoff relative to the non-merger sample. The error in the shaded region is the Poisson error reflecting the number of galaxies.

Overall, comparing the results of Illustris and EAGLE to TNG, I find that all three simulations qualitatively agree, demonstrating an increasing fractional excess with increasing luminosity. However, each simulation predicts a slightly different maximum fractional excess, ranging from a factor 2-4. In all three simulations, I find that post-mergers are more likely to undergo an 'AGN' event compared with non-mergers, and that there is the highest fractional excess in the highest luminosity AGN.

4.4 Effect of SMBH mass matching

In the previous section, I briefly commented on the possible presence of a SMBH mass offset in the post-mergers and control galaxies. In particular, the panel of SMBH masses in Illustris from Figure 4.6 suggests that Illustris post-mergers may have significantly different SMBH masses than their non-merger comparisons. In the following section, I will investigate how SMBH mass matching affects the main results of the research presented here by explicitly testing the difference in results when applying moderate and strict SMBH mass matching.

In the fiducial experiments in TNG, Illustris, and EAGLE, the post-merger galaxies are compared with non-mergers and controls at the same redshift, with a comparable stellar mass, gas mass, and environment. The motivation for matching in the above properties is to isolate the differences in the SMBH accretion in a post-merger that is due to the merger event, removing spurious results that result from comparing very different types of galaxies. However, it is less obvious whether or not one should include SMBH mass matching in the experiment. In one case, the merger event may result in post-mergers with larger than average SMBH masses, either from enhanced SMBH accretion rates or from the merger of the SMBHs, and enforcing a match in SMBH mass may select abnormal control galaxies (i.e. galaxies with an SMBH mass that is not typical for a non-merger galaxy of that stellar mass, gas mass, environment, etc.). On the other hand, recall from Section 2.1 that SMBH accretion rate is calculated from the simulations using a Bondi-Hoyle-Lyttleton subgrid recipe. The Bondi subrid model calculates the accretion rate as a function of the gas properties surrounding the SMBH (density and local sound speed) as well as a function of the SMBH mass, where $\dot{M}_{BH} \propto M_{BH}^2$. Therefore, the SMBH accretion rate in any galaxy will be very sensitive to changes in the SMBH mass. It is therefore important to understand the difference in SMBH mass between post-mergers and controls in or-

der to distinguish between enhancements in accretion rate that are a result of higher than average feeding vs. enhancements due to post-mergers having characteristically higher SMBH masses than controls.

In the following section, I perform tests where I modify the fiducial matching scheme to include SMBH mass matching. However, I do not wish to enforce an extremely strict match in SMBH mass, as the error tolerance on SMBH mass also significantly decreases the successfully matched post-merger sample size. In order to select an SMBH mass matching tolerance that is sufficient for the purposes of the following experiment, I calculate how the SMBH accretion rate enhancement depends on the difference between post-merger and control SMBH mass. I set up an idealized scenario in which a post-merger and control differ exclusively in SMBH mass (assuming the exact same density and local sound speed). Using the Bondi subgrid model, Eq. 2.1, I construct an equation for the relative enhancement in accretion rate as a function of the SMBH masses,

$$\Delta\dot{M}_{BH} = \log_{10}\Big(\frac{\dot{M}_{BH\,1}}{\dot{M}_{BH\,2}}\Big) = 2\log_{10}\Big(\frac{M_{BH\,1}}{M_{BH\,2}}\Big) = 2\Delta M_{BH}$$

where the factor 2 comes from $\dot{M}_{Bondi} \propto M_{BH}^2$. I find that, under the ideal assumption of *only* a difference in SMBH mass, the accretion rate enhancement will be equal to twice the offset in SMBH mass in dex. Considering the median $\Delta\dot{M}_{BH}$ for the instantaneous accretion rates in TNG was ~ 0.23 dex, an SMBH mass matching tolerance of $\Delta M_{BH} < 0.1$ dex is required. I therefore compare three matching schemes for each simulation. The first is the fiducial matching in which no SMBH mass matching is applied. The second matching scheme applies an intermediate mass matching with a base error tolerance of $\Delta M_{BH} < 0.1$ dex which can be increased 4 times by an additional 0.1 dex for a maximum $\Delta M_{BH} < 0.5$ dex. The final matching scheme applies a base error tolerance of $\Delta M_{BH} < 0.05$ dex which can be increased up to 4 times by an additional 0.01 dex for a maximum $\Delta M_{BH} < 0.1$ dex (technically $\Delta M_{BH} < 0.09$ dex).

4.4.1 SMBH mass matching: effect on $\Delta\dot{M}_{BH}$ in post-merger samples

The results for the three matching schemes are tabulated in Table 4.2, where I quote the number of successfully matched post-mergers and the median SMBH accretion

ΔM_{BH} [dex]	**matched post-mergers**	**median $\Delta\dot{M}_{BH}$ [dex]**	**simulation**
no match	1056	0.29	TNG
0.5	1056	0.29	TNG
0.1	705	0.27	TNG
no match	925	0.69	Illustris
0.5	905	0.57	Illustris
0.1	614	0.60	Illustris
no match	1744	0.31	EAGLE
0.5	1641	0.30	EAGLE
0.1	595	0.34	EAGLE

Table 4.2: Comparison of SMBH accretion rate enhancements for TNG, Illustris, and EAGLE for three matching schemes: no SMBH mass matching, $\Delta M_{BH} < 0.5$ dex, and $\Delta M_{BH} < 0.1$ dex.

rate enhancement for the post-merger sample. In addition, in Figure 4.10, I plot the offset between the SMBH mass of post-mergers and matched controls for each of the three matching schemes, where the median offset in SMBH mass is quoted in the legend.

From Table 4.2, I find that in all three simulations, the majority of post-mergers that are matched in the fiducial model are also matched in the $\Delta M_{BH} < 0.5$ dex model. However, a similar number of matched post-mergers does not mean that the majority of post-mergers are matched to controls within 0.5 dex in SMBH mass without explicit black hole mass matching, since the control matching algorithm may identify different controls. In fact, Figure 4.10 demonstrates that without explicit SMBH mass matching, Illustris and EAGLE have a non-negligible amount of post-mergers with SMBH mass offsets exceeding 0.5 dex.

In TNG and EAGLE, I find that the median $\Delta\dot{M}_{BH}$ is nearly identical between the fiducial and $\Delta M_{BH} < 0.5$ dex matching schemes. For TNG post-mergers in Figure 4.10 shown in green, the top and middle panels demonstrate that the median offset between the post-merger and control SMBH mass is nearly the same for the fiducial and $\Delta M_{BH} < 0.5$ dex schemes, and that without explicit SMBH mass matching the majority of post-mergers are matched in SMBH mass to within 0.5 dex. Therefore, I conclude the SMBH accretion rate enhancements are similar due to the majority of controls remaining the same. In contrast, EAGLE demonstrates a large number of largely offset SMBH masses, suggesting that SMBH mass in EAGLE is not strongly constrained by the other fiducial matching parameters, resulting in SMBH mass offsets

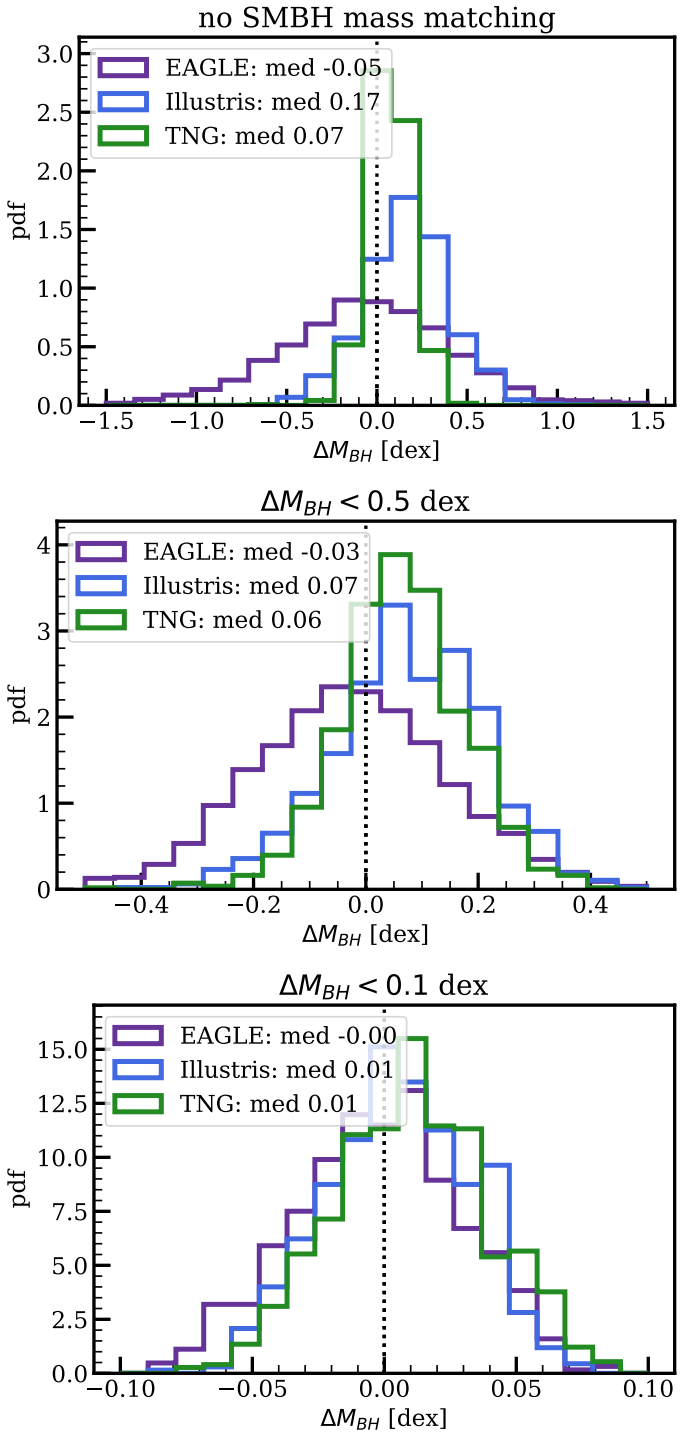

Figure 4.10: The offset between the SMBH mass of the post-mergers and matched controls for the three matching schemes: no SMBH mass matching (top), $\Delta M_{BH} < 0.5$ dex (middle), and $\Delta M_{BH} < 0.1$ dex (bottom).

sometimes exceeding 1 dex. However, the distribution is not significantly biased towards larger or smaller SMBH masses, which contributes to the stability of the median SMBH accretion rate enhancement for EAGLE post-mergers.

There is a significant change in Illustris between the fiducial and $\Delta M_{BH} < 0.5$ dex schemes, where the median enhancement decreases from 0.69 dex to 0.57 dex. Figure 4.10 demonstrates that without SMBH mass matching, post-mergers in Illustris are systematically matched to lower SMBH mass controls. The result suggests that in Illustris, post-mergers have an abnormally large SMBH mass, consistent with a strong enhancement in SMBH accretion rate that may significantly grow post-merger SMBHs.

Applying the strictest SMBH mass matching scheme, I find a significant decrease in the post-merger sample size, most dramatically in EAGLE. The large decrease in matched post-mergers in EAGLE may, in part, be due to post-mergers having larger SMBHs, making them difficult to control match with non-merger galaxies. However, I find that it is difficult, in general, to simultaneously match in all the fiducial parameters and introduce strict SMBH mass matching in EAGLE, with just as many of the non-merger sample of galaxies ($\sim$ 1000) failing to find 5 or more controls within error tolerances. Despite a significant drop in the number of matched post-mergers, I find that in all of the simulations the post-merger population still demonstrates enhanced SMBH accretion rates compared with controls when strictly matching in SMBH mass.

4.4.2 SMBH mass matching: effect on timescale of SMBH accretion rate enhancements

Finally, I explore how SMBH mass matching may affect the timescale of population averaged accretion rate enhancements. Figure 4.11 shows the timescale of SMBH accretion rate enhancements using the fiducial matching scheme (solid line), matching SMBH mass within $\Delta M_{BH} < 0.5$ dex (dashed line), and matching within $\Delta M_{BH} < 0.1$ dex (dash-dot line). Beginning with Illustris, I remind the reader that the enhancement of SMBH accretion rates in the fiducial matching scheme persists beyond 3 Gyrs from the merger event. Introducing progressively stricter matching in SMBH mass, I find that the accretion rates in post-mergers 'return to normal' around 2-3 Gyrs after the merger. I therefore determine that the prolonged enhancement in Illustris post-mergers was due to post-mergers having larger SMBH masses than con-

trols. In EAGLE and TNG, I find that all three matching schemes demonstrate similar time evolution. For the strictest matching scheme, despite the significant reduction in the number of matched post-mergers in EAGLE, I find that the timescale is very compatible with the timescale of the full sample. Therefore, all three simulations demonstrate, within the strictest tolerances in SMBH mass, that there exists a long lived enhancement in the accretion rate.

In Figure 4.11, I also find that there are notable differences between the time evolution of the accretion rate enhancements in Illustris, EAGLE, and TNG. First of all, TNG has a significantly smaller range of $\Delta\dot{M}_{BH}$ compared with Illustris and EAGLE, most noticeable in the distribution of the 25th and 75th percentiles shown in the shaded area. The smaller range in accretion rate enhancements in TNG is due to the feedback mode matching implemented in TNG. Recall from Figure 4.2 that the bimodal distribution in accretion rate in TNG corresponds to the two feedback modes. Applying feedback mode matching in TNG significantly reduces the range of SMBH accretion rates from which controls may be selected.

The second notable difference from Figure 4.11 between Illustris and EAGLE, compared with TNG, is in the behaviour immediately after the merger. In TNG, the highest accretion rate enhancement occurs at coalescence, and there is a decline in the median accretion rate enhancement from 0.3 dex to $\sim$ 0.05 dex in the first Gyr. In comparison, both Illustris and EAGLE show evidence for a peak accretion rate enhancement slightly after the merger. I note that the evidence of a delay in peak accretion rate enhancement in Illustris is much weaker than in EAGLE. In Illustris, the dip in the running median between coalescence and the first few hundred Myrs is comparable to the variation seen at other time post-merger bins, such as around 1.25 Gyrs. There is, however, more significant evidence in EAGLE that the accretion rate enhancement is strongest a few hundred Myrs after coalescence. A possible explanation for the delayed peak enhancement in EAGLE may be the higher temporal resolution ($\sim$ 60 Myrs between snipshots).

Finally, comparing the Illustris and EAGLE simulations to TNG, I find that Illustris and EAGLE have a stronger population averaged enhancements. At around 1 Gyr, Illustris and EAGLE have population averaged enhancements around $\sim$ 0.2-0.3 dex, compared to $\sim$ 0.05 at 1 Gyr for TNG. Therefore, even though EAGLE and TNG appear to have a similar enhancement in SMBH accretion rates in the immediate post-merger sample (around 0.3 dex), looking at the accretion rate enhancements over time demonstrates relatively stronger and longer lived enhancements in EAGLE.

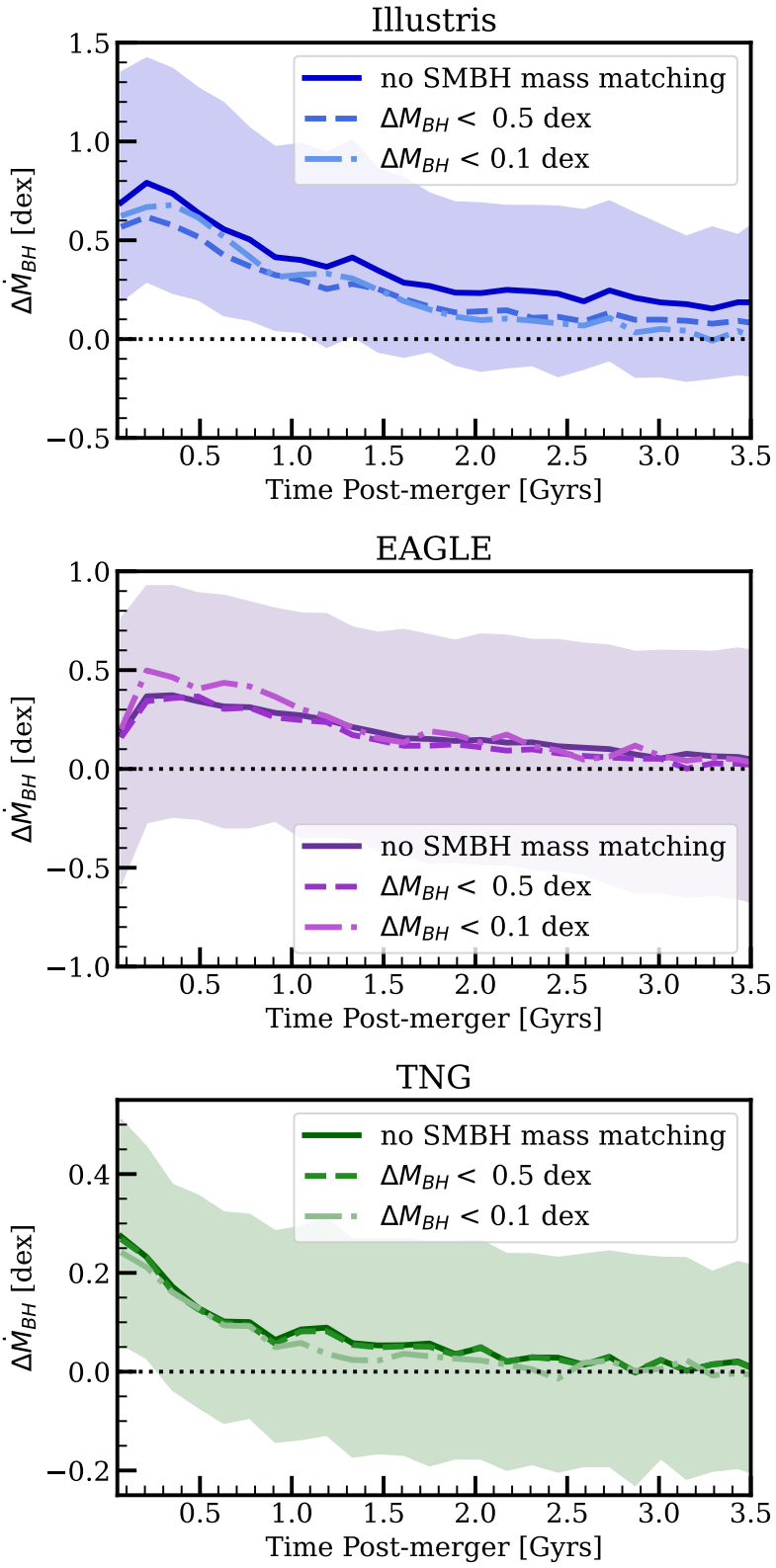

Figure 4.11: Time evolution of post-mergers $\Delta \dot{M}_{BH}$, comparing control matching schemes with no SMBH mass matching (solid line with shaded 25th and 75th percentiles), matching SMBH mass to within 0.5 dex (dashed line), and matching SMBH mass to within 0.1 dex (dash-dot line).

Chapter 5

Discussion and Concluding Remarks

5.1 Summary of results

In the research presented here, my aim was to investigate what modern cosmological scale simulations predict for an AGN-merger connection. In my research, I utilize the large and representative samples of post-mergers from cosmological simulations to perform a study of SMBH accretion rates within a diverse merger population. Through studying a population of mergers with a large range of galaxy properties and merger conditions, I answer questions such as: Do post-mergers, on average, demonstrate a significant enhancement in SMBH accretion rate? Do most post-mergers have enhanced SMBH accretion rates, and are there specific galaxy or merger properties that are more likely to generate SMBH enhancements? How much more likely are post-mergers to have an AGN, and how much do recent mergers contribute to the overall AGN population in the simulations?

In order to answer such questions, I select post-mergers, within redshift 0 to 1, from the cosmological simulations TNG, Illustris, and EAGLE. I apply a minimum stellar mass of $10^{10} M_{\odot}$ for resolution considerations and make additional selection cuts to ensure reliable measurements of stellar mass and SMBH accretion rate. I select control comparisons for each post-merger that represent a 'typical' galaxy of the same stellar mass, gas mass, and environment (and feedback type in TNG) that have not undergone a merger of stellar mass ratio at least 1:10 within the last 2 Gyrs. Using the matched controls, I quantitatively compare the SMBH accretion

rate of post-mergers with controls using the parameter $\Delta\dot{M}_{BH}$ (see Eq. 2.5), where a positive value indicates higher SMBH accretion rates than controls.

In all three simulations, I find that post-mergers demonstrate, on average, accretion rate enhancements (see Figures 3.1 and 4.7). I find a median SMBH accretion rates enhancement around 0.2-0.3 dex, or 1.5 to 2 times higher accretion rates than controls, in TNG and EAGLE. In Illustris, post-mergers have a median enhancement around 0.6-0.7 dex, or 4-5 times higher. I also demonstrate that not all post-mergers have SMBH accretion rates higher than controls, with zero or negative $\Delta\dot{M}_{BH}$ in $\sim 20\%$ of Illustris post-mergers, $\sim 30\%$ in TNG, and $\sim 40\%$ in EAGLE. Therefore, I demonstrate that most post-mergers have enhanced SMBH accretion rates, for the simulation snapshot immediately post-coalescence, when compared with controls.

In the TNG simulation, Figure 3.4 demonstrates that the strength of the accretion rate enhancement depends on gas mass and gas fraction, such that the gas poor/low gas fraction post-mergers are more likely to have average or below-average SMBH accretion rates, relative to controls. On the other hand, non-merger galaxies with high gas mass and gas fractions do not have higher SMBH accretion rates than their matched controls, demonstrating that it is a combination of a merger event and the presence of a significant amount of gas that allows for enhanced SMBH accretion rates in post-mergers.

In Section 3.2, I investigated the connection, in TNG, between post-mergers that demonstrate enhanced SMBH accretion and post-mergers that demonstrate enhanced star formation rate, finding that most post-mergers $> 50\%$ do not demonstrate co-incident enhancements in SMBH accretion rate and star formation rate, and that the strength of the two enhancements are, at best, weakly correlated (coefficient 0.28) within the first few hundred Myrs of coalescence. However, in Figure 3.8 I show that there is a both a significant correlation (coefficient 0.47) and a co-incident enhancement in the majority ($\sim 76\%$) of gas rich major mergers.

In all three simulations, I find that post-merger galaxies, on average, demonstrate sustained SMBH accretion rate enhancements for up to 2 to 3 Gyrs after coalescence (shown in Figures 3.6 and 4.8). Therefore, my results suggest that merger events may continue to influence SMBH accretion rates for many Gyrs beyond the immediate coalescence phase.

In Figures 3.11 and 4.9 I demonstrate that post-mergers are more likely to experience a high accretion rate event within 500 Myrs post-coalescence than non-merger galaxies within 500 Myrs of secular evolution. All three simulations demonstrate a

luminosity dependence in the fractional excess of post-mergers that experience an 'AGN phase', demonstrating that post-mergers are up to 2 to 4 times more likely to host the highest luminosity AGN. Finally, in Figure 3.12, I find that despite the higher likelihood that mergers host high luminosity AGN, the majority of high luminosity AGN in TNG ($\sim$ 90% at $L_{bol} > 10^{45}$erg/s) are not recent mergers (of stellar mass ratio > 1:10). Therefore, my results demonstrate that post-mergers are more likely to have AGN, but the majority of AGN are not recent mergers.

5.2 AGN-merger connection in simulations revisited

Now that the results of the research presented here have been outlined, I revisit the predictions from previous binary and cosmological simulations of mergers and AGN, and ask how the results of my work compare with the current and emerging picture for a simulated AGN-merger connection.

The first result of my research, the population averaged enhancement of SMBH accretion rate in post-merger galaxies (shown in Figures 3.1 and 4.7), demonstrates that the foundation for an AGN-merger connection is broadly applicable to a cosmological post-merger population. It is not obvious that there would be a population averaged signal of enhanced SMBH accretion rates in post-mergers. In fact, the results of my research also demonstrate that there is a large variation on a galaxy by galaxy basis, and that not all post-mergers show enhanced SMBH accretion rates in the snapshot immediately after coalescence. If post-mergers with enhanced SMBH accretion rates were rare, a large diverse sample of post-mergers would not have an averaged enhancement. Instead, I find that the majority (> 50%) of post-mergers, in all three cosmological simulations studied, have SMBH accretion rates higher than matched controls.

Furthermore, it is possible that temporal resolution and stochasticity contribute to the $\sim$ 20-40% (depending on the simulation) of post-mergers which do not show enhanced accretion rates. Stochasticity contributes to non-zero values in $\Delta\dot{M}_{BH}$ that are unrelated to a merger process, as demonstrated in the non-merger sample of Figure 3.1. In the case of temporal resolution, merger triggered enhancements to SMBH accretion may occur in the interval of time between snapshots, but are not represented in the calculation of $\Delta\dot{M}_{BH}$. Therefore, my result demonstrates that

despite the expected noise level due to stochasticity and the temporal constraint (both of which are also relevant in observations), the majority of mergers still demonstrate enhancements in SMBH accretion rate.

Returning to the variation on a galaxy by galaxy basis, it has been demonstrated in hydrodynamic simulations (Mihos and Hernquist 1996; Di Matteo et al. 2007; Capelo and Dotti 2016) that the strength of merger induced inflows will depend on various merger and galaxy properties, such as the availability of gas, the orbital configuration, or the initial morphologies of merging galaxies. In the work presented here, I demonstrate that, in TNG, the post-merger characteristic that is most influential for SMBH accretion rate enhancements is the gas mass and gas fraction. I reiterate that in comparison with previous works, it is important to note that I consider the dependence on the post-coalescence gas, rather than the initial gas of the merging system. For example, the post-coalescence gas does not represent the change in gas content (relative to pre-merger state) which has been shown to be relatively unimportant in the strength of merger induced gas flows (Di Matteo et al. 2007).

I further note that the dependence of SMBH accretion strength on gas fraction shown in Figure 3.4 is predominantly in the range of $0.01 < f_{gas} < 0.1$, corresponding to $M_\star/M_{gas}$ ratios around 100:1 to 10:1, a lower range than is studied in suites of disk mergers (e.g. Capelo et al. 2015). In the regime of higher gas fractions, $f_{gas} > 0.1$, I do not find a strong dependence with the accretion enhancement strength, suggesting that enhancement strength depends on a sufficient amount of gas, but is not necessarily strongest in the post-mergers with the highest gas fractions.

Additionally, in contrast to Capelo et al. (2015), I do not find the merger (stellar) mass ratio to be a good predictor of the relative strength of the SMBH accretion rate enhancement. Such a tension may once again be influenced by stochasticity and temporal resolution, since the SMBH accretion rate of major mergers immediately post-coalescence does not capture the full effect of the merger on SMBH accretion rates over the coalescence window. However, my result may instead demonstrate that mass ratio is not the dominant factor influencing the strength of SMBH accretion rate enhancements in a diverse population of mergers where the gas mass, orbital configurations, and morphology are not held constant. In fact, I investigate the combination of merger mass ratio and post-merger gas mass in Figure 3.10, and find that, enhancement in SMBH accretion rate occur most reliably in gas-rich major mergers (89% have enhanced SMBH accretion rate), compared with 68% of gas-rich minor mergers, 71% of gas-poor major mergers, and 61% of gas-poor minor mergers.

I therefore find that it is the combination of sufficient gas (in the post-merger) and a high merger mass ratio that results in the overwhelming majority of post-mergers having enhanced SMBH accretion rates.

A surprising result of my research is the long-lived enhancements in SMBH accretion rate. In fact, at face value, my result may seem at odds with the expected short-lived burst of high SMBH accretion rate shown in previous works (see Figure 1.7 from Hopkins et al. 2008; Capelo et al. 2015; Volonteri et al. 2015b; Capelo and Dotti 2016). However, there are important differences in the methodology of my experiment that affects the interpretation of my result and comparison with previous works. In Figure 3.1, I re-match the post-mergers (i.e. re-select suitable controls within the error tolerances) in the snapshots following coalescence. For each subsequent snapshot, a single post-merger may have enhanced, normal, or suppressed SMBH accretion rates however the population average in the post-mergers remains enhanced over a long timescale. Therefore, my experiment demonstrates the timescale over which the post-merger population becomes indistinguishable from the control population, in SMBH accretion rate.

The long-lived enhancements of SMBH accretion rate from my research suggest that a post-merger population may have enhanced SMBH growth and AGN feedback, at subtle levels, up to 2-3 Gyrs after the merger. In TNG, post-mergers have median SMBH accretion rates 0.1 dex, or $\sim$25% higher than controls at 1 Gyr after coalescence. Illustris and EAGLE both have median enhancements of 0.3 dex or $\sim$100% higher than controls after 1 Gyr. It has been demonstrated in EAGLE that despite an enhancement in SMBH accretion in major mergers, the majority of SMBH mass accretion occurs outside of major mergers (McAlpine et al. 2020), which is consistent with the modest (within an order of magnitude) enhancement to SMBH accretion found in the work presented here. However, subtle enhancements over a long period of time would affect the SMBH population of the post-merger population. In fact, a recent study on galaxy mergers in EAGLE cosmological zoom-in simulations by Davies et al. (2022) show evidence for long-lived SMBH accretion rate enhancements, demonstrating that a galaxy undergoing a major merger will have a larger z=0 SMBH mass compared with a similar simulated galaxy that does not undergo a major merger event.

Finally, I comment again on the incidence of high-accretion rate events in post-mergers, and the contribution of post-mergers to the AGN population. In my research, I demonstrate that post-mergers are more likely to have high accretion rates, com-

pared with matched controls, by a factor 2-4. I also demonstrate that post-mergers do not contribute significantly, at most 10-15% in TNG, to the highest luminosity AGN population. My results quantitatively agree well with the incidence of AGN in post-mergers found in EAGLE by McAlpine et al. (2020) and the percent of AGN that are recent mergers in both EAGLE (McAlpine et al. 2020) and Magneticum Pathfinder (Steinborn et al. 2018).

5.2.1 Connection to quenching

Recall from Figure 1.7 that the endpoint of the proposed evolutionary pathway for mergers was an elliptical type galaxy where star formation was rapidly quenched following a period of strong effective AGN feedback. In the work presented here, I have demonstrated that most post-mergers do have enhanced SMBH accretion rates, which will result in an increase in AGN feedback within those post-merger galaxies. I further demonstrate in Figure 3.8 that for TNG post-mergers that are experiencing effective AGN feedback, the star formation rate is lower than control comparisons for the first $\sim$ 500 Myrs. However, Quai et al. (2021) explicitly investigate quenching in post-merger galaxies in TNG and conclude that quenching is rare in post-merger galaxies, but that there is an excess of quenched post-mergers when compared with matched controls. Specifically, Quai et al. (2021) find that post-mergers accelerate quenching within galaxies that were already close to the transition (in TNG) for effective AGN feedback.

The AGN feedback model in TNG is important in reconciling the enhancement of SMBH accretion rates in post-mergers with the rarity of post-mergers that quench rapidly in TNG. In TNG, high SMBH accretion rates are associated with radiative mode feedback. Therefore, although we find post-mergers are more likely to have high SMBH accretion rates, nearly 4 times more likely to have an SMBH accretion rate higher than $0.1 M_{\odot}$/year, all of these post-mergers are using radiative mode AGN feedback. According to the feedback prescription in TNG, if energy is released through the AGN mode that is inefficient at quenching, the high SMBH accretion rates in post-mergers will not promote rapid quenching.

Alternatively, some post-mergers have enhanced SMBH accretion rates but remain in the low accretion rate state. In these post-mergers, the SMBH accretion rate enhancement will increase the amount of effective kinetic mode feedback. This scenario is consistent with the slight excess of quenched post-mergers found in Quai

et al. (2021), where an increase in the effective kinetic mode feedback can speed up quenching in the post-merger galaxies that are predisposed to quench.

Furthermore, it is also possible that the long-lived SMBH accretion rate enhancements found in TNG, Illustris, and EAGLE may have long-term consequences for the star formation rate in the host galaxy. In fact, Davies et al. (2022) find that quenching can be causally connected to a merger event that occurred many Gyrs prior, due to the disruption of the CGM by AGN feedback from the merger event. My research would additionally suggest that SMBH accretion rates, and therefore AGN feedback, remain influenced by a merger event for up to 2-3 Gyrs. Therefore, although most post-mergers do not demonstrate rapid quenching, long-lived enhancements in AGN feedback may promote quenching on longer timescales.

5.3 Insights for observational tensions

In Chapter 1, I commented on the tension that exists in observational studies on the subject of an AGN-merger connection. One of the primary goals of my research was to study AGNs and mergers in a simulation through methodology motivated by observational studies. For example, in many binary simulations (such as Di Matteo et al. 2005; Springel et al. 2005; Capelo et al. 2015), the AGN-merger connection is studied over the full merger timeline. However, observational studies cannot observe the changes in SMBH accretion rate over hundreds of Myrs before and after coalescence. The work presented here takes a more observational approach, looking at whether post-mergers demonstrate an enhanced SMBH accretion rates for a single snapshot (one instance in time) when compared with control galaxies matching the post-merger characteristics.

As mentioned in the previous section, I demonstrate that, despite galaxy by galaxy variation, there is a population averaged enhancement in SMBH accretion rate in post-mergers. In fact, a population averaged signal is in agreement with the many observational studies that find that AGN are more likely to appear in a post-merger or interacting galaxy sample when compared with undisturbed controls (Woods and Geller 2007; Alonso et al. 2007; Koss et al. 2010; Ellison et al. 2011; Ramos Almeida et al. 2012; Ellison et al. 2013; Satyapal et al. 2014; Weston et al. 2017; Hewlett et al. 2017; Ellison et al. 2019b; Gao et al. 2020; Kocevski et al. 2015; Hong et al. 2015; Chiaberge et al. 2015; Marian et al. 2020; Pierce et al. 2022; Rosario et al. 2015; Goulding et al. 2018). Therefore, the results of my research support a scenario where

mergers can trigger AGN.

The work presented here also demonstrates that despite an enhancement in SMBH accretion rates in post-mergers, most luminous AGN are not recent mergers, once again in agreement with many observational studies (Cisternas et al. 2011; Schawinski et al. 2011, 2012; Kocevski et al. 2012; Böhm et al. 2013; Villforth et al. 2014, 2017; Mechtley et al. 2016; Hewlett et al. 2017; Marian et al. 2019; Lambrides et al. 2021), however also in disagreement with some observational studies (Bennert et al. 2008; Bessiere et al. 2012; Treister et al. 2012; Glikman et al. 2015). One caveat to the disagreement with studies such as Treister et al. (2012) and Glikman et al. (2015) is that the highest luminosity in the observed AGN in those observational studies exceed the highest luminosity range that I am able to study in TNG, Illustris, and EAGLE with statistical significance. It is possible that while only 10-15% of AGN of $L_{bol} > 10^{45}$ erg/s are recent mergers, the trend of increased merger significance continues into the highest luminosity AGN, such that mergers become increasingly important for $L_{bol} > 10^{46}$ erg/s. Additionally, my research agrees with observational studies that find a luminosity dependence in the merger fraction of AGN (Schawinski et al. 2012; Pierce et al. 2022), such that the highest luminosity AGN are more likely connected to mergers, but is in disagreement with studies that find the most luminous systems are not more likely to have disturbed morphologies (Villforth et al. 2014; Mechtley et al. 2016; Villforth et al. 2017; Marian et al. 2019).

Finally, in the work presented here, I study the co-incidence of star formation rate and SMBH accretion rate enhancements on a galaxy by galaxy basis. The results of my research demonstrate that, when observing post-mergers for one instance in time, the strength of the star formation rate and SMBH accretion rate enhancements are not correlated, in agreement with simulations by Hickox et al. (2014); Volonteri et al. (2015b). However, I do find a connection between star formation rate and SMBH accretion rate in post-mergers with both a high mass ratio and significant amount of gas, as demonstrated in Figure 3.10. Such a connection may reflect the general preference for AGN to reside in gas rich and star forming galaxies, as demonstrated in simulations (Ward et al. 2022) and observations (Rosario et al. 2013; Bernhard et al. 2016; Ellison et al. 2019a; Jarvis et al. 2020; Shangguan et al. 2020; Xie et al. 2021; Koss et al. 2021). In addition, I demonstrate in Figure 3.10 numerous individual cases where a post-merger may have a strongly enhanced SMBH accretion rate and simultaneously suppressed or normal star formation rate relative to controls. My results are therefore consistent with observations which show that most AGN (not

strictly post-mergers) have typical rates of star formation (Rosario et al. 2013, 2015), although some observations demonstrate higher than normal star formation rates in the highest luminosity AGN (Schweitzer et al. 2006; Lutz et al. 2010; Shao et al. 2010; Santini et al. 2012).

5.4 Limitations

One of the largest challenges in comparing the results of my work to observational studies is the non-trivial connection between the observational definition of AGN and the implementation of AGN in simulations. Full cosmological scale simulations do not resolve many AGN physics processes that are important for AGN selection techniques such as the emission associated with synchrotron processes which are important for the selection of radio AGN. A better comparison with observations would require the relevant processes to be modelled as well as the use of radiative transfer code to generate mock observations (e.g. Blecha et al. 2018), which is challenging on a cosmological sample scale.

Furthermore, in cosmological simulations, enhancements in the central gas density direct relate to AGN activity (feedback) through the SMBH accretion subgrid recipes. However, theoretical models for SMBH accretion disks suggest the processes through which material in the accretion disk loses sufficient angular momentum to fall into the SMBH is quite complicated, and can depend on the local stellar and AGN feedback (Netzer 2015).

Although cosmological simulations provide the advantage of diverse and 'realistic' merger samples, the large scale of cosmological simulations necessitate a loss of resolution. Resolution will no doubt play an extensive role in processes occurring on parsec and subparsec scales such as SMBH accretion, as mentioned in the previous paragraph. However, resolution also has an impact on the subgrid recipes used in cosmological simulations. For example, Sivasankaran et al. (2022) demonstrate in high-resolution simulations of a galaxy merger, including a multiphase ISM and super-Lagrangian refinement surrounding the SMBH, that SMBH accretion rates measured using a Bondi model are even more stochastic, varying orders of magnitude on Myr timescales, due to the accretion of now resolved clumps of gas in the ISM surrounding the SMBH. Another simulation study by Negri and Volonteri (2017) looked at how well a Bondi accretion model, tested over progressively lower resolutions, estimates the 'true' accretion rate from a high-resolution reference simulation. Negri and

Volonteri (2017) demonstrate that the accuracy of the Bondi model is reduced with decreasing resolution. Negri and Volonteri (2017) also find that the accuracy is non-trivially related to how the local density and sound speed is sampled, with certain methods resulting in under or over-estimated accretion rates.

An additional limitation of this work has to do with the implementation of SMBH relocation in cosmological simulations, and the subsequent effect on SMBH accretion and SMBH mergers. Bahé et al. (2022) investigate the effects of SMBH repositioning in simulations using the EAGLE galaxy physics model, and demonstrate that the repositioning of SMBHs to the potential minima can result in significant boosts to SMBH accretion rate due to the increased density at the gravitational potential minima and the reduced relative velocity of the SMBH after repositioning. In addition, SMBH repositioning promotes early SMBH merging as it places the SMBHs of the merging galaxies in close proximity. A higher SMBH mass, due to 'pre-mature' merging, will promote higher accretion rates due to the dependence on SMBH mass in the Bondi model.

Finally, the last limitation to this work concerns the SMBH merger model used in all three cosmological simulations. In combination with the SMBH relocation scheme, SMBH mergers occur promptly in all three simulations. However, it is not well understood the timescale over which SMBH mergers take place, and how the interactions between SMBHs affect the accretion rates and AGN activity. Furthermore, SMBH mergers may further complicate the timescale and delay between processes like starbursts and AGN activity. For example, Ni et al. (2022) demonstrate using the ASTRID cosmological simulations, which do not anchor SMBH particles to the gravitational minima and instead include a subgrid recipe to compensate for unresolved dynamical friction, that there is a delay of ~ 200 Myrs between first close encounter of SMBH pairs and the SMBH merger.

5.5 Future directions

The last topic I wish to discuss is the future directions for the work presented here. In particular, I wish to highlight follow-up projects complimentary to my research.

First, there is the role of minor mergers. Recall from Figure 3.5, that I do not find a strong relationship between the relative SMBH accretion rate enhancement strength and the merger mass ratio. In fact, I find numerous individual cases of highly enhanced SMBH accretion rates in minor mergers (shown in Figure 3.10). In

our Universe, minor mergers are much more common, and if some can produce SMBH accretion rate enhancements of similar strength (up to 100 times higher than matched controls), it is possible that minor mergers may play a significant role in triggering AGN activity. I demonstrate that in TNG most high luminosity AGN are not recent mergers of mass ratio exceeding 1:10, however a follow up experiment to my work would be to investigate how much of a contribution is made by mergers of increasingly smaller mass ratio. In fact, in a suite of high resolution hydrodynamic simulations, Yang et al. (2019) demonstrate AGN luminosities $> 10^{43-44}$ erg/s for minor mergers (mass ratios of 1:10).

Finally, in my research, I have focused on AGN activity in post-mergers. However, a full picture of the connection between AGN and mergers warrants investigation of how AGN activity may be influenced in the pair interactions leading up to coalescence. Once again, I bring back the result that 90% of high luminosity AGN in TNG are not recent mergers. Understanding how much pre-merger interactions contribute to the 'missing 90%' is crucial to determine whether the majority of AGN activity in TNG is unrelated to galaxy interactions. In fact, Prieto et al. (2021) demonstrate in parsec scale simulations that pericentre interactions leading up to a merger can result in near Eddington rate SMBH accretion. In addition, a follow up study on the role of pair interactions will investigate how the diversity in the merging galaxy characteristics affect SMBH accretion rates. For example, I demonstrate the importance of post-merger gas mass in determining the strength of SMBH accretion rate enhancement. However future works can investigate, on a cosmological scale, the importance of the initial gas content of the merging pairs.

5.6 Concluding remarks

In the research presented here, I look at the connection between enhanced SMBH accretion rates and post-merger galaxies in cosmological simulations IllustrisTNG, Illustris, and EAGLE. I find that post-mergers have a population averaged enhancement in all three simulations, supporting the scenario where mergers can trigger AGN, and in agreement with observational studies finding that post-mergers are more likely to host AGN. The population averaged enhancements are long-lived, suggesting that the merger event influences SMBH accretion and AGN feedback up to 2-3 Gyrs after coalescence. I also demonstrate the significant variation of SMBH accretion rate enhancement on a galaxy by galaxy basis, where most (>50%) but not all (exclud-

ing 20-40%) post-mergers have enhanced accretion rates, highlighting that enhanced SMBH accretion rate is not ubiquitous in the post-merger sample. Finally, I find that the majority of high luminosity AGN in TNG are not recent mergers (of stellar mass ratio $>$ 1:10), in support of observational studies that find mergers do not majorly contribute to the AGN population.

Bibliography

Alonso, M. S., Lambas, D. G., Tissera, P., and Coldwell, G. (2007). Active galactic nuclei and galaxy interactions. *Monthly Notices of the Royal Astronomical Society*, 375(3):1017–1024.

Antonucci, R. (1993). Unified models for active galactic nuclei and quasars. *Annual Review of Astronomy and Astrophysics*, 31:473–521.

Bahé, Y. M., Schaye, J., Schaller, M., Bower, R. G., Borrow, J., Chaikin, E., Kugel, R., Nobels, F., and Ploeckinger, S. (2022). The importance of black hole repositioning for galaxy formation simulations. *Monthly Notices of the Royal Astronomical Society*.

Baldry, I. K., Glazebrook, K., Brinkmann, J., Ivezić, Ž., Lupton, R. H., Nichol, R. C., and Szalay, A. S. (2004). Quantifying the Bimodal Color-Magnitude Distribution of Galaxies. *The Astrophysical Journal*, 600(2):681–694.

Barnes, J. E. and Hernquist, L. E. (1991). Fueling Starburst Galaxies with Gas-rich Mergers. *The Astrophysical Journal Letters*, 370:L65.

Barton, E. J., Geller, M. J., and Kenyon, S. J. (2000). Tidally Triggered Star Formation in Close Pairs of Galaxies. *The Astrophysical Journal*, 530(2):660–679.

Baugh, C. M., Lacey, C. G., Frenk, C. S., Granato, G. L., Silva, L., Bressan, A., Benson, A. J., and Cole, S. (2005). Can the faint submillimetre galaxies be explained in the Λ cold dark matter model? *Monthly Notices of the Royal Astronomical Society*, 356(3):1191–1200.

Bennert, N., Canalizo, G., Jungwiert, B., Stockton, A., Schweizer, F., Peng, C., and Lacy, M. (2008). Fueling QSOs: the relevance of mergers. *Memoire della Societa Astronomica Italiana*, 79:1247.

Bernhard, E., Mullaney, J. R., Daddi, E., Ciesla, L., and Schreiber, C. (2016). An enhanced fraction of starbursting galaxies among high Eddington ratio AGNs. *Monthly Notices of the Royal Astronomical Society*, 460(1):902–916.

Bessiere, P. S., Tadhunter, C. N., Ramos Almeida, C., and Villar Martín, M. (2012). The importance of galaxy interactions in triggering type II quasar activity. *Monthly Notices of the Royal Astronomical Society*, 426(1):276–295.

Bhowmick, A. K., Blecha, L., and Thomas, J. (2020). Supermassive Black Hole Fueling in IllustrisTNG: Impact of Environment. *The Astrophysical Journal*, 904(2):150.

Bickley, R. W., Bottrell, C., Hani, M. H., Ellison, S. L., Teimoorinia, H., Yi, K. M., Wilkinson, S., Gwyn, S., and Hudson, M. J. (2021). Convolutional neural network identification of galaxy post-mergers in UNIONS using IllustrisTNG. *Monthly Notices of the Royal Astronomical Society*, 504(1):372–392.

Blecha, L., Snyder, G. F., Satyapal, S., and Ellison, S. L. (2018). The power of infrared AGN selection in mergers: a theoretical study. *Monthly Notices of the Royal Astronomical Society*, 478(3):3056–3071.

Blumenthal, K. A. and Barnes, J. E. (2018). Go with the Flow: Understanding inflow mechanisms in galaxy collisions. *Monthly Notices of the Royal Astronomical Society*, 479(3):3952–3965.

Böhm, A., Wisotzki, L., Bell, E. F., Jahnke, K., Wolf, C., Bacon, D., Barden, M., Gray, M. E., Hoeppe, G., Jogee, S., McIntosh, D. H., Peng, C. Y., Robaina, A. R., Balogh, M., Barazza, F. D., Caldwell, J. A. R., Heymans, C., Häußler, B., van Kampen, E., Lane, K., Meisenheimer, K., Sánchez, S. F., Taylor, A. N., and Zheng, X. (2013). AGN host galaxies at redshift z $\approx$ 0.7: peculiar or not? *Astronomy and Astrophysics*, 549:A46.

Brinchmann, J., Charlot, S., White, S. D. M., Tremonti, C., Kauffmann, G., Heckman, T., and Brinkmann, J. (2004). The physical properties of star-forming galaxies in the low-redshift Universe. *Monthly Notices of the Royal Astronomical Society*, 351(4):1151–1179.

Brinkmann, S. (2009). *On the numerical simulation of advection dominated accretion flows*. PhD thesis, Ruprecht-Karls University of Heidelberg, Germany.

Cao, C., Xu, C. K., Domingue, D., Buat, V., Cheng, Y.-W., Gao, Y., Huang, J., Jarrett, T. H., Lisenfeld, U., Lu, N., Mazzarella, J., Sun, W.-H., Wu, H., Yun, M. S., Ronca, J., and Jacques, A. (2016). Herschel Observations of Major Merger Pairs at z = 0: Dust Mass and Star Formation. *The Astrophysical Journal Supplement*, 222(2):16.

Capelo, P. R. and Dotti, M. (2016). Shocks and angular momentum flips: a different path to feeding the nuclear regions of merging galaxies. *Monthly Notices of the Royal Astronomical Society*, 465(3):2643–2653.

Capelo, P. R., Volonteri, M., Dotti, M., Bellovary, J. M., Mayer, L., and Governato, F. (2015). Growth and activity of black holes in galaxy mergers with varying mass ratios. *Monthly Notices of the Royal Astronomical Society*, 447(3):2123–2143.

Casteels, K. R. V., Conselice, C. J., Bamford, S. P., Salvador-Solé, E., Norberg, P. R., Agius, N. K., Baldry, I., Brough, S., Brown, M. J. I., Drinkwater, M. J., Driver, S. P., Graham, A. W., Bland-Hawthorn, J., Hopkins, A. M., Kelvin, L. S., López-Sánchez, A. R., Loveday, J., Robotham, A. S. G., and Vázquez-Mata, J. A. (2014). Galaxy And Mass Assembly (GAMA): refining the local galaxy merger rate using morphological information. *Monthly Notices of the Royal Astronomical Society*, 445(2):1157–1169.

Chiaberge, M., Gilli, R., Lotz, J. M., and Norman, C. (2015). Radio Loud AGNs are Mergers. *The Astrophysical Journal*, 806(2):147.

Cicone, C., Maiolino, R., Sturm, E., Graciá-Carpio, J., Feruglio, C., Neri, R., Aalto, S., Davies, R., Fiore, F., Fischer, J., García-Burillo, S., González-Alfonso, E., Hailey-Dunsheath, S., Piconcelli, E., and Veilleux, S. (2014). Massive molecular outflows and evidence for AGN feedback from CO observations. *Astronomy and Astrophysics*, 562:A21.

Cisternas, M., Jahnke, K., Inskip, K. J., Kartaltepe, J., Koekemoer, A. M., Lisker, T., Robaina, A. R., Scodeggio, M., Sheth, K., Trump, J. R., Andrae, R., Miyaji, T., Lusso, E., Brusa, M., Capak, P., Cappelluti, N., Civano, F., Ilbert, O., Impey, C. D., Leauthaud, A., Lilly, S. J., Salvato, M., Scoville, N. Z., and Taniguchi, Y. (2011). The Bulk of the Black Hole Growth Since z ~1 Occurs in a Secular Universe: No Major Merger-AGN Connection. *The Astrophysical Journal*, 726(2):57.

Conselice, C. J. (2014). The Evolution of Galaxy Structure Over Cosmic Time. *Annual Review of Astronomy and Astrophysics*, 52:291–337.

Daddi, E., Dickinson, M., Morrison, G., Chary, R., Cimatti, A., Elbaz, D., Frayer, D., Renzini, A., Pope, A., Alexander, D. M., Bauer, F. E., Giavalisco, M., Huynh, M., Kurk, J., and Mignoli, M. (2007). Multiwavelength Study of Massive Galaxies at z~2. I. Star Formation and Galaxy Growth. *The Astrophysical Journal*, 670(1):156–172.

Davies, J. J., Crain, R. A., Oppenheimer, B. D., and Schaye, J. (2020). The quenching and morphological evolution of central galaxies is facilitated by the feedback-driven expulsion of circumgalactic gas. *Monthly Notices of the Royal Astronomical Society*, 491(3):4462–4480.

Davies, J. J., Pontzen, A., and Crain, R. A. (2022). Galaxy mergers can initiate quenching by unlocking an AGN-driven transformation of the baryon cycle. *arXiv e-prints*, page arXiv:2203.08157.

Di Matteo, P., Bournaud, F., Martig, M., Combes, F., Melchior, A. L., and Semelin, B. (2008). On the frequency, intensity, and duration of starburst episodes triggered by galaxy interactions and mergers. *Astronomy and Astrophysics*, 492(1):31–49.

Di Matteo, P., Combes, F., Melchior, A. L., and Semelin, B. (2007). Star formation efficiency in galaxy interactions and mergers: a statistical study. *Astronomy and Astrophysics*, 468(1):61–81.

Di Matteo, T., Springel, V., and Hernquist, L. (2005). Energy input from quasars regulates the growth and activity of black holes and their host galaxies. *Nature*, 433(7026):604–607.

Donnari, M., Pillepich, A., Nelson, D., Vogelsberger, M., Genel, S., Weinberger, R., Marinacci, F., Springel, V., and Hernquist, L. (2019). The star formation activity of IllustrisTNG galaxies: main sequence, UVJ diagram, quenched fractions, and systematics. *Monthly Notices of the Royal Astronomical Society*, 485(4):4817–4840.

Dunn, R. J. H., Fender, R. P., Körding, E. G., Belloni, T., and Cabanac, C. (2010). A global spectral study of black hole X-ray binaries. *Monthly Notices of the Royal Astronomical Society*, 403(1):61–82.

Ellison, S. L., Brown, T., Catinella, B., and Cortese, L. (2019a). Atomic gas fractions in active galactic nucleus host galaxies. *Monthly Notices of the Royal Astronomical Society*, 482(4):5694–5703.

Ellison, S. L., Mendel, J. T., Patton, D. R., and Scudder, J. M. (2013). Galaxy pairs in the Sloan Digital Sky Survey - VIII. The observational properties of post-merger galaxies. *Monthly Notices of the Royal Astronomical Society*, 435(4):3627–3638.

Ellison, S. L., Patton, D. R., Mendel, J. T., and Scudder, J. M. (2011). Galaxy pairs in the Sloan Digital Sky Survey - IV. Interactions trigger active galactic nuclei. *Monthly Notices of the Royal Astronomical Society*, 418(3):2043–2053.

Ellison, S. L., Patton, D. R., Simard, L., and McConnachie, A. W. (2008). GALAXY PAIRS IN THE SLOAN DIGITAL SKY SURVEY. i. STAR FORMATION, ACTIVE GALACTIC NUCLEUS FRACTION, AND THE LUMINOSITY/MASS-METALLICITY RELATION. *The Astronomical Journal*, 135(5):1877–1899.

Ellison, S. L., Viswanathan, A., Patton, D. R., Bottrell, C., McConnachie, A. W., Gwyn, S., and Cuillandre, J.-C. (2019b). A definitive merger-AGN connection at z ~ 0 with CFIS: mergers have an excess of AGN and AGN hosts are more frequently disturbed. *Monthly Notices of the Royal Astronomical Society*, 487(2):2491–2504.

Ellison, S. L., Wong, T., Sánchez, S. F., Colombo, D., Bolatto, A., Barrera-Ballesteros, J., García-Benito, R., Kalinova, V., Luo, Y., Rubio, M., and Vogel, S. N. (2021). The EDGE-CALIFA survey: central molecular gas depletion in AGN host galaxies - a smoking gun for quenching? *Monthly Notices of the Royal Astronomical Society*, 505(1):L46–L51.

Fan, L., Han, Y., Fang, G., Gao, Y., Zhang, D., Jiang, X., Wu, Q., Yang, J., and Li, Z. (2016). THE MOST LUMINOUS HEAVILY OBSCURED QUASARS HAVE a HIGH MERGER FRACTION: MORPHOLOGICAL STUDY OF WISE -SELECTED HOT DUST-OBSCURED GALAXIES. *The Astrophysical Journal*, 822(2):L32.

Ferrarese, L. and Merritt, D. (2000). A Fundamental Relation between Supermassive Black Holes and Their Host Galaxies. *The Astrophysical Journal Letters*, 539(1):L9–L12.

Gao, F., Wang, L., Pearson, W. J., Gordon, Y. A., Holwerda, B. W., Hopkins, A. M., Brown, M. J. I., Bland-Hawthorn, J., and Owers, M. S. (2020). Mergers trigger active galactic nuclei out to z $\sim$ 0.6. *Astronomy and Astrophysics*, 637:A94.

Genel, S., Vogelsberger, M., Springel, V., Sijacki, D., Nelson, D., Snyder, G., Rodriguez-Gomez, V., Torrey, P., and Hernquist, L. (2014). Introducing the Illustris project: the evolution of galaxy populations across cosmic time. *Monthly Notices of the Royal Astronomical Society*, 445(1):175–200.

Glikman, E., Simmons, B., Mailly, M., Schawinski, K., Urry, C. M., and Lacy, M. (2015). Major Mergers Host the Most-luminous Red Quasars at z ~2: A Hubble Space Telescope WFC3/IR Study. *The Astrophysical Journal*, 806(2):218.

Goulding, A. D., Greene, J. E., Bezanson, R., Greco, J., Johnson, S., Leauthaud, A., Matsuoka, Y., Medezinski, E., and Price-Whelan, A. M. (2018). Galaxy interactions trigger rapid black hole growth: An unprecedented view from the Hyper Suprime-Cam survey. *Publications of the Astronomical Society of Japan*, 70:S37.

Habouzit, M., Li, Y., Somerville, R. S., Genel, S., Pillepich, A., Volonteri, M., Davé, R., Rosas-Guevara, Y., McAlpine, S., Peirani, S., Hernquist, L., Anglés-Alcázar, D., Reines, A., Bower, R., Dubois, Y., Nelson, D., Pichon, C., and Vogelsberger, M. (2021). Supermassive black holes in cosmological simulations I: M_{BH} - $M_\star$ relation and black hole mass function. *Monthly Notices of the Royal Astronomical Society*, 503(2):1940–1975.

Habouzit, M., Somerville, R. S., Li, Y., Genel, S., Aird, J., Anglés-Alcázar, D., Davé, R., Georgiev, I. Y., McAlpine, S., Rosas-Guevara, Y., Dubois, Y., Nelson, D., Banados, E., Hernquist, L., Peirani, S., and Vogelsberger, M. (2022). Supermassive black holes in cosmological simulations - II: the AGN population and predictions for upcoming X-ray missions. *Monthly Notices of the Royal Astronomical Society*, 509(2):3015–3042.

Hani, M. H., Gosain, H., Ellison, S. L., Patton, D. R., and Torrey, P. (2020). Interacting galaxies in the IllustrisTNG simulations – II: star formation in the post-merger stage. *Monthly Notices of the Royal Astronomical Society*, 493(3):3716–3731.

Harrison, C. (2014). *Observational constraints on the influence of active galactic nuclei on the evolution of galaxies*. PhD thesis, Durham University, UK.

Hernández-Toledo, H. M., Avila-Reese, V., Conselice, C. J., and Puerari, I. (2005). The Structural Properties of Isolated Galaxies, Spiral-Spiral Pairs, and Mergers: The Robustness of Galaxy Morphology during Secular Evolution. *The Astronomical Journal*, 129(2):682–697.

Hernquist, L. (1989). Tidal triggering of starbursts and nuclear activity in galaxies. *Nature*, 340(6236):687–691.

Hewlett, T., Villforth, C., Wild, V., Mendez-Abreu, J., Pawlik, M., and Rowlands, K. (2017). The redshift evolution of major merger triggering of luminous AGNs: a slight enhancement at z $\sim$ 2. *Monthly Notices of the Royal Astronomical Society*, 470(1):755–770.

Hickox, R. C. and Alexander, D. M. (2018). Obscured Active Galactic Nuclei. *Annual Review of Astronomy and Astrophysics*, 56:625–671.

Hickox, R. C., Mullaney, J. R., Alexander, D. M., Chen, C.-T. J., Civano, F. M., Goulding, A. D., and Hainline, K. N. (2014). Black Hole Variability and the Star Formation-Active Galactic Nucleus Connection: Do All Star-forming Galaxies Host an Active Galactic Nucleus? *The Astrophysical Journal*, 782(1):9.

Hong, J., Im, M., Kim, M., and Ho, L. C. (2015). CORRELATION BETWEEN GALAXY MERGERS AND LUMINOUS ACTIVE GALACTIC NUCLEI. *The Astrophysical Journal*, 804(1):34.

Hopkins, P. F., Hernquist, L., Cox, T. J., and Kereš, D. (2008). A Cosmological Framework for the Co-Evolution of Quasars, Supermassive Black Holes, and Elliptical Galaxies. I. Galaxy Mergers and Quasar Activity. *The Astrophysical Journal Supplement*, 175(2):356–389.

Hubble, E. P. (1926). Extragalactic nebulae. *The Astrophysical Journal*, 64:321–369.

Inayoshi, K., Ostriker, J. P., Haiman, Z., and Kuiper, R. (2018). Low-density, radiatively inefficient rotating-accretion flow on to a black hole. , 476(1):1412–1426.

Jahnke, K. and Macciò, A. V. (2011). The Non-causal Origin of the Black-hole-galaxy Scaling Relations. *The Astrophysical Journal*, 734(2):92.

Jarvis, M. E., Harrison, C. M., Mainieri, V., Calistro Rivera, G., Jethwa, P., Zhang, Z. Y., Alexander, D. M., Circosta, C., Costa, T., De Breuck, C., Kakkad, D., Kharb,

P., Lansbury, G. B., and Thomson, A. P. (2020). High molecular gas content and star formation rates in local galaxies that host quasars, outflows, and jets. *Monthly Notices of the Royal Astronomical Society*, 498(2):1560–1575.

Knapen, J. H., Cisternas, M., and Querejeta, M. (2015). Interacting galaxies in the nearby Universe: only moderate increase of star formation. *Monthly Notices of the Royal Astronomical Society*, 454(2):1742–1750.

Kocevski, D. D., Brightman, M., Nandra, K., Koekemoer, A. M., Salvato, M., Aird, J., Bell, E. F., Hsu, L.-T., Kartaltepe, J. S., Koo, D. C., Lotz, J. M., McIntosh, D. H., Mozena, M., Rosario, D., and Trump, J. R. (2015). Are Compton-thick AGNs the Missing Link between Mergers and Black Hole Growth? *The Astrophysical Journal*, 814(2):104.

Kocevski, D. D., Faber, S. M., Mozena, M., Koekemoer, A. M., Nandra, K., Rangel, C., Laird, E. S., Brusa, M., Wuyts, S., Trump, J. R., Koo, D. C., Somerville, R. S., Bell, E. F., Lotz, J. M., Alexander, D. M., Bournaud, F., Conselice, C. J., Dahlen, T., Dekel, A., Donley, J. L., Dunlop, J. S., Finoguenov, A., Georgakakis, A., Giavalisco, M., Guo, Y., Grogin, N. A., Hathi, N. P., Juneau, S., Kartaltepe, J. S., Lucas, R. A., McGrath, E. J., McIntosh, D. H., Mobasher, B., Robaina, A. R., Rosario, D., Straughn, A. N., van der Wel, A., and Villforth, C. (2012). CANDELS: Constraining the AGN-Merger Connection with Host Morphologies at z ~2. *The Astrophysical Journal*, 744(2):148.

Kormendy, J. and Gebhardt, K. (2001). Supermassive black holes in galactic nuclei. In Wheeler, J. C. and Martel, H., editors, *20th Texas Symposium on relativistic astrophysics*, volume 586 of *American Institute of Physics Conference Series*, pages 363–381.

Kormendy, J. and Ho, L. C. (2013). Coevolution (Or Not) of Supermassive Black Holes and Host Galaxies. *Annual Review of Astronomy and Astrophysics*, 51(1):511–653.

Koss, M., Mushotzky, R., Veilleux, S., and Winter, L. (2010). Merging and Clustering of the Swift BAT AGN Sample. *The Astrophysical Journal Letters*, 716(2):L125–L130.

Koss, M. J., Strittmatter, B., Lamperti, I., Shimizu, T., Trakhtenbrot, B., Saintonge, A., Treister, E., Cicone, C., Mushotzky, R., Oh, K., Ricci, C., Stern, D., Ananna,

T. T., Bauer, F. E., Privon, G. C., Bär, R. E., De Breuck, C., Harrison, F., Ichikawa, K., Powell, M. C., Rosario, D., Sanders, D. B., Schawinski, K., Shao, L., Megan Urry, C., and Veilleux, S. (2021). BAT AGN Spectroscopic Survey. XX. Molecular Gas in Nearby Hard-X-Ray-selected AGN Galaxies. *The Astrophysical Journal Supplement*, 252(2):29.

Lambrides, E. L., Chiaberge, M., Heckman, T., Kirkpatrick, A., Meyer, E. T., Petric, A., Hall, K., Long, A., Watts, D. J., Gilli, R., Simons, R., Tchernyshyov, K., Rodriguez-Gomez, V., Vito, F., de la Vega, A., Davis, J. R., Kocevski, D. D., and Norman, C. (2021). Lower-luminosity Obscured AGN Host Galaxies Are Not Predominantly in Major-merging Systems at Cosmic Noon. *The Astrophysical Journal*, 919(2):129.

Liu, B. (2013). Coupling of the accretion disk and corona around black holes. *Proceedings of the International Astronomical Union*, 8:62–65.

Liu, B. F., Mineshige, S., Meyer, F., Meyer-Hofmeister, E., and Kawaguchi, T. (2002). Two-Temperature Coronal Flow above a Thin Disk. , 575(1):117–126.

Lotz, J. M., Jonsson, P., Cox, T. J., Croton, D., Primack, J. R., Somerville, R. S., and Stewart, K. (2011). The Major and Minor Galaxy Merger Rates at z ¡ 1.5. *The Astrophysical Journal*, 742(2):103.

Lotz, J. M., Jonsson, P., Cox, T. J., and Primack, J. R. (2008). Galaxy merger morphologies and time-scales from simulations of equal-mass gas-rich disc mergers. *Monthly Notices of the Royal Astronomical Society*, 391(3):1137–1162.

Luo, Y., Li, Z., Kang, X., Li, Z., and Wang, P. (2020). What has quenched the massive spiral galaxies? *Monthly Notices of the Royal Astronomical Society*, 496(1):L116–L121.

Lutz, D., Mainieri, V., Rafferty, D., Shao, L., Hasinger, G., Weiß, A., Walter, F., Smail, I., Alexander, D. M., Brandt, W. N., Chapman, S., Coppin, K., Förster Schreiber, N. M., Gawiser, E., Genzel, R., Greve, T. R., Ivison, R. J., Koekemoer, A. M., Kurczynski, P., Menten, K. M., Nordon, R., Popesso, P., Schinnerer, E., Silverman, J. D., Wardlow, J., and Xue, Y. Q. (2010). The LABOCA Survey of the Extended Chandra Deep Field South: Two Modes of Star Formation in Active Galactic Nucleus Hosts? *The Astrophysical Journal*, 712(2):1287–1301.

Madau, P. and Dickinson, M. (2014). Cosmic Star-Formation History. *Annual Review of Astronomy and Astrophysics*, 52:415–486.

Marian, V., Jahnke, K., Andika, I., Bañados, E., Bennert, V. N., Cohen, S., Husemann, B., Kaasinen, M., Koekemoer, A. M., Mechtley, M., Onoue, M., Schindler, J.-T., Schramm, M., Schulze, A., Silverman, J. D., Smirnova-Pinchukova, I., van der Wel, A., Villforth, C., and Windhorst, R. A. (2020). A Significant Excess in Major Merger Rate for AGNs with the Highest Eddington Ratios at z ¡ 0.2. *The Astrophysical Journal*, 904(1):79.

Marian, V., Jahnke, K., Mechtley, M., Cohen, S., Husemann, B., Jones, V., Koekemoer, A., Schulze, A., van der Wel, A., Villforth, C., and Windhorst, R. A. (2019). Major Mergers Are Not the Dominant Trigger for High-accretion AGNs at z $\sim$ 2. *The Astrophysical Journal*, 882(2):141.

Marinacci, F., Vogelsberger, M., Pakmor, R., Torrey, P., Springel, V., Hernquist, L., Nelson, D., Weinberger, R., Pillepich, A., Naiman, J., and Genel, S. (2018). First results from the IllustrisTNG simulations: radio haloes and magnetic fields. *Monthly Notices of the Royal Astronomical Society*, 480(4):5113–5139.

McAlpine, S., Harrison, C. M., Rosario, D. J., Alexander, D. M., Ellison, S. L., Johansson, P. H., and Patton, D. R. (2020). Galaxy mergers in EAGLE do not induce a significant amount of black hole growth yet do increase the rate of luminous AGN. *Monthly Notices of the Royal Astronomical Society*, 494(4):5713–5733.

McAlpine, S., Helly, J. C., Schaller, M., Trayford, J. W., Qu, Y., Furlong, M., Bower, R. G., Crain, R. A., Schaye, J., Theuns, T., Dalla Vecchia, C., Frenk, C. S., McCarthy, I. G., Jenkins, A., Rosas-Guevara, Y., White, S. D. M., Baes, M., Camps, P., and Lemson, G. (2016). The EAGLE simulations of galaxy formation: Public release of halo and galaxy catalogues. *Astronomy and Computing*, 15:72–89.

McCarthy, I. G., Babul, A., Bower, R. G., and Balogh, M. L. (2008). Towards a holistic view of the heating and cooling of the intracluster medium. *Monthly Notices of the Royal Astronomical Society*, 386(3):1309–1331.

McNamara, B. R. and Nulsen, P. E. J. (2007). Heating Hot Atmospheres with Active Galactic Nuclei. *Annual Review of Astronomy and Astrophysics*, 45(1):117–175.

Mechtley, M., Jahnke, K., Windhorst, R. A., Andrae, R., Cisternas, M., Cohen, S. H., Hewlett, T., Koekemoer, A. M., Schramm, M., Schulze, A., Silverman, J. D., Villforth, C., van der Wel, A., and Wisotzki, L. (2016). Do the Most Massive Black Holes at z = 2 Grow via Major Mergers? *The Astrophysical Journal*, 830(2):156.

Meyer-Hofmeister, E., Liu, B. F., and Meyer, F. (2012). Coronae above accretion disks around black holes: the effect of Compton cooling. , 544:A87.

Mihos, J. C. and Hernquist, L. (1996). Gasdynamics and Starbursts in Major Mergers. *The Astrophysical Journal*, 464:641.

Müller, A. (2004). *Black hole astrophysics: magnetohydrodynamics on the Kerr geometry*. PhD thesis, -.

Naiman, J. P., Pillepich, A., Springel, V., Ramirez-Ruiz, E., Torrey, P., Vogelsberger, M., Pakmor, R., Nelson, D., Marinacci, F., Hernquist, L., Weinberger, R., and Genel, S. (2018). First results from the IllustrisTNG simulations: a tale of two elements – chemical evolution of magnesium and europium. *Monthly Notices of the Royal Astronomical Society*, 477(1):1206–1224.

Negri, A. and Volonteri, M. (2017). Black hole feeding and feedback: the physics inside the 'sub-grid'. *Monthly Notices of the Royal Astronomical Society*, 467(3):3475–3492.

Nelson, D., Pillepich, A., Springel, V., Weinberger, R., Hernquist, L., Pakmor, R., Genel, S., Torrey, P., Vogelsberger, M., Kauffmann, G., Marinacci, F., and Naiman, J. (2017). First results from the IllustrisTNG simulations: the galaxy colour bimodality. *Monthly Notices of the Royal Astronomical Society*, 475(1):624–647.

Nelson, E. J., Tacchella, S., Diemer, B., Leja, J., Hernquist, L., Whitaker, K. E., Weinberger, R., Pillepich, A., Nelson, D., Terrazas, B. A., Nevin, R., Brammer, G. B., Burkhart, B., Cochrane, R. K., van Dokkum, P., Johnson, B. D., Marinacci, F., Mowla, L., Pakmor, R., Skelton, R. E., Speagle, J., Springel, V., Torrey, P., Vogelsberger, M., and Wuyts, S. (2021). Spatially resolved star formation and inside-out quenching in the TNG50 simulation and 3D-HST observations. *Monthly Notices of the Royal Astronomical Society*, 508(1):219–235.

Netzer, H. (2015). Revisiting the Unified Model of Active Galactic Nuclei. *Annual Review of Astronomy and Astrophysics*, 53:365–408.

Ni, Y., Di Matteo, T., Bird, S., Croft, R., Feng, Y., Chen, N., Tremmel, M., DeGraf, C., and Li, Y. (2022). The ASTRID simulation: the evolution of supermassive black holes. *Monthly Notices of the Royal Astronomical Society*, 513(1):670–692.

Noeske, K. G., Weiner, B. J., Faber, S. M., Papovich, C., Koo, D. C., Somerville, R. S., Bundy, K., Conselice, C. J., Newman, J. A., Schiminovich, D., Le Floc'h, E., Coil, A. L., Rieke, G. H., Lotz, J. M., Primack, J. R., Barmby, P., Cooper, M. C., Davis, M., Ellis, R. S., Fazio, G. G., Guhathakurta, P., Huang, J., Kassin, S. A., Martin, D. C., Phillips, A. C., Rich, R. M., Small, T. A., Willmer, C. N. A., and Wilson, G. (2007). Star Formation in AEGIS Field Galaxies since z=1.1: The Dominance of Gradually Declining Star Formation, and the Main Sequence of Star-forming Galaxies. *The Astrophysical Journal Letters*, 660(1):L43–L46.

Padovani, P., Alexander, D. M., Assef, R. J., De Marco, B., Giommi, P., Hickox, R. C., Richards, G. T., Smolčić, V., Hatziminaoglou, E., Mainieri, V., and Salvato, M. (2017). Active galactic nuclei: what's in a name? *Astronomy and Astrophysics Review*, 25(1):2.

Patton, D. R., Grant, J. K., Simard, L., Pritchet, C. J., Carlberg, R. G., and Borne, K. D. (2005). A Hubble Space Telescope Snapshot Survey of Dynamically Close Galaxy Pairs in the CNOC2 Redshift Survey. *The Astronomical Journal*, 130(5):2043–2057.

Patton, D. R., Qamar, F. D., Ellison, S. L., Bluck, A. F. L., Simard, L., Mendel, J. T., Moreno, J., and Torrey, P. (2016). Galaxy pairs in the Sloan Digital Sky Survey - XI. A new method for measuring the influence of the closest companion out to wide separations. *Monthly Notices of the Royal Astronomical Society*, 461(3):2589–2604.

Patton, D. R., Torrey, P., Ellison, S. L., Mendel, J. T., and Scudder, J. M. (2013). Galaxy pairs in the Sloan Digital Sky Survey - VI. The orbital extent of enhanced star formation in interacting galaxies. *Monthly Notices of the Royal Astronomical Society*, 433(1):L59–L63.

Patton, D. R., Wilson, K. D., Metrow, C. J., Ellison, S. L., Torrey, P., Brown, W., Hani, M. H., McAlpine, S., Moreno, J., and Woo, J. (2020). Interacting galaxies in the IllustrisTNG simulations - I: Triggered star formation in a cosmological context. *Monthly Notices of the Royal Astronomical Society*, 494(4):4969–4985.

Peng, Y.-j., Lilly, S. J., Kovač, K., Bolzonella, M., Pozzetti, L., Renzini, A., Zamorani, G., Ilbert, O., Knobel, C., Iovino, A., Maier, C., Cucciati, O., Tasca, L., Carollo, C. M., Silverman, J., Kampczyk, P., de Ravel, L., Sanders, D., Scoville, N., Contini, T., Mainieri, V., Scodeggio, M., Kneib, J.-P., Le Fèvre, O., Bardelli, S., Bongiorno, A., Caputi, K., Coppa, G., de la Torre, S., Franzetti, P., Garilli, B., Lamareille, F., Le Borgne, J.-F., Le Brun, V., Mignoli, M., Perez Montero, E., Pello, R., Ricciardelli, E., Tanaka, M., Tresse, L., Vergani, D., Welikala, N., Zucca, E., Oesch, P., Abbas, U., Barnes, L., Bordoloi, R., Bottini, D., Cappi, A., Cassata, P., Cimatti, A., Fumana, M., Hasinger, G., Koekemoer, A., Leauthaud, A., Maccagni, D., Marinoni, C., McCracken, H., Memeo, P., Meneux, B., Nair, P., Porciani, C., Presotto, V., and Scaramella, R. (2010). Mass and Environment as Drivers of Galaxy Evolution in SDSS and zCOSMOS and the Origin of the Schechter Function. *The Astrophysical Journal*, 721(1):193–221.

Pierce, J. C. S., Tadhunter, C. N., Gordon, Y., Ramos Almeida, C., Ellison, S. L., O'Dea, C., Grimmett, L., Makrygianni, L., Bessiere, P. S., and Doña Girón, P. (2022). Do AGN triggering mechanisms vary with radio power? - II. The importance of mergers as a function of radio power and optical luminosity. *Monthly Notices of the Royal Astronomical Society*, 510(1):1163–1183.

Pillepich, A., Nelson, D., Hernquist, L., Springel, V., Pakmor, R., Torrey, P., Weinberger, R., Genel, S., Naiman, J. P., Marinacci, F., and Vogelsberger, M. (2017a). First results from the IllustrisTNG simulations: the stellar mass content of groups and clusters of galaxies. *Monthly Notices of the Royal Astronomical Society*, 475(1):648–675.

Pillepich, A., Springel, V., Nelson, D., Genel, S., Naiman, J., Pakmor, R., Hernquist, L., Torrey, P., Vogelsberger, M., Weinberger, R., and Marinacci, F. (2017b). Simulating galaxy formation with the IllustrisTNG model. *Monthly Notices of the Royal Astronomical Society*, 473(3):4077–4106.

Piotrowska, J. M., Bluck, A. F. L., Maiolino, R., and Peng, Y. (2021). On the quenching of star formation in observed and simulated central galaxies: Evidence for the role of integrated AGN feedback. *Monthly Notices of the Royal Astronomical Society*.

Prieto, J., Escala, A., Privon, G. C., and d'Etigny, J. (2021). Black hole fuelling in

galaxy mergers: a high-resolution analysis. *Monthly Notices of the Royal Astronomical Society*, 508(3):3672–3683.

Quai, S., Hani, M. H., Ellison, S. L., Patton, D. R., and Woo, J. (2021). Interacting galaxies in the IllustrisTNG simulations – III. (The rarity of) quenching in post-merger galaxies. *Monthly Notices of the Royal Astronomical Society*, 504(2):1888–1901.

Ramos Almeida, C., Bessiere, P. S., Tadhunter, C. N., Pérez-González, P. G., Barro, G., Inskip, K. J., Morganti, R., Holt, J., and Dicken, D. (2012). Are luminous radio-loud active galactic nuclei triggered by galaxy interactions? *Monthly Notices of the Royal Astronomical Society*, 419(1):687–705.

Ramos Almeida, C. and Ricci, C. (2017). Nuclear obscuration in active galactic nuclei. *Nature Astronomy*, 1:679–689.

Rodighiero, G., Daddi, E., Baronchelli, I., Cimatti, A., Renzini, A., Aussel, H., Popesso, P., Lutz, D., Andreani, P., Berta, S., Cava, A., Elbaz, D., Feltre, A., Fontana, A., Förster Schreiber, N. M., Franceschini, A., Genzel, R., Grazian, A., Gruppioni, C., Ilbert, O., Le Floch, E., Magdis, G., Magliocchetti, M., Magnelli, B., Maiolino, R., McCracken, H., Nordon, R., Poglitsch, A., Santini, P., Pozzi, F., Riguccini, L., Tacconi, L. J., Wuyts, S., and Zamorani, G. (2011). The Lesser Role of Starbursts in Star Formation at z = 2. *The Astrophysical Journal Letters*, 739(2):L40.

Rodriguez-Gomez, V., Genel, S., Vogelsberger, M., Sijacki, D., Pillepich, A., Sales, L. V., Torrey, P., Snyder, G., Nelson, D., Springel, V., Ma, C.-P., and Hernquist, L. (2015). The merger rate of galaxies in the Illustris simulation: a comparison with observations and semi-empirical models. *Monthly Notices of the Royal Astronomical Society*, 449(1):49–64.

Rodríguez Montero, F., Davé, R., Wild, V., Anglés-Alcázar, D., and Narayanan, D. (2019). Mergers, starbursts, and quenching in the SIMBA simulation. *Monthly Notices of the Royal Astronomical Society*, 490(2):2139–2154.

Roos, N. and Norman, C. A. (1979). Galaxy collisions and their influence on the dynamics and evolution of groups and clusters of galaxies. *Astronomy and Astrophysics*, 76(1):75–85.

Rosario, D. J., McIntosh, D. H., van der Wel, A., Kartaltepe, J., Lang, P., Santini, P., Wuyts, S., Lutz, D., Rafelski, M., Villforth, C., Alexander, D. M., Bauer, F. E., Bell, E. F., Berta, S., Brandt, W. N., Conselice, C. J., Dekel, A., Faber, S. M., Ferguson, H. C., Genzel, R., Grogin, N. A., Kocevski, D. D., Koekemoer, A. M., Koo, D. C., Lotz, J. M., Magnelli, B., Maiolino, R., Mozena, M., Mullaney, J. R., Papovich, C. J., Popesso, P., Tacconi, L. J., Trump, J. R., Avadhuta, S., Bassett, R., Bell, A., Bernyk, M., Bournaud, F., Cassata, P., Cheung, E., Croton, D., Donley, J., DeGroot, L., Guedes, J., Hathi, N., Herrington, J., Hilton, M., Lai, K., Lani, C., Martig, M., McGrath, E., Mutch, S., Mortlock, A., McPartland, C., O'Leary, E., Peth, M., Pillepich, A., Poole, G., Snyder, D., Straughn, A., Telford, O., Tonini, C., and Wandro, P. (2015). The host galaxies of X-ray selected active galactic nuclei to z = 2.5: Structure, star formation, and their relationships from CANDELS and Herschel/PACS. *Astronomy and Astrophysics*, 573:A85.

Rosario, D. J., Trakhtenbrot, B., Lutz, D., Netzer, H., Trump, J. R., Silverman, J. D., Schramm, M., Lusso, E., Berta, S., Bongiorno, A., Brusa, M., Förster-Schreiber, N. M., Genzel, R., Lilly, S., Magnelli, B., Mainieri, V., Maiolino, R., Merloni, A., Mignoli, M., Nordon, R., Popesso, P., Salvato, M., Santini, P., Tacconi, L. J., and Zamorani, G. (2013). The mean star-forming properties of QSO host galaxies. *Astronomy and Astrophysics*, 560:A72.

Rosas-Guevara, Y. M., Bower, R. G., Schaye, J., Furlong, M., Frenk, C. S., Booth, C. M., Crain, R. A., Dalla Vecchia, C., Schaller, M., and Theuns, T. (2015). The impact of angular momentum on black hole accretion rates in simulations of galaxy formation. *Monthly Notices of the Royal Astronomical Society*, 454(1):1038–1057.

Rowan-Robinson, M. (1995). A new model for the infrared emission of quasars. *Monthly Notices of the Royal Astronomical Society*, 272(4):737–748.

Salim, S., Rich, R. M., Charlot, S., Brinchmann, J., Johnson, B. D., Schiminovich, D., Seibert, M., Mallery, R., Heckman, T. M., Forster, K., Friedman, P. G., Martin, D. C., Morrissey, P., Neff, S. G., Small, T., Wyder, T. K., Bianchi, L., Donas, J., Lee, Y.-W., Madore, B. F., Milliard, B., Szalay, A. S., Welsh, B. Y., and Yi, S. K. (2007). UV Star Formation Rates in the Local Universe. *The Astrophysical Journal Supplement*, 173(2):267–292.

Sandage, A. (1961). *The Hubble Atlas of Galaxies*.

Sanders, D. B., Soifer, B. T., Elias, J. H., Madore, B. F., Matthews, K., Neugebauer, G., and Scoville, N. Z. (1988). Ultraluminous Infrared Galaxies and the Origin of Quasars. *The Astrophysical Journal*, 325:74.

Santini, P., Rosario, D. J., Shao, L., Lutz, D., Maiolino, R., Alexander, D. M., Altieri, B., Andreani, P., Aussel, H., Bauer, F. E., Berta, S., Bongiovanni, A., Brandt, W. N., Brusa, M., Cepa, J., Cimatti, A., Daddi, E., Elbaz, D., Fontana, A., Förster Schreiber, N. M., Genzel, R., Grazian, A., Le Floc'h, E., Magnelli, B., Mainieri, V., Nordon, R., Pérez Garcia, A. M., Poglitsch, A., Popesso, P., Pozzi, F., Riguccini, L., Rodighiero, G., Salvato, M., Sanchez-Portal, M., Sturm, E., Tacconi, L. J., Valtchanov, I., and Wuyts, S. (2012). Enhanced star formation rates in AGN hosts with respect to inactive galaxies from PEP-Herschel observations. *Astronomy and Astrophysics*, 540:A109.

Satyapal, S., Ellison, S. L., McAlpine, W., Hickox, R. C., Patton, D. R., and Mendel, J. T. (2014). Galaxy pairs in the Sloan Digital Sky Survey - IX. Merger-induced AGN activity as traced by the Wide-field Infrared Survey Explorer. *Monthly Notices of the Royal Astronomical Society*, 441(2):1297–1304.

Schawinski, K., Simmons, B. D., Urry, C. M., Treister, E., and Glikman, E. (2012). Heavily obscured quasar host galaxies at z $\sim$ 2 are discs, not major mergers. *Monthly Notices of the Royal Astronomical Society*, 425(1):L61–L65.

Schawinski, K., Treister, E., Urry, C. M., Cardamone, C. N., Simmons, B., and Yi, S. K. (2011). HST WFC3/IR Observations of Active Galactic Nucleus Host Galaxies at z ~2: Supermassive Black Holes Grow in Disk Galaxies. *The Astrophysical Journal Letters*, 727(2):L31.

Schawinski, K., Urry, C. M., Simmons, B. D., Fortson, L., Kaviraj, S., Keel, W. C., Lintott, C. J., Masters, K. L., Nichol, R. C., Sarzi, M., Skibba, R., Treister, E., Willett, K. W., Wong, O. I., and Yi, S. K. (2014). The green valley is a red herring: Galaxy Zoo reveals two evolutionary pathways towards quenching of star formation in early- and late-type galaxies. *Monthly Notices of the Royal Astronomical Society*, 440(1):889–907.

Schaye, J., Crain, R. A., Bower, R. G., Furlong, M., Schaller, M., Theuns, T., Dalla Vecchia, C., Frenk, C. S., McCarthy, I. G., Helly, J. C., Jenkins, A., Rosas-Guevara, Y. M., White, S. D. M., Baes, M., Booth, C. M., Camps, P., Navarro, J. F., Qu,

Y., Rahmati, A., Sawala, T., Thomas, P. A., and Trayford, J. (2015). The EAGLE project: simulating the evolution and assembly of galaxies and their environments. *Monthly Notices of the Royal Astronomical Society*, 446(1):521–554.

Schweitzer, M., Lutz, D., Sturm, E., Contursi, A., Tacconi, L. J., Lehnert, M. D., Dasyra, K. M., Genzel, R., Veilleux, S., Rupke, D., Kim, D. C., Baker, A. J., Netzer, H., Sternberg, A., Mazzarella, J., and Lord, S. (2006). Spitzer Quasar and ULIRG Evolution Study (QUEST). I. The Origin of the Far-Infrared Continuum of QSOs. *The Astrophysical Journal*, 649(1):79–90.

Schweizer, F. (1986). Colliding and Merging Galaxies. *Science*, 231(4735):227–234.

Scudder, J. M., Ellison, S. L., Momjian, E., Rosenberg, J. L., Torrey, P., Patton, D. R., Fertig, D., and Mendel, J. T. (2015). Galaxy pairs in the Sloan Digital Sky Survey - X. Does gas content alter star formation rate enhancement in galaxy interactions? *Monthly Notices of the Royal Astronomical Society*, 449(4):3719–3740.

Scudder, J. M., Ellison, S. L., Torrey, P., Patton, D. R., and Mendel, J. T. (2012). Galaxy pairs in the Sloan Digital Sky Survey - V. Tracing changes in star formation rate and metallicity out to separations of 80 kpc. *Monthly Notices of the Royal Astronomical Society*, 426(1):549–565.

Shah, E. A., Kartaltepe, J. S., Magagnoli, C. T., Cox, I. G., Wetherell, C. T., Vanderhoof, B. N., Calabro, A., Chartab, N., Conselice, C. J., Croton, D. J., Donley, J., de Groot, L., de la Vega, A., Hathi, N. P., Ilbert, O., Inami, H., Kocevski, D. D., Koekemoer, A. M., Lemaux, B. C., Mantha, K. B., Marchesi, S., Martig, M., Masters, D. C., McGrath, E. J., McIntosh, D. H., Moreno, J., Nayyeri, H., Pampliega, B. A., Salvato, M., Snyder, G. F., Straughn, A. N., Treister, E., and Weston, M. E. (2020). Investigating the Effect of Galaxy Interactions on the Enhancement of Active Galactic Nuclei at 0.5 ¡ z ¡ 3.0. *The Astrophysical Journal*, 904(2):107.

Shangguan, J., Ho, L. C., Bauer, F. E., Wang, R., and Treister, E. (2020). AGN Feedback and Star Formation of Quasar Host Galaxies: Insights from the Molecular Gas. *The Astrophysical Journal*, 899(2):112.

Shao, L., Lutz, D., Nordon, R., Maiolino, R., Alexander, D. M., Altieri, B., Andreani, P., Aussel, H., Bauer, F. E., Berta, S., Bongiovanni, A., Brandt, W. N., Brusa,

M., Cava, A., Cepa, J., Cimatti, A., Daddi, E., Dominguez-Sanchez, H., Elbaz, D., Förster Schreiber, N. M., Geis, N., Genzel, R., Grazian, A., Gruppioni, C., Magdis, G., Magnelli, B., Mainieri, V., Pérez García, A. M., Poglitsch, A., Popesso, P., Pozzi, F., Riguccini, L., Rodighiero, G., Rovilos, E., Saintonge, A., Salvato, M., Sanchez Portal, M., Santini, P., Sturm, E., Tacconi, L. J., Valtchanov, I., Wetzstein, M., and Wieprecht, E. (2010). Star formation in AGN hosts in GOODS-N. *Astronomy and Astrophysics*, 518:L26.

Sijacki, D., Vogelsberger, M., Genel, S., Springel, V., Torrey, P., Snyder, G. F., Nelson, D., and Hernquist, L. (2015). The Illustris simulation: the evolving population of black holes across cosmic time. *Monthly Notices of the Royal Astronomical Society*, 452(1):575–596.

Silk, J. and Rees, M. J. (1998). Quasars and galaxy formation. *Astronomy and Astrophysics*, 331:L1–L4.

Sivasankaran, A., Blecha, L., Torrey, P., Kelley, L. Z., Bhowmick, A., Vogelsberger, M., Losacco, R., Weinberger, R., Hernquist, L., Marinacci, F., Sales, L. V., and Qi, J. (2022). Simulations of black hole fueling in isolated and merging galaxies with an explicit, multiphase ISM. *arXiv e-prints*, page arXiv:2203.14985.

Somerville, R. S. and Davé, R. (2015). Physical Models of Galaxy Formation in a Cosmological Framework. *Annual Review of Astronomy and Astrophysics*, 53:51–113.

Somerville, R. S., Hopkins, P. F., Cox, T. J., Robertson, B. E., and Hernquist, L. (2008). A semi-analytic model for the co-evolution of galaxies, black holes and active galactic nuclei. *Monthly Notices of the Royal Astronomical Society*, 391(2):481–506.

Springel, V. (2005). The cosmological simulation code GADGET-2. *Monthly Notices of the Royal Astronomical Society*, 364(4):1105–1134.

Springel, V. (2010). E pur si muove: Galilean-invariant cosmological hydrodynamical simulations on a moving mesh. *Monthly Notices of the Royal Astronomical Society*, 401(2):791–851.

Springel, V., Di Matteo, T., and Hernquist, L. (2005). Modelling feedback from stars and black holes in galaxy mergers. *Monthly Notices of the Royal Astronomical Society*, 361(3):776–794.

Springel, V., Pakmor, R., Pillepich, A., Weinberger, R., Nelson, D., Hernquist, L., Vogelsberger, M., Genel, S., Torrey, P., Marinacci, F., and Naiman, J. (2017). First results from the IllustrisTNG simulations: matter and galaxy clustering. *Monthly Notices of the Royal Astronomical Society*, 475(1):676–698.

Starkenburg, T. K., Tonnesen, S., and Kopenhafer, C. (2019). What Is Inside Matters: Simulated Green Valley Galaxies Have too Centrally Concentrated Star Formation. *The Astrophysical Journal Letters*, 874(2):L17.

Steinborn, L. K., Hirschmann, M., Dolag, K., Shankar, F., Juneau, S., Krumpe, M., Remus, R.-S., and Teklu, A. F. (2018). Cosmological simulations of black hole growth II: how (in)significant are merger events for fuelling nuclear activity? *Monthly Notices of the Royal Astronomical Society*, 481(1):341–360.

Strateva, I., Ivezić, Ž., Knapp, G. R., Narayanan, V. K., Strauss, M. A., Gunn, J. E., Lupton, R. H., Schlegel, D., Bahcall, N. A., Brinkmann, J., Brunner, R. J., Budavári, T., Csabai, I., Castander, F. J., Doi, M., Fukugita, M., Győry, Z., Hamabe, M., Hennessy, G., Ichikawa, T., Kunszt, P. Z., Lamb, D. Q., McKay, T. A., Okamura, S., Racusin, J., Sekiguchi, M., Schneider, D. P., Shimasaku, K., and York, D. (2001). Color Separation of Galaxy Types in the Sloan Digital Sky Survey Imaging Data. *The Astronomical Journal*, 122(4):1861–1874.

Sturm, E., González-Alfonso, E., Veilleux, S., Fischer, J., Graciá-Carpio, J., Hailey-Dunsheath, S., Contursi, A., Poglitsch, A., Sternberg, A., Davies, R., Genzel, R., Lutz, D., Tacconi, L., Verma, A., Maiolino, R., and de Jong, J. A. (2011). Massive Molecular Outflows and Negative Feedback in ULIRGs Observed by Herschel-PACS. *The Astrophysical Journal Letters*, 733(1):L16.

Terrazas, B. A., Bell, E. F., Pillepich, A., Nelson, D., Somerville, R. S., Genel, S., Weinberger, R., Habouzit, M., Li, Y., Hernquist, L., and Vogelsberger, M. (2020). The relationship between black hole mass and galaxy properties: examining the black hole feedback model in IllustrisTNG. *Monthly Notices of the Royal Astronomical Society*, 493(2):1888–1906.

Thorp, M. D., Ellison, S. L., Simard, L., Sánchez, S. F., and Antonio, B. (2019). Spatially resolved star formation and metallicity profiles in post-merger galaxies from MaNGA. *Monthly Notices of the Royal Astronomical Society*, 482(1):L55–L59.

Toomre, A. and Toomre, J. (1972). Galactic Bridges and Tails. *The Astrophysical Journal*, 178:623–666.

Treister, E., Schawinski, K., Urry, C. M., and Simmons, B. D. (2012). Major Galaxy Mergers Only Trigger the Most Luminous Active Galactic Nuclei. *The Astrophysical Journal Letters*, 758(2):L39.

Tremaine, S., Gebhardt, K., Bender, R., Bower, G., Dressler, A., Faber, S. M., Filippenko, A. V., Green, R., Grillmair, C., Ho, L. C., Kormendy, J., Lauer, T. R., Magorrian, J., Pinkney, J., and Richstone, D. (2002). The Slope of the Black Hole Mass versus Velocity Dispersion Correlation. *The Astrophysical Journal*, 574(2):740–753.

Urry, C. M. and Padovani, P. (1995). Unified Schemes for Radio-Loud Active Galactic Nuclei. *Publications of the Astronomical Society of the Pacific*, 107:803.

Villforth, C., Hamann, F., Rosario, D. J., Santini, P., McGrath, E. J., van der Wel, A., Chang, Y. Y., Guo, Y., Dahlen, T., Bell, E. F., Conselice, C. J., Croton, D., Dekel, A., Faber, S. M., Grogin, N., Hamilton, T., Hopkins, P. F., Juneau, S., Kartaltepe, J., Kocevski, D., Koekemoer, A., Koo, D. C., Lotz, J., McIntosh, D., Mozena, M., Somerville, R., and Wild, V. (2014). Morphologies of z $\sim$ 0.7 AGN host galaxies in CANDELS: no trend of merger incidence with AGN luminosity. *Monthly Notices of the Royal Astronomical Society*, 439(4):3342–3356.

Villforth, C., Hamilton, T., Pawlik, M. M., Hewlett, T., Rowlands, K., Herbst, H., Shankar, F., Fontana, A., Hamann, F., Koekemoer, A., Pforr, J., Trump, J., and Wuyts, S. (2017). Host galaxies of luminous z $\sim$ 0.6 quasars: major mergers are not prevalent at the highest AGN luminosities. *Monthly Notices of the Royal Astronomical Society*, 466(1):812–830.

Villumsen, J. V. (1982). Simulations of galaxy mergers. *Monthly Notices of the Royal Astronomical Society*, 199:493–516.

Vogelsberger, M., Genel, S., Sijacki, D., Torrey, P., Springel, V., and Hernquist, L. (2013). A model for cosmological simulations of galaxy formation physics. *Monthly Notices of the Royal Astronomical Society*, 436(4):3031–3067.

Vogelsberger, M., Genel, S., Springel, V., Torrey, P., Sijacki, D., Xu, D., Snyder, G., Bird, S., Nelson, D., and Hernquist, L. (2014a). Properties of galaxies reproduced by a hydrodynamic simulation. *Nature*, 509(7499):177–182.

Vogelsberger, M., Genel, S., Springel, V., Torrey, P., Sijacki, D., Xu, D., Snyder, G., Nelson, D., and Hernquist, L. (2014b). Introducing the Illustris Project: simulating the coevolution of dark and visible matter in the Universe. *Monthly Notices of the Royal Astronomical Society*, 444(2):1518–1547.

Volonteri, M., Capelo, P. R., Netzer, H., Bellovary, J., Dotti, M., and Governato, F. (2015a). Black hole accretion versus star formation rate: theory confronts observations. *Monthly Notices of the Royal Astronomical Society*, 452(1):L6–L10.

Volonteri, M., Capelo, P. R., Netzer, H., Bellovary, J., Dotti, M., and Governato, F. (2015b). Growing black holes and galaxies: black hole accretion versus star formation rate. *Monthly Notices of the Royal Astronomical Society*, 449(2):1470–1485.

Walters, D., Woo, J., and Ellison, S. L. (2022). Quenching time-scales in the IllustrisTNG simulation. *Monthly Notices of the Royal Astronomical Society*, 511(4):6126–6142.

Ward, S. R., Harrison, C. M., Costa, T., and Mainieri, V. (2022). Cosmological simulations predict that AGN preferentially live in gas-rich, star-forming galaxies despite effective feedback. *Monthly Notices of the Royal Astronomical Society*, 514(2):2936–2957.

Weinberger, R., Springel, V., Hernquist, L., Pillepich, A., Marinacci, F., Pakmor, R., Nelson, D., Genel, S., Vogelsberger, M., Naiman, J., and Torrey, P. (2016). Simulating galaxy formation with black hole driven thermal and kinetic feedback. *Monthly Notices of the Royal Astronomical Society*, 465(3):3291–3308.

Weston, M. E., McIntosh, D. H., Brodwin, M., Mann, J., Cooper, A., McConnell, A., and Nielsen, J. L. (2017). Incidence of WISE -selected obscured AGNs in major

mergers and interactions from the SDSS. *Monthly Notices of the Royal Astronomical Society*, 464(4):3882–3906.

White, S. D. M. (1978). Simulations of merging galaxies. *Monthly Notices of the Royal Astronomical Society*, 184(2):185–203.

White, S. D. M. and Frenk, C. S. (1991). Galaxy Formation through Hierarchical Clustering. *The Astrophysical Journal*, 379:52.

White, S. D. M. and Rees, M. J. (1978). Core condensation in heavy halos: a two-stage theory for galaxy formation and clustering. *Monthly Notices of the Royal Astronomical Society*, 183:341–358.

Wild, V., Heckman, T., and Charlot, S. (2010). Timing the starburst-AGN connection. *Monthly Notices of the Royal Astronomical Society*, 405(2):933–947.

Woods, D. F. and Geller, M. J. (2007). Minor Galaxy Interactions: Star Formation Rates and Galaxy Properties. *The Astronomical Journal*, 134(2):527–540.

Woods, D. F., Geller, M. J., and Barton, E. J. (2006). Tidally Triggered Star Formation in Close Pairs of Galaxies: Major and Minor Interactions. *The Astronomical Journal*, 132(1):197–209.

Woods, D. F., Geller, M. J., Kurtz, M. J., Westra, E., Fabricant, D. G., and Dell'Antonio, I. (2010). Triggered Star Formation in Galaxy Pairs at z = 0.08-0.38. *The Astronomical Journal*, 139(5):1857–1870.

Xie, Y., Ho, L. C., Zhuang, M.-Y., and Shangguan, J. (2021). The Infrared Emission and Vigorous Star Formation of Low-redshift Quasars. *The Astrophysical Journal*, 910(2):124.

Xu, G. (1995). A New Parallel N-Body Gravity Solver: TPM. *The Astrophysical Journal Supplement*, 98:355.

Yang, C., Ge, J.-Q., and Lu, Y.-J. (2019). Hydrodynamical simulations of the triggering of nuclear activities by minor mergers of galaxies. *Research in Astronomy and Astrophysics*, 19(12):177.